# SSR MITIGATION WITH TCSC IN POWER SYSTEMS

THESIS SUBMITTED FOR THE DEGREE OF

DOCTOR OF PHILOSOPHY

RUI ZHENG

School of Engineering

Cardiff University

Cardiff, 2017

# Declaration

This work has not been submitted in substance for any other degree or award at this or any other university or place of learning, nor is being submitted concurrently in candidature for any degree or other award.

Signed ………………………………(candidate) Date ……………….………………………

## STATEMENT 1

This thesis is being submitted in partial fulfillment of the requirements for the degree of ………(insert MCh, MD, MPhil, PhD etc, as appropriate)

Signed ………………………………(candidate) Date ……………….………………………

## STATEMENT 2

This thesis is the result of my own independent work/investigation, except where otherwise stated, and the thesis has not been edited by a third party beyond what is permitted by Cardiff University's Policy on the Use of Third Party Editors by Research Degree Students. Other sources are acknowledged by explicit references.  The views expressed are my own.

Signed ………………………………(candidate) Date ……………….………………………

## STATEMENT 3

I hereby give consent for my thesis, if accepted, to be available online in the University's Open Access repository and for inter-library loan, and for the title and summary to be made available to outside organisations.

Signed ………………………………(candidate) Date ……………….………………………

## STATEMENT 4: PREVIOUSLY APPROVED BAR ON ACCESS

I hereby give consent for my thesis, if accepted, to be available online in the University's Open Access repository and for inter-library loans **after expiry of a bar on access previously approved by the Academic Standards & Quality Committee.**

Signed ………………………………(candidate) Date ……………….………………………

# Abstract

Thyristor-Controlled Series Capacitor (TCSC) is considered as solutions to the fast increasing demand in modern power systems. The TCSC project located at Hutton substation in the Great Britain (GB) power system is used to reinforce the existing transmission line to meet the 2020 target by introducing more renewable energy into the network. It is also able to provide system stability improvement and Sub-Synchronous Resonance (SSR) mitigation with its flexbile operational princinples. SSR problems in power systems are caused by the interaction between the mechanical turbine shaft system and the electrical system resonance. The capability of TCSC in SSR mitigation in High Voltage Alternative Current (HVAC) systems is investigated.

The study is conducted in two aspects, the inherent capability of TCSC to mitigate SSR and the active control scheme of TCSC for SSR damping. The operational principle of TCSC and the dynamic performance of TCSC under SSR impacts are analysed. It is found that the regulation of thyristors allows TCSC to transform sub-synchronous components into fundamental components. This ability of TCSC contributes to an improvement in SSR damping.

A Sub-Synchronous Damping Controller (SSDC) for TCSC is to secure the mitigation of SSR. But conventional SSDC has its limitations and challenges in implementation. These limitations include communication delays due to remote information transmitting at the generator side and the poor performance of bandpass filters due to its variable frequency response. A new SSDC scheme is proposed to solve the limitations and to improve the performance of SSR damping.

A physical TCSC device is designed and implemented at the laboratory scale. By interconnecting with Real-Time Digital Simulation (RTDS) and Power Amplifier (PA),

a TCSC platform is set up to perform experimental tests. The effectiveness of the proposed SSDC scheme is validated with both simulation software on PSCAD/EMTDC and the TCSC platform. The simulation results agree with the experimental test results. The developed TCSC platform can be utilised for testing other control schemes for SSR mitigations.

# Acknowledgements

I am particularly thankful to my parents, for their intellectual contributions to my academic nature. More importantly, I appreciate for their unconditionally support, incessant encouragement and undoubted faith in my succeeding the Ph.D. career throughout all these years. I also appreciate the help from Miss Lijie Yang, who helped me with proofreading and encouraged me during the hard period.

# TABLE OF CONTENTS

IX

# LIST OF TABLES

# LIST OF FIGURES

XIII

# List of abbreviations

| | |
|---|---|
| A/D | Analogue/Digital |
| AC | Alternate Current |
| CC | Constant-Current |
| CI | Constant-Impedance |
| CT | Current Transducers |
| DC | Direct Current |
| ERCOT | Electric Reliability Council of Texas |
| FACTS | Flexible AC Transmission System |
| FFT | Fast Fourier Transform |
| FSC | Fixed Series Compensation |
| HVAC | High Voltage AC |
| HVDC | High-Voltage Direct Current |
| IEEE | Institute of Electrical and Electronics Engineers |
| IGE | Induction Generator Effect |
| LCC | Line Commuted Converter |
| LQR | Linear-Quadratic Regulator |
| MOV | Metal Oxide Varistor |
| MTDC | Multi-Terminal DC |
| NGET | National Grid Electricity Transmission |
| PA | Power Amplifier |
| PCB | Printed Circuit Board |
| PLL | Phase Locked Loop |
| PMSG | Permanent-Magnetic Synchronous Generators |
| PMU | Phasor Measurement Units |

| | |
|---|---|
| RF | Resonant Filters |
| RTDS | Real Time Digital Simulator |
| RTI | Real Time Interface |
| SPT | Scottish Power Transmission |
| SSCI | Sub-Synchronous Control Interaction |
| SSDC | Sub-Synchronous Damping Controller |
| SSI | Sub-Synchronous Interaction |
| SSR | Sub-Synchronous Resonance |
| SSSC | Static Synchronous Series Compensator |
| SSTI | Sub-Synchronous Torsional Interaction |
| STATCOM | Static Synchronous Compensator |
| SVC | Static Var Compensator |
| SVR | Synchronous Voltage Reversal |
| TCR | Thyristor-Controlled Reactor |
| TCSC | Thyristor Controlled Series Capacitor |
| T-G | Turbine-Generator |
| TI | Torsional Interaction |
| TSO | Transmission System Operators |
| TTE | Transient Torque Effect |
| UPFC | Unified Power Flow Controller |
| VT | Voltage Transducers |
| WAMS | Wide-Area Measurement System |

# Chapter 1

# Introduction

This chapter introduces the background of the GB power system, motivation of this research, and contributions of the thesis. The structure of the thesis is also given.

## 1.1 DEVELOPMENT OF THE GB POWER SYSTEM

To face the challenges caused by environment and climate changes, the GB power system is experiencing great changes. The continuously developing economy results in increased demands for electrical power generation and transmission. The existing power system requires reinforcements to meet the demand for higher and more stable power transfer, as its power transfer capability is approaching the limit.

### 1.1.1  The UK future energy policy

Global warming and climate change resulted by greenhouse gas emissions have raised a lot of concern. To help contribute to preventing the climate change, the UK government announced the 2020 target in 2010 to source 15% of all energy consumption and 10% of transport fuels from renewables [1]. According to the plan, the following sub-objectives are to be achieved:

- 30% of total electricity from renewable generation

- 12% of the heat energy from renewable resources

- 10% of energy consumption in transport from renewable generation

The statistic indicates that the UK is expected to exceed the 30% electricity sub-target but may fail the other two sub-targets in transport fuels and heat. Fig. 1.1 shows

the electricity generation shares in the second quarter of year 2016 and 2017 [2]. The result indicates electricity generations from renewables achieve 29.8% which is 13.6% higher than it was in the second quarter of year 2016.
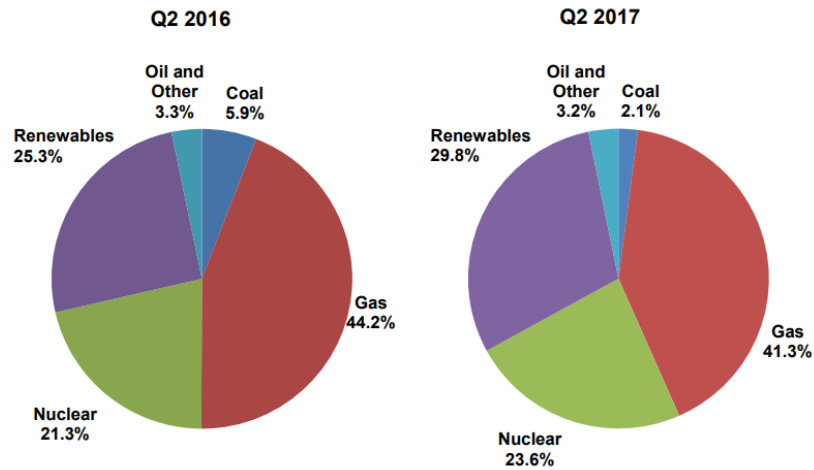


Fig. 1.1 Comparisons of the UK electricity generation in the 2$^{nd}$ quarter of year 2016 and 2017 [2]

To meet the 2020 target, the wind power is expected to play the leading role. According to the government's delivery Roadmap [3], by 2020, wind power generation within the UK could contribute between 3.7% and 5.8% of the estimated total energy consumption.

The development of wind power has progressed rapidly over the past 20 years. Up to Q3 in 2017, the wind power capacity in the UK has reached around 18 GW, and generated around 32.6 GWh in the first 3 quarters of 2017, which contributes 15% to the total electricity consumption throughout this year.

Locations of wind generation are unevenly distributed. Fig. 1.2 shows the geographical distribution of the wind generation [3]. The wind generation is centralised in the coastal area, especially in the Scotland and northern England.
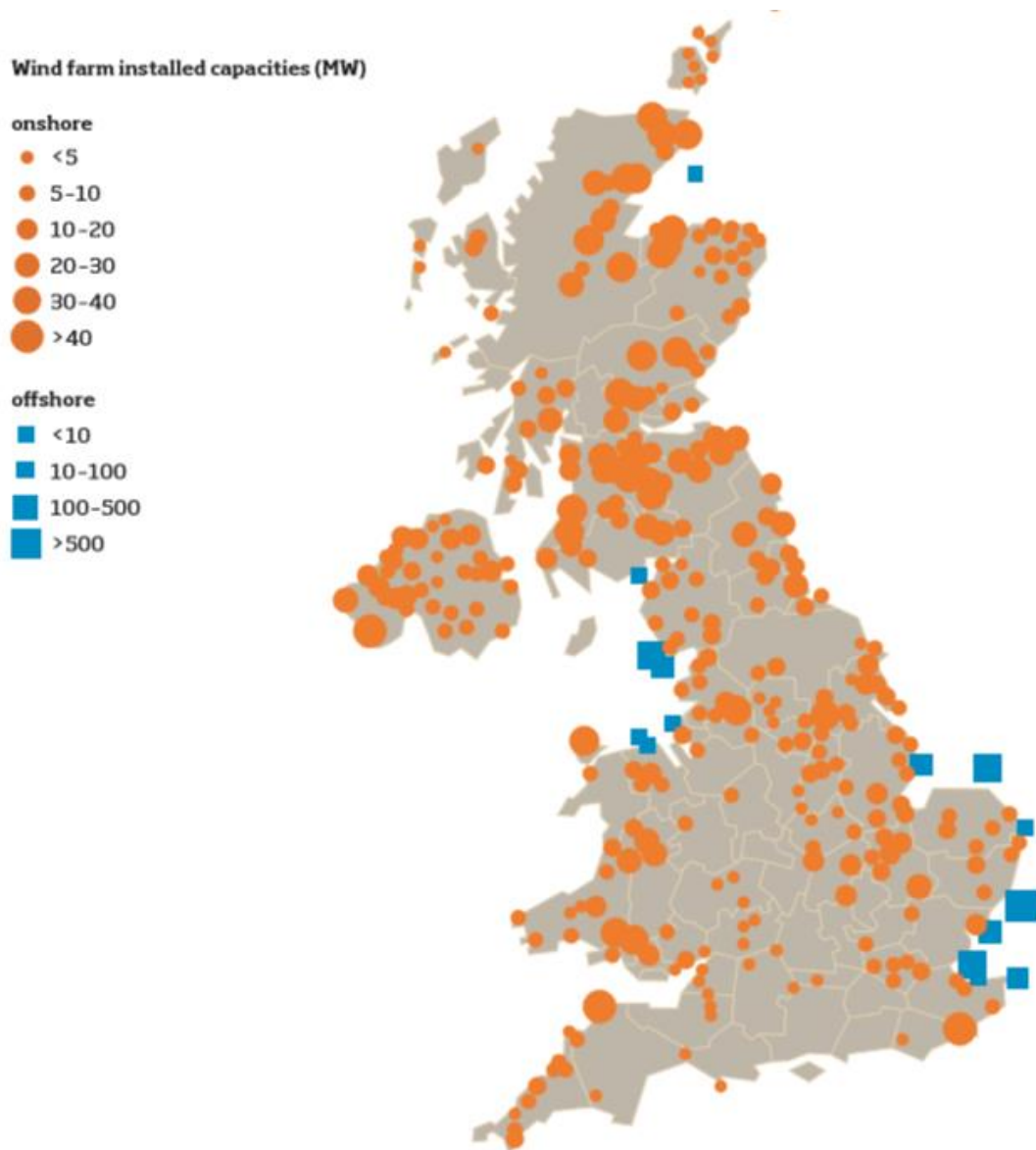
Fig. 1.2 Geographical locations of wind generation [3]

## 1.1.2 Reinforcing the existing GB power system

The integration of renewable generation requires reinforcements to the existing GB power system to meet the power transfer requirements. Reinforcements include series compensation techniques placed at the main transmission routes and additional HVDC links based on power electronics converters. Fig. 1.3 demonstrates the locations of reinforcements to the existing power system [4].
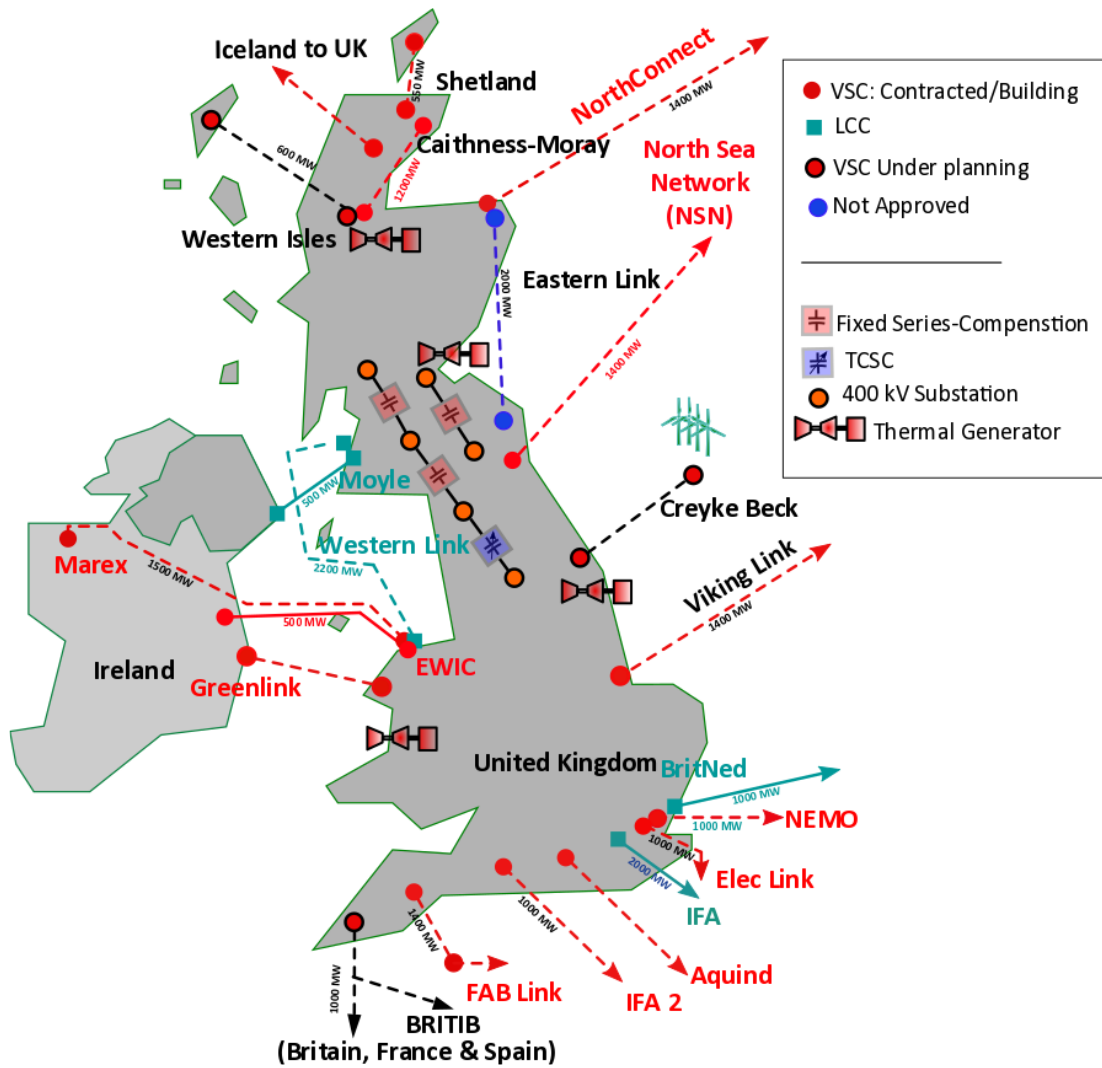
Fig. 1.3 Reinforcements in the GB power system to meet the 2020 target [4]

According to Fig. 1.3, three Fixed Series Compensation (FSC) projects and a Thyristor Controlled Series Capacitor (TCSC) project are installed interconnecting the Scottish system to the north of England. The power transfer capacity is boosted from 1100 MW to 4400 MW through these compensators. However, as the first application of series capacitor in the UK, the potential interaction and risks of SSR problems need to be addressed.

## 1.2 RESEARCH MOTIVATION

Generating units, especially wind turbine generators and thermal turbine generators are vulnerable to Sub-Synchronous Resonance (SSR) risks introduced by series compensation techniques in the GB power system.

One way to solve the potential SSR risks is to install conventional countermeasures based on a detailed study about which generating units are under SSR risks, i.e. filters or damping circuits to prevent sub-synchronous currents from flowing back to generating units. This is a time-consuming task and requires experienced engineers to design or modify the existing control systems or protection schemes. However, the better solution is to utilise the benefits of the controllable TCSC due to the installation of TCSC is located at the main corridor interconnecting generating units and the demand. Since the FSC and TCSC projects are in series and placed in the main corridor that interconnects the Scottish system and the England system, SSR risks caused by FSC can be eliminated by TCSC without investing in extra devices.

The TCSC project at the Hutton substation is the first project of this kind in the UK. The Transmission System Operators (TSO) in the UK still lack the experience and confidence in the operation of TCSC and its capability in solve SSR problems, as the mechanism of TCSC inherent capability in SSR mitigation is still not clear. The National Grid UK has conducted case studies which indicate the SSR risk has been eliminated by use of TCSC [5]. The system electrical damping is found to be positive enough to damp all SSR modes between 12 Hz and 38 Hz, which covers all the range of concerned mechanical frequencies. However, with the construction of new wind turbines, or with an un-scheduled configuration changing, SSR may still occur at

unexpected frequencies. This is because that newly installed turbine generators may have new SSR modes.

## 1.3 OBJECTIVES AND CONTRIBUTIONS OF THE THESIS

The objectives and contributions of the Ph. D research are outlined as follow:

- Investigate the impact of TCSC device on the GB power system in terms of SSR.

  A detailed study about the inherent characteristic of TCSC has been conducted and the dynamic performance of TCSC under impacts of SSR events has been investigated. The selection of TCSC parameters in a hybrid compensation system with both FSC and TCSC has been studied, to provide a guidance to TSOs in designing TCSC projects.

- Set up an experimental platform with physical TCSC device for validations.

  A TCSC device has been designed and built based in the laboratory environment. The device is connected to the grid emulator, which consists a Real Time Digital Simulator (RTDS) and a Power Amplifier (PA). SSR problems have been replicated on the platform and the effectiveness of TCSC's capability in SSR mitigation have been validated. This platform can be extended for other studies on compensation-related issues.

- Propose a novel control scheme for TCSC to mitigate SSR events with higher adaptability to future system conditions.

  A novel control scheme for TCSC in SSR mitigation have been proposed to improve the adaptability in practical projects. Unlike traditional control strategies, which requires remote communication links to be established

between generating units and TCSC device, this control scheme considers local measurements for SSR detection and discrimination to provide a faster response and easier access to control system modifications.

## 1.4 THESIS STRUCTURE

The rest chapters of the thesis are structured as follow.

**Chapter 2** provides the literature review of the development of series compensation technique, and the definition and classification of SSR. Some commonly used study methods for SSR phenomenon are introduced, with special attention to the complex torque coefficient method, which is used in the study of SSR within this thesis. Last, the state-of-the-art of conventional solutions to SSR problems is presented.

**Chapter 3** reviews the technology of TCSC, including its history, commissioned projects and relevant research topics. The operational principle and performance of TCSC are presented, mainly operated under the capacitive mode. The principle in selecting TCSC parameters to avoid the dual-resonance phenomenon is also demonstrated.

**Chapter 4** investigates the inherent characteristic of TCSC and the response of TCSC to SSR events. A theory is proposed that TCSC operated with constant firing angle control still has the ability to improve SSR damping by transforming sub-synchronous components into synchronous components. This theory is validated by comparing the energy at different frequencies before and after the regulation of thyristors. Case studies have been conducted to show the damping performance improved by the application of TCSC is highly related to the energy conversion ability of TCSC. The performance of a hybrid compensation scheme with both TCSC and

FSC contributing different percentages of compensation levels is studied to provide a guidance in designing series compensation projects.

**Chapter 5** demonstrates the procedure of establishing the TCSC platform. The design for the TCSC device is presented, including the topology, protection schemes and parameter selections. The control system is developed, and the involved software and firmware are introduced.

**Chapter 6** describes the capability of TCSC in SSR mitigation with its controllability. Limitations of conventional damping schemes based on TCSC controller are discussed. Some modifications are proposed to eliminate the limitations and contribute to a novel SSR damping scheme. The effectiveness of the proposed damping scheme is validated with simulation case studies and experimental tests.

**Chapter 7** presents the conclusion drawn from this thesis, and the recommended future work.

# Chapter 2

# Literature review

## 2.1 INTRODUCTION

In AC power systems, series capacitors are connected in series with transmission line to reduce the overall equivalent impedance of the transmission system. This helps to increase the maximum power transfer capability and improve the system stability. Because of these benefits, Fixed Series Capacitor (FSC) technologies are widely used around the world.

However, one drawback of FSC technology is the SSR phenomenon. Turbine generator shaft is consist of many individual masses with different inertias. When rotating as a whole shaft, the torque between different adjacent masses has an inherent resonant frequency, which is also referred as a SSR mode. An electrical resonance at a complementary frequency to the shaft inherent frequency may interact with the SSR mode and amplfy the torsional oscillation on the shaft. This electro-mechanical phenomenon can reduce the lifetime of turbine generator shafts or even break down the shaft to cause severe accidents.

In 2013, FSC installations were commissioned at Moffat, Eccles and Gretna [6-8] to interconnect the Scottish Power Transmission (SPT) and National Grid Electricity Transmission (NGET), and TCSC installtions were completed by the end of 2014. Since this is the first series compensation technique adopted in the GB power system, the concern of SSR events also rises. This chapter reviews the background of FSC and SSR, and commonly used technologies for SSR mitigation.

## 2.2 A REVIEW OF SERIES COMPENSATION TECHNOLOGY

### 2.2.1 Benefits of series compensation techniques

The application of the series compensation dates back to 1930s. In AC transmission system, the maximum active power transferable over a certain power transmission line is inversely proportional to the series impedance of the transmission line. Thus, by using a series capacitor and compensating the series impedance to a certain level, the transmission line is electrically shortened, and higher power transfer can be achieved. This is a cost-effective solution to face bulk power transmission challenges compared with building extra transmission lines [7]. Besides, the series capacitor can balance voltage drops caused by the line impedance. Consequently, the voltage stability is also improved.

The active power transfer through a transmission line is determined by its terminal voltages at each end, and is inversely proportional to the overall impedance of the transmission system. The relationship can be expressed in (2.1).

$$P = \frac{V_S V_R}{X_t} sin\delta \qquad (2.1)$$

where $V_S \; and \; V_R$ are the sending and receiving terminal voltages, and $\delta$ is their phase angle difference. $X_t$ is the overall impedance of the transmission system.

Considering that the terminal voltage magnitudes are kept constant, the maximum power transfer occurs when the phase angle difference $\delta$ becomes 90°.

Application of the FSC technique can help to improve the maximum power transfer without building extra transmission lines. The relationship between the inserted FSC impedance and the transmission line impedance is defined as the series compensation level, denoted by $k$.

$$k = \frac{X_{FSC}}{X_T} \tag{2.2}$$

where $X_{FSC}$ is the impedance of inserted FSC, and $X_T$ is the total impedance of the transmission system before compensating. The compensation level $k$ is smaller than 100%.

Thus, the reduced impedance of the overall transmission system can be derived in terms of the compensation level, as:

$$X_{eff} = X_T - X_{FSC} = X_T(1 - k) \tag{2.3}$$

where $X_{eff}$ is the effective impedance of the compensated transmission line. The maximum power flow in terms of the series compensation level is given as:

$$P = \frac{V_S V_R}{X_T(1-k)} sin\delta \tag{2.4}$$

Considering that the sending and receiving end voltages are constant at 1 pu, the power-angle curve regarding different compensation levels can be presented as Fig. 2.1.
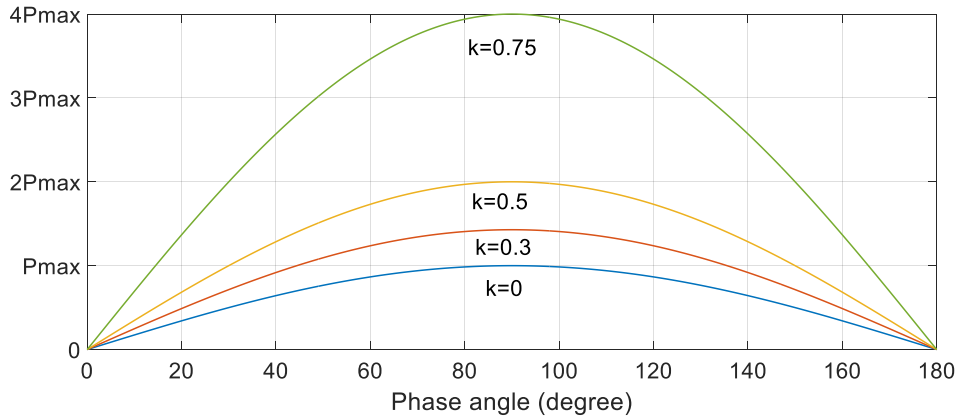


Fig. 2.1 Power-angle curve considering different compensation levels

According to Fig. 2.1, the power transfer capability is greatly affected by the compensation level. Given that the compensation level is at 30%, the power transfer

11

capability is boosted by 50%. If the compensation level achieves 75%, the power

transfer capability is boosted to 400% of the non-compensated capability.

## 2.2.2 Installation of FSC in the GB power system

FSC technique has become a mature and cost-effective solution to bulk AC power

transmission. A typical layout of a FSC installation in industrial projects is given in

Fig. 2.2.
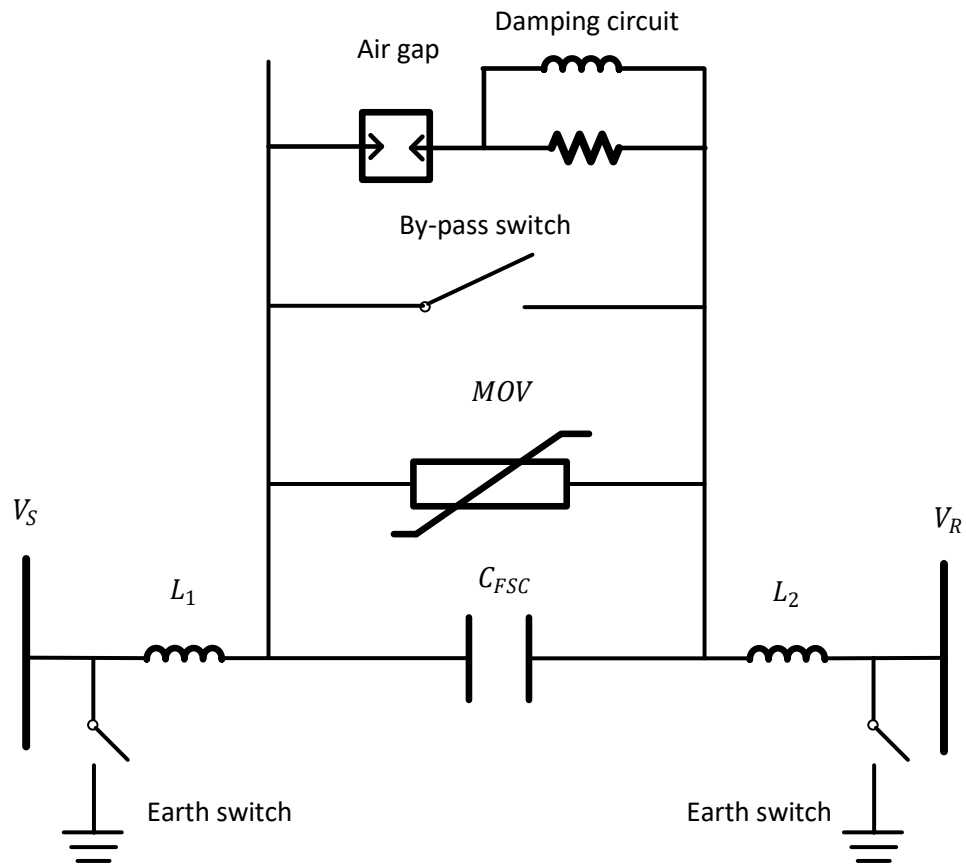


Fig. 2.2 Typical layout of a FSC [10]

In industrial projects, FSC is equipped with MOV to protect it from over-voltage

events. A paralleled switch is used to insert or by-pass FSC from the network, denoted

as the By-pass switch in Fig. 2.2. When FSC is by-passed, its stored energy needs to

be discharged through a closed circuit containing a damping circuit to limit the

discharging current. The damping circuit is controlled through a damping switch and it is open-circuit during normal operations. Two earth switches are used to protect FSC from fault events.

Table 2.1 Ratings of FSC installations in the UK

|  | Moffat | Gretna | Eccles 1 | Eccles 2 |
|---|---|---|---|---|
| Voltage rating | 400 kV | 400 kV | 400 kV | 400 kV |
| Power rating | 560 MVAr | 560 MVAr | 442 MVAr | 442 MVAr |

The FSC projects in the UK are installed at Moffat, Eccles and Gretna, and their ratings are listed in Table 2.1 [9]. These capacitor banks are equipped with SSR filters and help to reduce the overall impedance between Strathaven and Harker and Eccles and Stella by 35% [10].

Generally, the design of the compensation level should consider following aspects:

- The voltage at the terminal substaion;
- The voltage distrubition along the transmission line;
- Requirements of the system stability;
- Power flows between paralleled transmission lines.

A reasonable compensation level should be within 20% - 80% [11] depending on site requirements and considerations listed above. When FSC is installed on a transmission corridor directly connected to turbine generator units, the risk of SSR problems needs to be addressed.

## 2.2.3 Operations of FSC

In the design of industrial FSC projects, specifications of the continuous and fault currents flowing through a FSC must be given. According to [11], an industrial standard of 1000kV FSC's capability in over-current operations is given in Table 2.2.

Table 2.2 Over-current capability requirements for a 1000kV FSC bank

| Current | Typical duration | Typical over-current value |
|---|---|---|
| Rated current | Continuous | 1.0 pu |
| 1.10*rated current | 8 hours in every 12 hours | 1.10 pu |
| 1.20*rated current | 2 hours in every 8 hours | 1.20 pu |
| 1.35*rated current | 30 mins in every 6 hours | 1.35 pu |
| 1.50*rated current | 10 mins in every 2 hours | 1.50 pu |
| Current swings | 1s – 10 s | 1.70 pu – 2 pu |

Table 2.2 shows typical operational requirements for FSC under industrial standards. It indicates that the current rating of FSC bank should be higher than the system current rating considering the maximum power transfer under continuous operations. This allows system operators to flexibly utilise the FSC's capability in over-current operations to face fault conditions or power transfer requirements in an emergency.

## 2.3 AN OVERVIEW OF SUB-SYNCHRONOUS INTERACTION (SSI)

## 2.3.1 Classification of Sub-Synchronous Interaction

Interactions within sub-synchronous frequency ranges in power systems are defined as Sub-Synchronous Interaction (SSI). In power systems, SSI can be various. According to [12], reasons of SSI can be installations of FSC or converter control systems. Generally, there are three types of SSI events based on involved devices and the source of sub-synchronous components, Sub-Synchronous Resonance (SSR), Sub-Synchronous Torsional Interaction (SSTI) and Sub-Synchronous Control Interaction (SSCI).

SSR occurs due to the addition of series compensation onto the system, while SSTI is due to the integration of High-Voltage Direct Current (HVDC) links. The potential effect of both SSR and SSTI on the network is the interaction with generator shafts, and in severe cases they can both cause shaft fatigues and failures. Another type of SSI, known as SSCI, occurs between the control system and the electrical transmission network at complementary frequencies of control system torsional modes. The severity of SSI problems is increasing with the development of series compensation techniques and HVDC techniques in the GB power system.
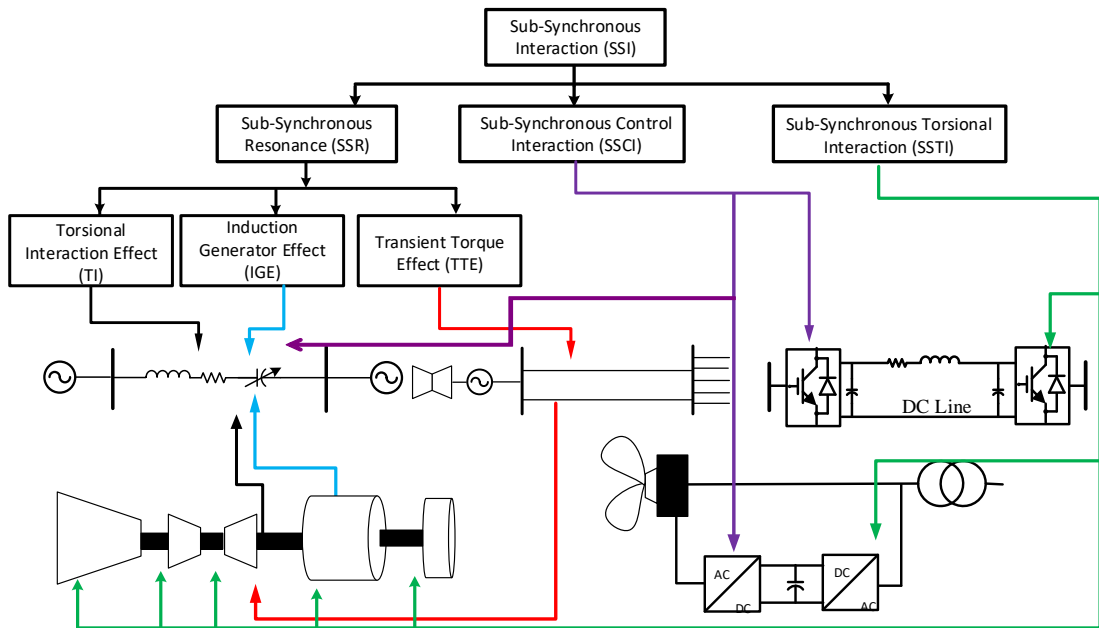
Fig. 2.3 Classification of SSI and their relationships between different devices involved

However, it should be noted that the classification of SSI still exists with crossing-overs and disagreements among academics and industries. In this thesis, it adopts the classification accepted by most European and US researchers and the UK National Grid. Fig. 2.3 shows this classification of SSI phenomenon and the devices involved in corresponding SSI events.

**Sub-Synchronous Resonance :**

SSR is caused by the installation of series capacitors and is an interaction between the turbine generator shaft system and the compensated electrical network. There are three types of commonly observed SSR events which are discussed in section 2.4.

**Sub-Synchronous Control Interaction:**

SSCI occurs between the control system of power electronics and the series capacitor [13-17]. The first SSCI event was observed in 2009 between power electronics control systems in wind turbines and the series capacitor in Electric Reliability Council of

Texas (ERCOT). The wind turbines then suffered crossbar failures caused by the oscillating current with heavy sub-synchronous distortions. After this event, ERCOT requires a detailed study on all wind turbines that are directly connected to series capacitors to address SSCI risks.

**Sub-Synchronous Torsional Interaction:**

The first SSTI event was observed in 1977 at Square Butte, between the classic Line Commuted Converter (LCC) in a HVDC link and the turbine generator. This led to an extensive research on SSTI to find out the mechanism of SSTI [18-21]. The reason of SSTI is that the converter working as a rectifier reduces the electrical damping within sub-synchronous frequency ranges. Therefore, the system induces sub-synchronous harmonics that cannot be damped by the electrical network, and these sub-synchronous components may interact with the natural torsional modes of the turbine generator to cause SSTI. A solution to SSTI is to design and equip the converter with Sub-Synchronous Damping Controller (SSDC) [20, 21].

## 2.3.2 New SSI phenomenon

The classification shown in Fig. 2.3 is based on previous SSI events. However, as the complexity of modern power systems has increased, more SSI phenomena are observed, and they belong to none of the listed classifications.

In 2014, a sub-synchronous power oscillation was captured by the Wide-Area Measurement System (WAMS) in XinJiang Province, northwestern China. These sub-synchronous oscillations were oriented from some directly-drive Permanent-Magnetic Synchronous Generators (PMSG), but then spread rapidly to nearby AC grids [22-24]. Fig. 2.4 presents the occurrence of the newly found SSI event.
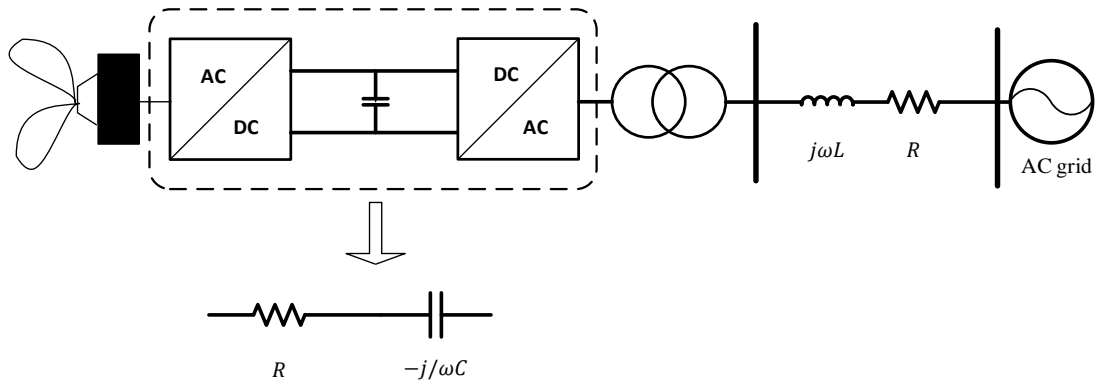
Fig. 2.4 Demonstration of the mechanism of the new SSI event

In this new SSI event, the interaction is found between a non-compensated weak AC grid and the wind turbine converter. Study in [24] found that the converter control system performs negative resistive and capacitive at sub-synchronous frequencies. This forms a R-L-C circuit along with the AC grid and induces sub-synchronous currents. These currents then interact with particular torsional modes of the converter control system. This new SSI event is a pure electrical event without interacting with the mechanical turbine system. Fig. 2.5 shows the phase A current and power oscillations during this event.
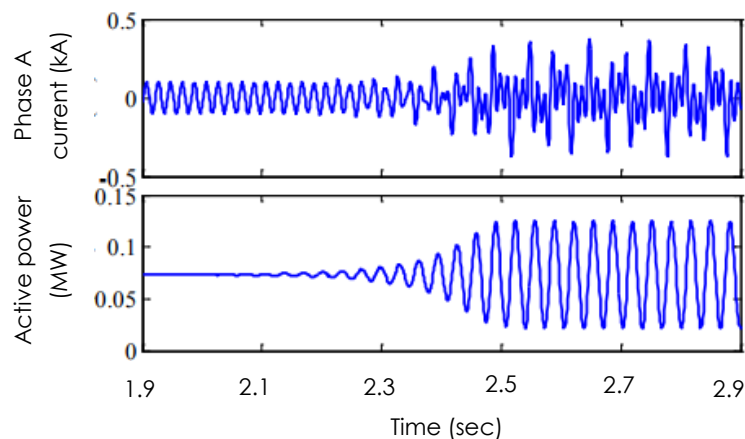


Fig. 2.5 Dynamics of the PSMG under the new SSI event

There are still many research topics in SSI, however, limited by time, the scope for this thesis focuses on SSR-TI only.

## 2.4 REVIEW ON SSR PHENOMENON

### 2.4.1 Definition of SSR

SSR can cause severe damages to power devices and is the most common concern among other SSI problems. Though numerous studies have been made on previous SSR events, the short distance transmission system in the UK makes a different case for SSR concerns. Especially in the UK, with the newly-installed series compensation devices, study of SSR and its impacts on the GB power system are of particular interests.

The discovery of SSR dates back to 1930s when FSC was first adopted in transmission systems. Engineers discovered the potential interaction between the capacitor and turbine generators and proposed the first paper on SSR in 1937 [25], but the first SSR event was not observed until 1970 at the Mohave units in the USA [26]. This event caused a big black-out in the Texas area and drew lots of attention from both industries and academics, while a second event followed in the next year. Lots of researches have been conducted after the SSR events on turbine generator modelling [27-29] and system modelling [30-32].

To study the mechanism of SSR event, a general model for study was proposed by the IEEE working group as the First Benchmark model [27]. This model is based on the Navajo project including a 892.4 MVA turbine generator and a 500 kV transmission line with series compensation. It provides a guidance of how to study SSR events. In 1979, a first paper was published by the IEEE working group to propose terms and definitions for SSR [33]. These definitions and symbols were soon accepted

by both industries and academics. Another extended paper of definitions and symbols to describe SSR event was followed in 1985 by IEEE working group to give a more detailed guidance for SSR phenomenon [34].

According to [35], the formal definition of SSR is:

"Subsynchronous resonance is an electric power system condition where the electric network exchanges energy with a turbine generator at one or more of the natural frequencies of the combined system below the synchronous frequency of the system."

The definition of SSR includes any possible conditions that an interaction or energy exchange at sub-synchronous frequencies. Typically, there are two types of modes, the natural mode and the forced mode [36]. A natural mode of oscillation refers to the inherent system characteristic, and a most common example is the series compensation which forms a R-L-C network with a series resonant frequency below synchronous frequency. As for a forced mode, it refers to an oscillation driven by controllable devices or the control system.

## 2.4.2  Classification of different SSR interactions

The interaction between the electrical system and the turbine generator can occur in different ways in terms of sub-synchronous frequencies. Among them, there are three types of SSR interactions [37] most commonly studied and concerned. They are:

- Induction Generator Effect (IGE)

- Torsional Interaction (TI)

- Transient Torque Effect (TTE)

**Induction Generator Effect**

The IGE is resulted by the self-excitation of the electrical system [169, 170]. As seen in Fig. 2.6, the rotor resistance, viewed from the armature, can become negative under the impact of sub-synchronous current. When sub-synchronous current, at frequency of $f_n$, is flowing through the rotor, the rotor behaves like an induction machine running at above synchronous speed. Then the slip becomes negative which is determined by (2.5).

$$s = \frac{f_n - f_0}{f_n} \tag{2.5}$$

Since the frequency of sub-synchronous current, $f_n$, is determined by the series compensation level, the apparent negative rotor resistance can exceed the positive resistance of the armature. In that case, the overall resistance, denoted as $R_{eff}$, becomes negative and this reduces the stability of the system, according to (2.6).

$$R_{eff} = \frac{1-s}{s} R_r + R_a \tag{2.6}$$

The IGE is a pure electrical phenomenon and is independent from the turbine shaft characteristic.
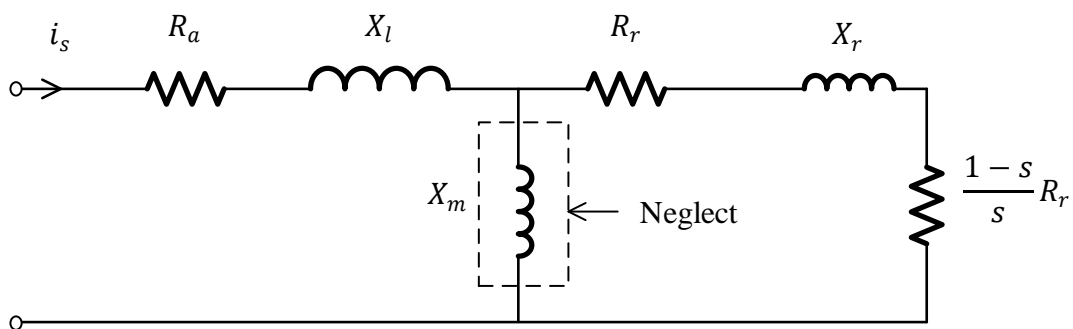


Fig. 2.6 Simplified synchronous machine equivalent circuit regarding to induction generator effect

**Torsional Interaction**

The TI occurs between the electrical system and the mechanical turbine shaft system, this is an electro-mechanical phenomenon.

To summarise, the occurrence of TI-SSR must fulfil the following conditions:

- A mechanical torsional mode at a frequency within sub-synchronous frequency ranges

- The generator mass must participate with one of other swinging masses at the torsional mode frequency

- The electrical system must induce a resonant component at a complementary frequency to the mechanical frequency

For given turbine generators, their turbine shafts may have some fixed mechanical torsional modes that lie within sub-synchronous frequencies ranges. The relationship between the mechanical torsional frequency and the electrical resonant frequency that can excite a torsional mode can be expressed as:

$$f_{TM} \approx f_{sys} - f_{ele} \tag{2.7}$$

where $f_{TM}$ is the frequency of a torsional mode, $f_{sys}$ and $f_{ele}$ are the system frequency and the frequency of the electrical component.

A torsional mode can be excited when there is a sub-synchronous component at the complementary frequency, and if the overall damping is not enough, the oscillation grows and SSR event happens. The electrical sub-synchronous component can be found in different cases, but most commonly in series compensated AC systems or can be found with power electronic devices. In this thesis, the scope is limited to series

compensated AC systems. Then, the determination of the electrical sub-synchronous component frequency is given as:

$$f_{ele} = f_{sys} \cdot \sqrt{X_C / X_T} \qquad (2.8)$$

here $X_C$ is the impedance of series compensator, and $X_T$ is the total impedance of the system, including the transmission line impedance, connected transformer leakage impedance and the load impedance. The term $X_C / X_T$ is the compensation level provided by series compensators.

**Transient Torque Effect**

TTE is mainly caused by system disturbances and the induced transient current. In AC systems, sudden changes in the network can result in large transient current which tends to oscillate at the natural frequency of the network. If there are no series capacitors, the transient current is only DC current that can be damped quickly by the system natural damping. However, with series capacitors, the transient current tends to oscillate at a frequency determined by (2.8), which is below the synchronous frequency. If there are more capacitor banks located in the network, there can be multiple oscillation frequencies in the transient current. Similar to TI effect, if the frequency of the sub-synchronous current is at complementary frequency of a torsional frequency of the turbine shaft, a large torque oscillation can be excited since the magnitude of torque oscillation is proportional to the magnitude of the transient current. The TTE is a severe event since the fault current can cause a very high peak torque and the situation in real power systems is very complex with many different sub-synchronous frequencies.

## 2.4.3  Typical waveforms to describe SSR event

The SSR event affects both the mechanical system and the electrical system. It can be observed in the Turbine-Generator (T-G) torque or in the line current flow.
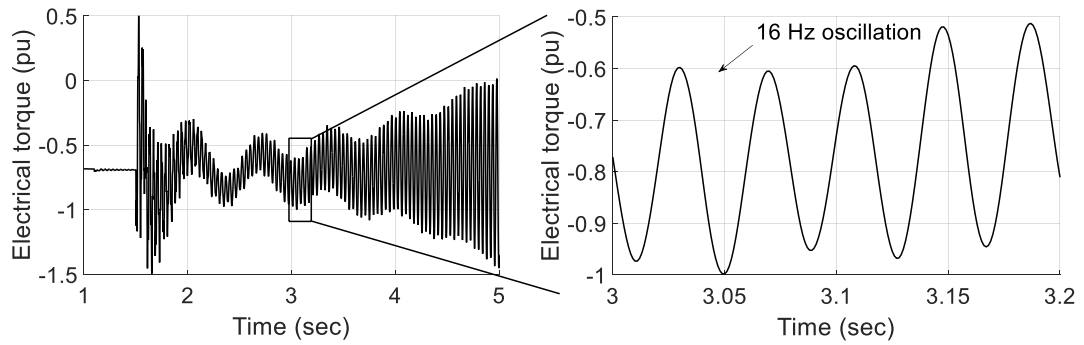


(a) Electrical torque waveform and its zoom-in plot under SSR event
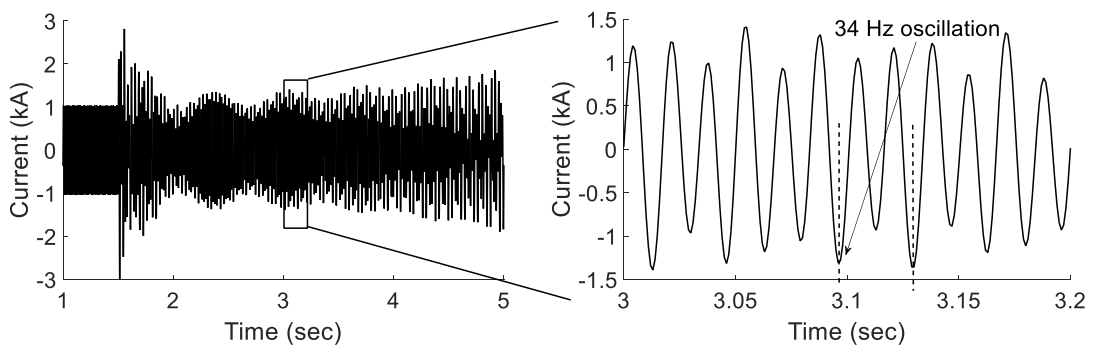


(b) Current waveform and its zoom-in plot under SSR event

Fig. 2.7 Typical waveforms and their zoom-in plots under SSR events

Fig. 2.7 gives typical waveforms for the T-G electrical torque and the line current under the impact of SSR. The SSR is triggered at 1.5s by applying a large disturbance and the torsional mode is at 16 Hz which is reflected in the electrical torque. The complementary frequency to this torsional mode is 34 Hz and this sub-synchronous current is found in the line current along with the synchronous component at 50 Hz.

SSR problem is very severe in real projects since it may break turbine shaft down if unattended for a long time. The torsional oscillation can cause shaft masses to suffer

24

metal fatigue which will dramatically reduce the lifetime of the shaft system. In the first SSR event, 1970, the turbine shaft broke down and was blown to miles away. Therefore, SSR must be avoided in power systems with suitable countermeasures, i.e. static and dynamic filters [38], dynamic stabilizer [39], and excitation system damper [40].

## 2.5 STUDY METHODS FOR SSR

### 2.5.1 Frequency scanning

There are several analytical methods to investigate SSR, the frequency scanning method is a widely used and effective tool for SSR study [41-46] , especially in IGE study.

Frequency scanning technique calculates the equivalent circuit resistance and impedance seen from the generator side, usually behind the stator windings of the generator to consider the rotor resistance for IGE study. If the equivalent resistance and impedance occur to be close to or below zero, the circuit can be expected to be suffering oscillations. However, this is also the limitation of frequency scanning method. The system impedance has to be seen from a certain generator side and the rest components are equivalent to a passive circuit. In complex networks, to identify SSR risks for different generating units, the frequency scanning must be repeated for different system conditions at each generator terminal of interest.

In [47-49], some modifications were made to improve the performance of frequency scanning method in large scale power system with higher complexities. The function is also extended to SSCI study by optimising the discrimination algorithms.

## 2.5.2 Eigenvalue analysis

The dynamic behaviour of The dynamic behaviour of a power system can be described with a set of non-linear first order differential equations [50]:

$$\dot{x} = f(x, u) \tag{2.9}$$

$$y = g(x, u) \tag{2.10}$$

where

**f** is the vector containing the set of first-order non-linear differential equations, **x** and **u** are the vectors containing the state variables and input variables respectively. **g** is the vector of non-linear algebraic equations, and **y** is the vector containing output variables.

Linearising the system allows investigation on the system's response to small disturbances. Detailed linearization can be found in [50-51]. Then the vector **x** and **y** in 2.9 and 2.10 can be expressed as:

$$\dot{\Delta x} = A\Delta x + B\Delta u \tag{2.11}$$

$$\Delta y = C\Delta x + D\Delta u \tag{2.12}$$

where

$$A = \begin{bmatrix} \frac{\partial f_1}{\partial x_1} & \cdots & \frac{\partial f_1}{\partial x_n} \\ \vdots & \ddots & \vdots \\ \frac{\partial f_n}{\partial x_1} & \cdots & \frac{\partial f_n}{\partial x_n} \end{bmatrix} \qquad B = \begin{bmatrix} \frac{\partial f_1}{\partial u_1} & \cdots & \frac{\partial f_1}{\partial u_n} \\ \vdots & \ddots & \vdots \\ \frac{\partial f_n}{\partial u_1} & \cdots & \frac{\partial f_n}{\partial u_n} \end{bmatrix}$$

$$C = \begin{bmatrix} \frac{\partial g_1}{\partial x_1} & \cdots & \frac{\partial g_1}{\partial x_n} \\ \vdots & \ddots & \vdots \\ \frac{\partial g_n}{\partial x_1} & \cdots & \frac{\partial g_n}{\partial x_n} \end{bmatrix} \qquad D = \begin{bmatrix} \frac{\partial g_1}{\partial u_1} & \cdots & \frac{\partial g_1}{\partial u_n} \\ \vdots & \ddots & \vdots \\ \frac{\partial g_n}{\partial u_1} & \cdots & \frac{\partial g_n}{\partial u_n} \end{bmatrix}$$

Therefore, the matrices **A, B, C** and **D** contain the partial derivatives of the functions in **f** and **g** to the state variables **x** and the input variables **u**. The characteristic equation of matrix **A** is given in 2.13, and values of s which satisfy 2.13 are known as eigenvalues of matrix **A**.

$$\det(s\boldsymbol{I} - \boldsymbol{A}) = 0 \qquad\qquad (2.13)$$

The stability in a small non-linear system can be obtained by the eigenvalues of the matrix **A** [53]:

a. If the eigenvalues have negative real parts, the system is asymptotically stable;

b. If there are at least one eigenvalues having a positive real part, the system is unstable;

c. If the eigenvalues have real parts that equal to zero, the system stability cannot be determined based on the first approximation.


The disadvantage of eigenvalue analysis method is that only small system can be analysed. Eigenvalue analysis method requires modelling of the system with necessary state variables to describe the system condition. In large systems, the system matrix can be of 500th order or more, which makes the computation a time-consuming task. Some work has been done to solve large systems by selecting necessary state variables only and optimising the programming [53-54].

### 2.5.3 Complex torque coefficient method

Complex torque coefficient method has been extensively applied in the SSR analysis since it was first proposed by I. M. Canay [64]. Compared with the other tools for SSR study like eigenvalue analysis and frequency scanning, the complex torque

coefficient method is easier to realize as it does not require linearization of complex power systems. While the limitation is that the complex torque coefficient method can be only applied to single T-G system with other components to be fixed frequency sources [65]. But since the study system in this chapter is based on the single transmission line system with one T-G, this disadvantage is not a problem.

To a T-G under study, its electromechanical dynamic under small signal disturbance can be represented by the following relationship:

$$\Delta T_e = K_S \Delta \delta + K_D \Delta \omega \qquad (2.14)$$

where $\Delta T_e$ is the increment in the electrical torque, $K_S$ and $K_D$ are the synchronous torque coefficient and damping torque coefficient, $\Delta \delta$ and $\Delta \omega$ are the increment in the power angle and the generator rotor speed respectively. The relationship between power angle $\delta$ and rotor speed $\omega$ is:

$$\Delta \omega = \frac{1}{\omega_0} \frac{d\Delta \delta}{dt} \qquad (2.15)$$

Assume a small disturbance at sub-synchronous frequency of $\rho \omega_0$ ($\rho < 1$) is injected onto the rotor speed, then the phasor expression of (2.14) and (2.15) can be derived as

$$\Delta \overline{\omega} = \frac{1}{\omega_0} (j\rho \omega_0) \Delta \overline{\delta} = j\rho \Delta \overline{\delta} \qquad (2.16)$$

and

$$\Delta \overline{T_e} = K_S(\rho) \Delta \overline{\delta} + K_D(\rho) \Delta \overline{\omega} \qquad (2.17)$$

where the term with a bar over it means it is in phasor form. Therefore, dividing (2.17) with $\Delta \overline{\omega}$ gives the expression for the damping torque coefficient at different sub-synchronous frequencies depending on $\rho$:

$$\frac{\Delta \overline{T_e}}{\Delta \overline{\omega}} = -j \frac{1}{\rho} K_S(\rho) + K_D(\rho) \tag{2.18}$$

Here $K_D(\rho)$ represents the damping factor at sub-synchronous frequency $\rho \omega_0$ for the electrical system. If the mechanical damping is neglected, the requirement for a stable SSR mode is related to $K_D(\rho)$ that

$$K_D(\rho) > 0 \tag{2.19}$$

Therefore, the steps to obtain the $K_D(\rho)$ in time domain simulation can be summarized as follow:

(a). For a certain operating point, inject a small disturbance onto the mechanical torque input of the T-G:

$$T_m = T_{m0} + \Delta T_m = T_{m0} + T_\rho \cos(\rho \omega_0 t + \varphi_\rho) \tag{2.20}$$

Here $T_{m0}$ is the initial mechanical torque input, and $\rho \omega_0$ represents the sub-synchronous frequency ($\rho < 1$).

(b). After the injection of sub-synchronous torque $\Delta T_m$, simulate the system until it reaches steady state again, and obtain the electrical torque $T_e$ and rotor speed $\omega$.

(c). Use Fourier Transform to obtain the phasor information of $T_e$ and $\omega$, for $\Delta \overline{T_e}$ and $\Delta \overline{\omega}$ at different frequencies $\rho \omega_0$, then calculate $K_D(\rho)$.
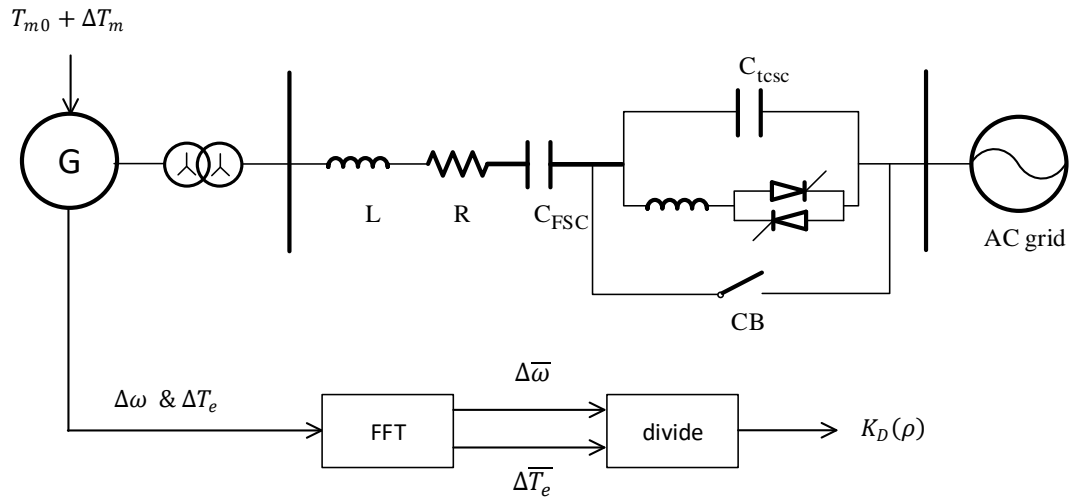
Fig. 2.8 An application of the complex torque coefficient method in measuring the electrical torque in power systems

Fig. 2.8 shows the implementation of the complex torque coefficient method in the FBM system. The electrical system including transmission line, series compensator, TCSC and the AC grid, is equivalent to a circuit from the generator side.

## 2.6 CONVENTIONAL SOLUTIONS TO SSR PROBLEMS

Thefollowing solutions have been used to help reduce impacts of SSR on power systems and generating units:

**Static filter:**

A static filter with specified bandwidth is suitable for known SSR modes in a power system [66-67]. The configuration of a static filter can be either a L-C filter or a damping circuit. When placed at the generator side, the filter needs to be in series to block sub-synchronous currents to flow back to generator. Or the static filter can be placed in parallel with the FSC as a damping circuit.

**Dynamic filter:**

A dynamic filter is an active device with self-adaptability to different SSR modes [68-69]. The dynamic filter is placed in series with the generator and picks the rotor speed derivation as input to extract the frequency of the SSR event. When sub-synchronous component is detected, the dynamic filter can induce a sub-synchronous voltage in opposite direction to compensate the sub-synchronous voltage in the armature.

**Dynamic stabiliser:**

Dynamic stabiliser is achieved by thyristor controlled shunt reactors connected to the generator to regulate sub-synchronous oscillations [71-72]. Generally, a shunt reactor is placed at the low voltage winding of the generator to absorb the reactive power. With the regulation of thyristor modules, the thyristor-controlled shunt reactor can be extended for SSR mitigation. The input is the generator rotor speed derivation and the thyristor regulation can induce suitable waveforms circulating in the shunt circuit to damp the sub-synchronous oscillation.

**Protective relays:**

Protective relays are commonly used methods among SSR countermeasures [73-74]. A relay can detect SSR event in the network and send control signals to trigger other units like by-pass switches or circuit breakers. The detection of SSR event can be achieved by either sensing rotor speed or sensing the generator armature current flow.

**NGH scheme:**

In 1981, a configuration based on thyristor modules was proposed by N. G. Hingorani [55]. This configuration consists of a series capacitor in parallel with a resistor which is regulated by an anti-paralleled thyristor module. When sub-synchronous current flows through the series capacitor, the voltage across the capacitor is also impacted by the sub-synchronous distortion. By regulating thyristor gate pulses, the parallel circuit can provide additional damping to mitigate SSR event.

According to [31], the mitigation of SSR events in the GB power system is mainly achieved by installing filters and protective relays. However, there are some potential solutions based on FACTS technology that have been proposed by researchers. Some damping schemes are based on the controllability of power electronics, including Static Var Compensator (SVC) [56-58], Static Synchronous Compensator (STATCOM) [59-62] and TCSC [63].

In this thesis, the scope is limited to solutions with TCSC only.

## 2.7 SUMMARY

This chapter presents the background of series compensation technology and SSI phenomena. The review highlights the FSC and SSR.

FSC in modern power systems allows a cost-effective solution to bulk power transfer requirements though it has the drawback of bringing in potential SSR risks. The design of a FSC requires system analysis over the power flow and the voltage distribution. In industrial projects, a typical FSC is installed along with a damping circuit and MOV arresters for protection. The design of FSC ratings is usually determined higher than the system rating to face transient high current flow and emergencies.

The term SSI is an overall definition including all interactions that occur within sub-synchronous frequency ranges. The classification of SSI is generally divided into three categories: SSR, SSCI and SSTI. This classification is based on the devices that are involved in the interaction. However, with the development of power systems and the integration of more controllable power electronics devices, new type of interaction also occurs. A new type of SSI happened between the HVDC converter control system and a weak AC grid in China. So far there is no definition about this type of SSI.

SSR events have been observed in 1970 and studied since that. SSR is caused by the interaction between the turbine shaft natural torsional modes and the electrical resonant component induced by the series R-L-C circuit. There are several study tools to study SSR events, including frequency scanning, eigenvalue analysis, and complex torque coefficient. In industrial projects, some countermeasures to SSR have been applied, but the low adaptability to new system conditions and difficulties in modifications limit their applications. Therefore, the current focus is on the mitigation of SSR with FACTS devices.

# Chapter 3

# Principles of Thyristor Controlled Series Capacitor

TCSC is an advanced series compensator and is considered a solution to SSR problems. As one of the members of Flexible AC Transmission System (FACTS) family, TCSC has been used in modern power systems as a reinforcement.

In this chapter, a brief introduction about the development of FACTS devices is given. The basic principles of TCSC and installed TCSC projects along with applications are presented.

## 3.1 DEVELOPMENT OF FACTS DEVICES

Developments of FACTS devices have been moving rapidly during the past decades. In HVAC systems, the main objective is to transfer power flow with the highest security. However, with passive components, this task can be challenging since system operators have a limited controllability over the impedance of power systems when failures or problems occur. FACTS devices are proposed to allow a better control over the power system in many key parameters, i.e. the system impedance or the terminal voltage.

FACTS devices are based on power electronics technology which allows a very fast response to system dynamics [75]. This fills the gap between different system control levels and allow a much higher controllability for operators to smoothly operate the system.

A variety of FACTS devices have been proposed to contribute to a flexible control of system parameters. In the conventional power flow control, methods are limited to

the generator side, the transmission line compensator switching and voltage regulations [76]. The fixed characteristics of the apparatus result in fixed power angles which limit the stability of the whole power system. But with FACTS devices, the smooth controllability allows a continuous variation in the system impedance and the power angle, which is reflected by a higher stability in the power transfer.

The success of power electronics applications in power systems has promoted the development of a production of more cost-effective devices with the capability to withstand high voltage and current along with a fast response time. Among them, some most widely used devices are listed here.

**Static VAr Compensator (SVC):** A shunt-connected device capable of providing or consuming the reactive power. It can be used in the voltage control, the reactive power compensation, the low-frequency oscillation damping and the stability improvement.

**Static Synchronous Series Compensator (SSSC):** SSSC is a voltage source inverter connected in series with the transmission line via a coupling transformer. It allows flexible control over the system impedance by regulating the voltage and current phase angles. Therefore, SSSC can be used to control the energy storage system and to control the power flow and the system stability.

**Unified Power Flow Controller (UPFC)**: UPFC is capable of controlling power flow between parallel corridors, improving the system transient stability and mitigating system oscillations. A typical UPFC configuration consists of an excitation transformer, a boosting transformer and two voltage source converters.

**Static Synchronous Compensator (STATCOM):** STATCOM is similar to SVC but it provides a faster response in the reactive power control to voltage variations.

**Thyristor-Controlled Series Compensator (TCSC):** This is a series connected device aiming to provide a flexible control over the system impedance. It consists of a series capacitor bank in parallel with a Thyristor-Controlled Reactor (TCR). TCSC is majorly used for the power flow control and boosting, the stability improvement and the SSR mitigation. In this thesis, the scope is limited to TCSC only.

## 3.2 THYRISTOR-CONTROLLED SERIES CAPACITOR

TCSC is an advanced series compensation technique with all benefits provided by Fixed Series Capacitor (FSC) but is also capable of controlling the inserted impedance, primary in a capacitive mode. The main objective of using TCSC is to improve the power transfer capability but there are other benefits[77-80]:

- Improving the system stability

- Mitigating SSR problems

In AC power systems, the power transfer capability is determined by the terminal voltage magnitudes at sending and receiving nodes, their phase angle difference, and the overall impedance between the two ends.

Conventional solutions to reduce the overall impedance include building extra transmission lines in parallel and inserting series capacitors which are controlled by mechanical switches. Building extra lines is not a cost-effective method since it requires a large amount of investment and may cause large impacts on the environment nearby. This solution is not adopted by most system operators around the world. Putting FSC is a common solution since series capacitors can compensate the voltage drop caused by the line inductance and increase the power transfer capability by reducing the overall inductive impedance of the system.

In the past decades, FSC controlled by mechanical switches has been used; however, there are several limitations [77]:

- Lack of an effective controllability at high compensation levels

- Lack of a smooth controllability in variations of the compensation levels

- Re-inserting capacitors can cause a voltage offset across capacitors

- Low damping performance within sub-synchronous frequency ranges can cause SSR

Compared with FSC, TCSC provides a more reliable performance in solving above limitations, and this has been proved in practical projects around the world. The configurations of a TCSC compensated system is shown in Fig. 3.1.

The configuration of a TCSC device is similar to a FSC device, except for the Thyristor-Controlled Reactor (TCR) denoted as $L_{TCR}$. $L_1$ and $L_2$ are two parts of a transmission line. $C_{TCSC}$ is the physical capacitor of TCSC which determines the minimum capacitance of TCSC. A Metal Oxide Varistor (MOV) is used to protect TCSC from over voltage conditions, and the By-pass switch allows disconnecting TCSC from the network under fault conditions. A damping circuit is designed to safely discharge the energy stored in capacitors with a spark-gap which triggers when the discharging current is high.
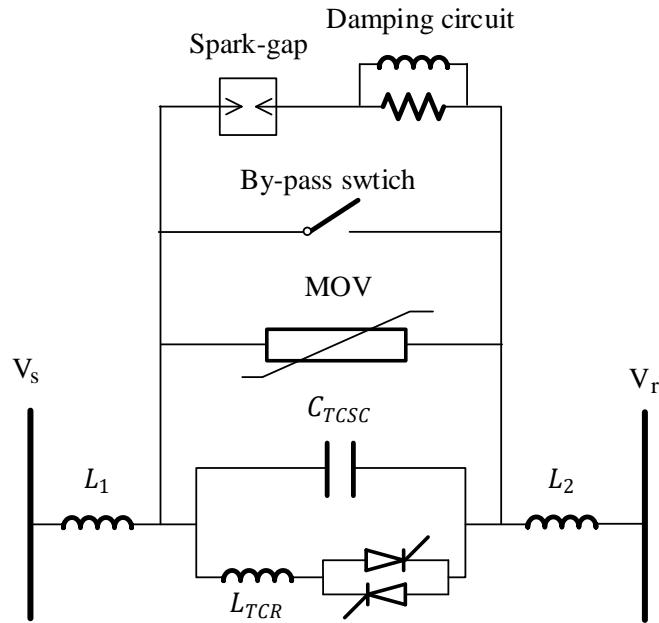
Fig. 3.1 A typical configuration of series compensated systems with TCSC

## 3.3 PRINCIPLES OF TCSC OPERATIONS

### 3.3.1 TCSC control

The controllability of TCSC is enabled by thyristor modules. Firing instants of thyristors are defined by the variable, firing angle α. This α is operated between 90° and 180° for the forward thyristor, with reference to the positive-going zero-crossing points of the capacitor voltage. In this way, thyristor conducting instants are synchronised with the capacitor voltage zero-crossing points. Fig. 3.2 shows the typical components of interests in a TCSC [82]. Terms $i_L$ and $i_{line}$ are the TCR current and the line current respectively, while $i_C$ and $u_C$ is the capacitor current and voltage. $T_1$ and $T_2$ are the gate signals to the positive and negative thyristors respectively.
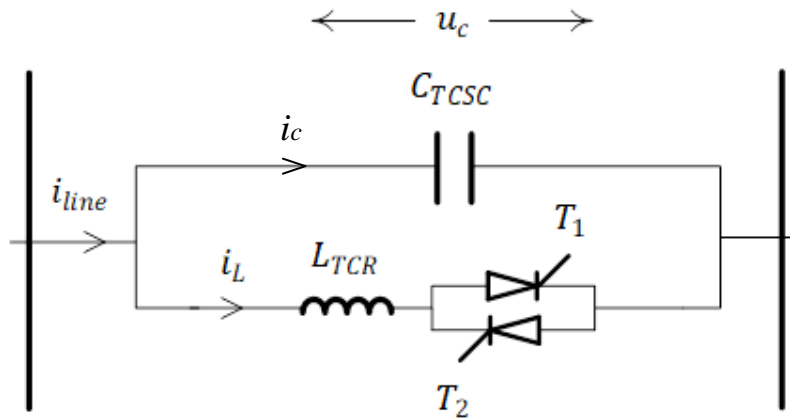
Fig. 3.2 A simplified configuration of TCSC [84]
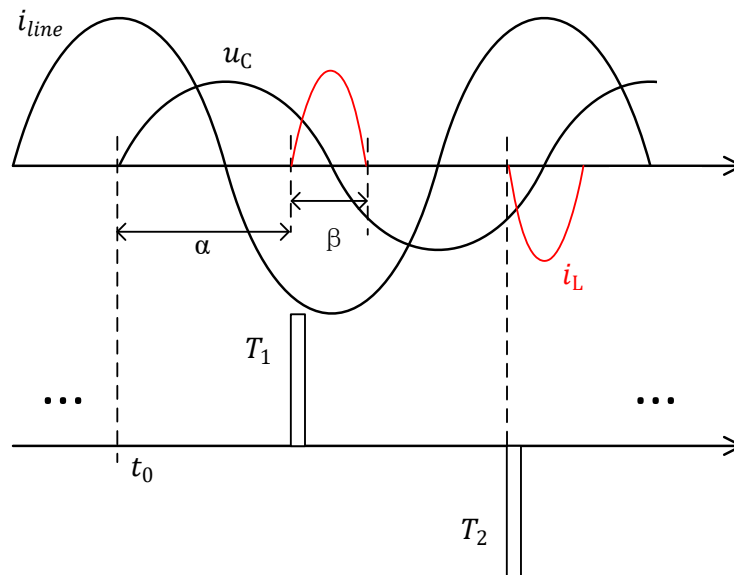


Fig. 3.3 Typical waveforms in TCSC

When a TCSC device is fired under steady state conditions, the typical waveforms of its TCR current ($i_L$), the capacitor voltage ($u_C$) and the line current ($i_{line}$) , and the relationship between $\alpha$ and $u_C$ are shown in Fig. 3.3. Once the thyristor is conducting, the current is generated by the capacitor voltage and the thyristor turn-off time is determined at the instant when the current drops to zero. The period of the thyristor conduction is denoted as $\beta$, in degrees. Assume the resistance of TCSC is neglected,

the relationship between the firing angle $\alpha$ and the conduction angle $\beta$ can be derived as:

$$\alpha = \pi - \frac{\beta}{2} \qquad (3.1)$$

When thyristors are on, the current begins to circulate within the parallel circuit of TCSC and provokes the capacitor voltage with a boost. This results in the capacitor current to be boosted with small humps, as shown in Fig. 3.4. This circulating current usually results in a higher peak current flow in the capacitor. Therefore, the design of TCSC capacitor requires case studies and a higher current rating than the system current rating.
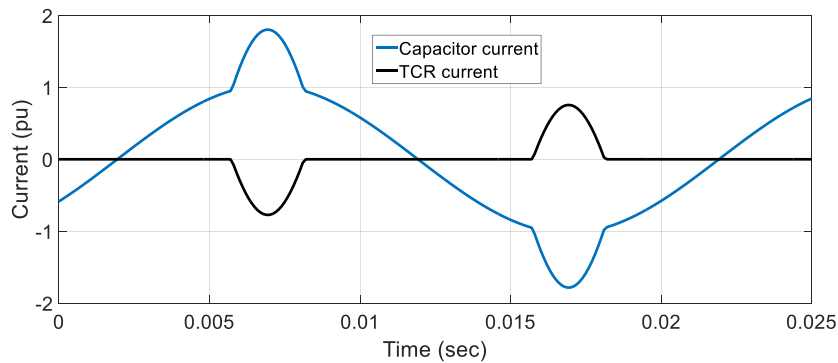


Fig. 3.4 Typical waveforms of TCR current and the capacitor current in TCSC

### 3.3.2 Operational modes of TCSC

TCSC is usually operated in three different modes, aiming for different objectives: the thyristor-blocked mode, the thyristor-bypassed mode and the Vernier mode [81]. The corresponding firing angles for these modes are 180°, 90°, and between 90° to 180°. TCSC is supposed to work within 90° to 180° and shall not go beyond this range.

**The thyristor blocked mode:** In this mode, thyristors are fully blocked and no current is flowing through the TCR branch. This can be achieved by either sending no triggering signals or setting the firing angle to 180°. In this case TCSC is just a series capacitor and all conditions for FSC apply. Fig. 3.5 shows directions of current flows in this mode.
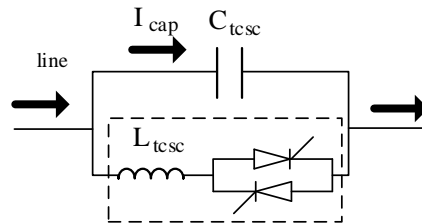


Fig. 3.5 TCSC current flows in the thyristor blocked mode [81]

**The thyristor bypassed mode:** This mode occurs when the firing angle is set to 90° and thyristors are fully conducted. In this case, TCSC becomes a parallel L-C circuit, and the overall impedance of TCSC becomes inductive. Fig. 3.6 shows the current flows within TCSC in this mode.
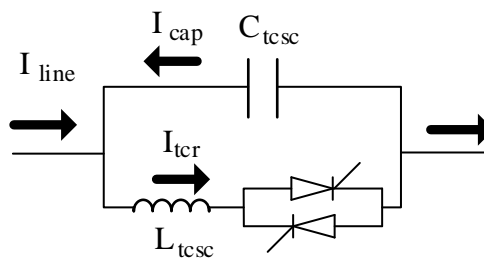


Fig. 3.6 TCSC current flows in the thyristor bypassed mode [81]

**The Vernier mode:** Vernier mode refers to the condition where discrete current flow within the TCR branch and it happens when the firing angle is between 90° to 180°. Due to the regulation of thyristors in the current flow through the TCR branch, the RMS value of the TCR current can vary thus making the equivalent impedance of

41

TCR changing from the base value of the TCR inductance to infinite. Depending on the design of TCSC parameters, usually two vernier regions exist based on whether TCSC apparent impedance is inductive or capacitive. Fig. 3.7 shows the current flow in either modes respectively.



(a)



(b)
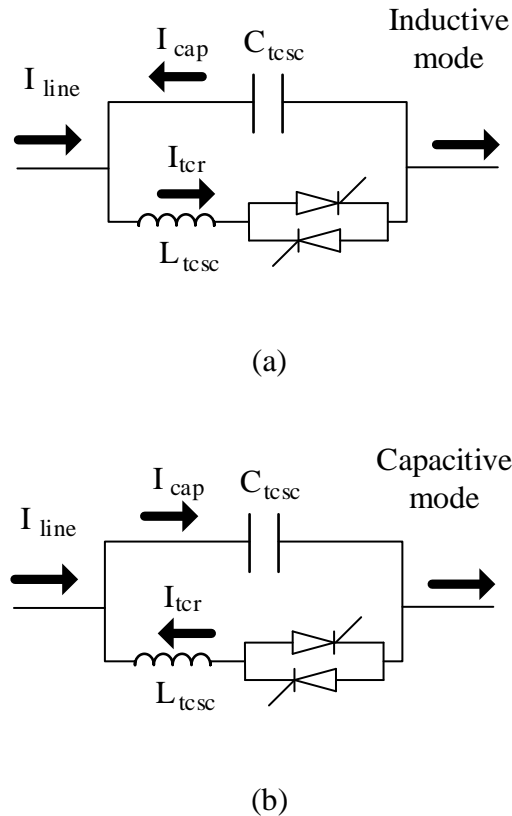
Fig. 3.7 TCSC current flows in two Vernier modes (a) inductive mode, (b) capacitive mode [81]

### 3.3.3  Mathematical models of TCSC

Unlike FSC, TCSC has a very complex characteristic. The non-linearity due to thyristors triggering makes it difficult to derive a mathematical representation suitable for all frequency bands. Therefore, the commonly used model of TCSC is based on its dynamics at the synchronous frequency, and the apparent impedance of TCSC at the synchronous frequency can be derived [82]:

$$X_{\text{TCSC}}(\alpha) = -X_C + C_1\big(2(\pi - \alpha) + \sin(2(\pi - \alpha))\big)$$

$$-C\_2 \cos{}^\wedge 2 \, (\pi - \alpha)(\omega \tan(\omega(\pi - \alpha)) - \tan(\pi - \alpha)) \qquad (3.2)$$

where

$$C_1 = \frac{X_C + X_{LC}}{\pi} \qquad\qquad (3.3)$$

$$C_2 = 4\frac{X_{LC}^2}{X_L \pi} \qquad\qquad (3.4)$$

$$X_{LC} = \frac{X_C X_L}{X_C - X_L} \qquad\qquad (3.5)$$

$$\omega = \sqrt{\frac{X_C}{X_L}} \qquad\qquad (3.6)$$

and $L$ and $C$ are the inductance and the capacitance of TCSC.

According to (3.2), TCSC impedance against firing angle characteristic can be plotted.
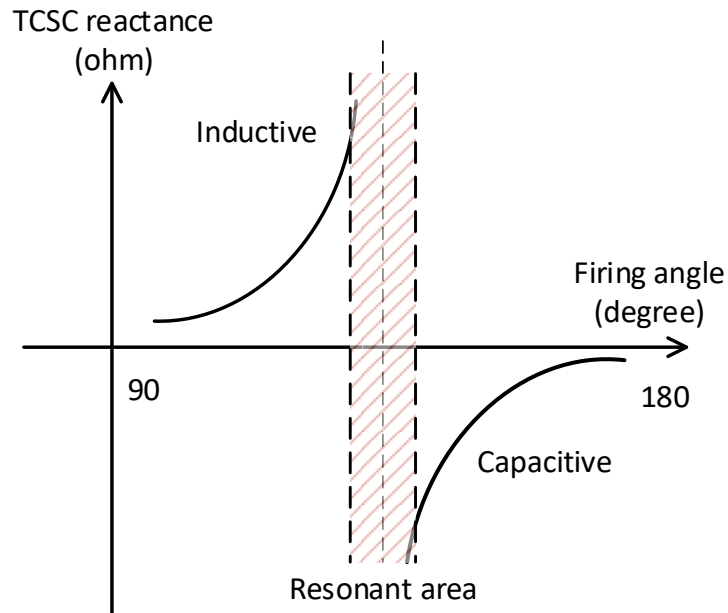


Fig. 3.8 TCSC impedance-firing angle characteristic

Fig. 3.8 shows a typical TCSC impedance-firing angle characteristic. When the firing angle is synchronised with the capacitor voltage, its operational range varies within 90° to 180°, and the limits represent the fully conducted mode and the fully blocked mode respectively. When the firing angle approaches to the middle of the range, as indicated as the resonant area in Fig. 3.8, the TCSC impedance control becomes more sensitive to changes in firing angles and the boost factor is moving to a higher level. A boost factor is the ratio between the effective impedance of TCSC and the base capacitor impedance of TCSC. In this case, even small distortions may lead to a large variation in the TCSC impedance and the system can become unstable. Therefore, there are limitations for the TCSC operational range and the boost factor, which determines TCSC effective impedance over its base impedance, i.e. boost factor < 3. Additionally, in practical projects, TCSC under high boost factors can only be operated for a short term, i.e. <10 mins.

## 3.4 THE SELECTION OF TCSC PARAMETERS TO AVOID DUAL-RESONANCE

The selection of the base capacitance in the design of TCSC project is based on the system requirement. The base capacitance determines the compensation TCSC can provide when TCSC is operated at the thyristor-blocked mode. Based on the transmission system line impedance and the expectation for future power demands, the capacitor of TCSC is chosen at a reasonable level. However, the selection of TCR inductance can be varied to adjust the performance of TCSC according to system requirements, i.e. a larger capacitive operational range [83, 84].

A factor, defined as $\omega$ in (3.6), is used to determine the ratio between the TCSC base capacitance and the TCR inductance. From (3.2), it indicates that the factor $\omega$

44

affects the characteristic of TCSC. Normally, as indicated in Fig. 3.8, TCSC has two operational regions, the inductive region and the capacitive region. The effective impedance of the TCSC varies with firing angles smoothly in the two regions. However, there is a resonant region between the inductive region and the capacitive region where TCSC effective impedance approaches to infinity. Therefore, the relationship between the firing angle and TCSC operational regions can be summarised in Table 3. 1.

Table 3. 1 indicates that $\alpha_{Llim}$ and $\alpha_{Clim}$ determine the ranges of different regions. Here $\alpha_{Llim}$ and $\alpha_{Clim}$ are the higher and lower limits for the inductive region and the capacitive region respectively. The determination of $\alpha_{Llim}$ and $\alpha_{Clim}$ is only affected by the factor ω.

Table 3.1 The relationship between TCSC operational regions and firing angles

| Range of firing angles | Operational region |
| --- | --- |
| $90° \leq \alpha \leq \alpha_{Llim}$ | Inductive |
| $\alpha_{Llim} \leq \alpha \leq \alpha_{Clim}$ | Resonant |
| $\alpha_{Clim} \leq \alpha \leq 180°$ | Capacitive |

An example is given considering the TCSC base capacitance, $X_C$, to be 1 pu. By varying ω, the TCSC impedance vs. firing angle characteristics are obtained with Matlab plots, as shown in Fig. 3.9.
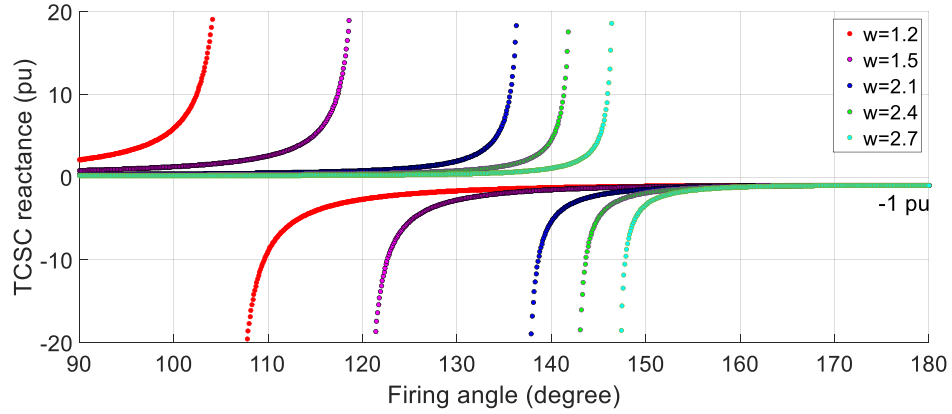
Fig. 3.9 The TCSC impedance against firing angle characteristics with different factor **ω** values

From Fig. 3.9, it can be concluded that TCSC operational regions are affected by the factor ω. When ω is varied between 1<ω<3, the range of the capacitive region is increased with a smaller ω value, while the inductive region is narrowed.

However, if ω lies beyond the range 1< ω<3, the characteristic is changed. When ω equals to 1, the configuration becomes a parallel resonant circuit, which must be avoided. And if ω drops below 1, the effective impedance of the TCR, denoted as $X_{TCR,eff}$, is always larger than the capacitor impedance $X_C$. The effective impedance of TCSC is always capacitive as

$$X_{TCSC,eff} = -\frac{X_{TCR,eff}*X_C}{X_{TCR,eff}-X_C} < 0 \tag{3.7}$$

Fig. 3.10 shows the TCSC impedance vs. firing angle characteristic when the factor ω is selected to be 0.7. It indicates that TCSC can only be operated under the capacitive mode in this case. There is no resonant area in this case. When the firing angle is at 180°, thyristors are fully blocked and TCSC provides the minimum compensation level.
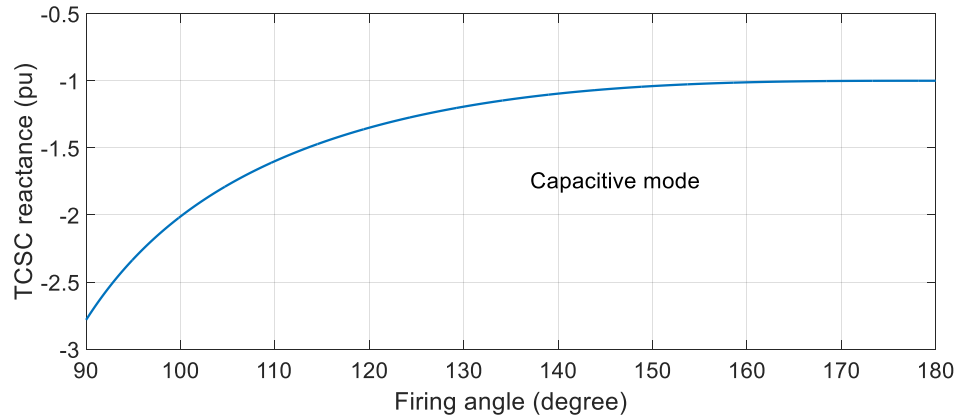
Fig. 3.10 The TCSC impedance characteristic plot when **ω** is smaller than 1

If ω further increases to be higher than 3, a situation occurs as the multi-resonance. Fig. 3.11 shows an example of the TCSC impedance characteristic with ω set to 3.3.
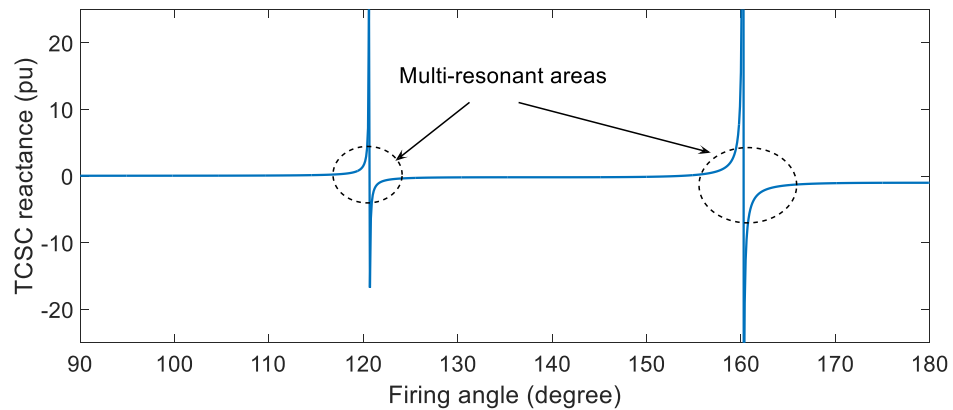


Fig. 3.11 The TCSC impedance characteristic with **ω** higher than 3

From Fig. 3.11, within the operational range of TCSC, between 90° and 180°, there are two resonant areas. This reduces the span of the TCSC operation in either the inductive mode or the capacitive mode.

The flexible operational modes and the smooth controllability are the main benefits of TCSC. To utilise these benefits, a reasonable selection of the factor ω is advised between 2.3 and 2.8 [85, 86].

### 3.5 APPLICATIONS OF TCSC IN POWER SYSTEMS

## 3.5.1 Installed TCSC projects

There have been 10 TCSC projects commissioned in the world, located in the US, Sweden, China, India and Brazil. The latest TCSC project was commissioned in the GB power system by the National Grid in 2014. These TCSC projects are installed to meet different system contingencies including the transient stability, power oscillations, and SSR, etc.

**The Kayenta TCSC project:** The first TCSC project in the world is the Kayenta TCSC project in 1990, referred to as the Advanced Series Capacitor before.

The Kayenta TCSC device is placed on a 230 kV transmission line of 320 km between Shiprock to Glen Canyon [87]. The compensation is provided by two capacitor modules of 55 ohms each. One of the capacitor module is split into two segments of 40 ohms and 15 ohms. A TCR is placed in parallel with the 15 ohms capacitor to form TCSC and to control the effective impedance. The main objective of the Kayenta TCSC project is to improve the power transfer capability from 300 MW to 400 MW.

**The Slatt TCSC project**: The second TCSC project is at Slatt substation on a 500 kV transmission line in 1995 in the US.

The Slatt TCSC device is split into six separate TCSC modules with individual by-pass switches. Each TCSC module can provide a continuous capacitive impedance between 4 $\Omega$ to 8 $\Omega$ and can be independently controlled from other modules. This configuration of TCSC allows more control over the system impedance since each

TCSC sub-module is independent from other modules, but it also increases the investment cost due to more components [88].

**The Stode TCSC project:** This TCSC project commissioned in 1997 in Sweden is to reinforce the 400 kV transmission system connecting the hydro and nuclear power generation in the north and the load centre in the south. The initial plan was to install FSC to provide a compensation level of 70%, but the system was found affected by SSR [89]. To mitigate SSR problems, the compensation is re-designed with FSC providing 49% compensation level while TCSC providing 21% compensation level.

**The Imperatriz TCSC project and The Serra da Mesa TCSC project:** The two TCSC projects were commissioned in 1999 to reinforce the North-South interconnection line in Brazil [90].

The transmission line is around 1020 km long working at 500 kV, provided with a total compensation level of 66%. A hybrid compensation scheme with both FSC and TCSC are used, where FSC contributes 54% and TCSC contributes 12%. The installation of these compensation allows the power transfer capability to be boosted to 1300 MW. The main purpose of TCSC installation is to damp low-frequency oscillations in the system [91-92].

**TCSC projects in India**: There have been three TCSC projects in India, the Kanpur - Ballabhgarh TCSC project, the Rourkela – Raipur TCSC project and the Purnea-Gorakhpur TCSC Project.

The Kanpur - Ballabhgarh TCSC project is the first TCSC project in India on a 400 kV, 400 km transmission line. TCSC is used in combination with FSC to provide a total of 55% compensation, of which 20% is provided by TCSC [93, 94].

The Rourkela – Raipur TCSC project [95] is completed in 2004, providing a maximum compensation level of 10% to a 400 kV system. The min purpose of the TCSC project is to improve the power transfer.

The Purnea-Gorakhpur TCSC Project [96] is completed in 2012 as the largest TCSC project in the world. The rating of the TCSC device is 1.7 GVAr to improve the power transfer capability from 9.5 GW to 30 GW to power the northern industrial region.

**TCSC projects in China:** The first TCSC project in China is commissioned in 2000 [97-98] at Fengtun site. The 500 kV transmission line is boosted from 1.6 GW to 2 GW. The installation of TCSC is to avoid building an extra line in parallel [99].

Another Chinese TCSC project is at Pingguo substation in southern China to improve the system transient stability and to solve SSR. The overall compensation level is 40%, of which 35% is provided by FSC and 5% is provided by TCSC [100].

**The Hutton TCSC project:** The latest TCSC project in the world is commissioned in late 2014 at Hutton substation in the GB power system [101]. This project is to help meet the 2020 target in the UK as reinforcements to the Anglo-Scottish circuit. Studies indicates that the power capacity is boosted by 33% from 3.3 GW to 4.4 GW [102].

The Hutton TCSC project reinforces the main 400 kV corridor that interconnects the wind generations in Scotland and the load centre in England. TCSC is used to provide 35% compensation level. Passive filter technology is chosen to prevent the production of SSR [103]. Case studies in [103] indicates that TCSC could improve the system transient stability and damp SSR.

### 3.5.2 Applications of TCSC

Applications of TCSC are enabled by the various control strategies in response to different system problems, including the power oscillation damping, the power system transient stability, the coordination with other controllers and the SSR damping [116].

**The Power oscillation damping (POD)** is a feature of TCSC to solve the power oscillation problems in large power systems. With a longer transmission distance and a higher power transfer, the inter-area oscillation is an inherent problem which can lead to instability.

To solve this problem, researchers proposed different methods to optimise the performance and parameters of the POD controller, including the $H_\infty$ optimisation technique [104-107], the pole placement technique [108-110], and the Linear-Quadratic Regulator (LQR) technique [111-112]. Some work was conducted to investigate the optimised location of TCSC device based on economic considerations and utilisation of device efficiency [40]. There have been different methods to find out the optimised location including the sensitivity index based technique and the linear programming technique [115].

**The transient stability** is caused by major system disturbances including circuit breaker operations and relay system operations. Some papers presented the risk analysis on transient instability in power system [117-118].

Authors in [119-120] mainly discussed the improvements in system transient stability with installations of TCSC without designing extra controllers. The effectiveness was studied in different system topologies and different system conditions. Results indicated that the system transient stability can be improved by an optimised placement of TCSC.

Additionally, some control algorithms for TCSC to improve the transient stability were proposed in [121-122].

**The coordinated control** was discussed in [123-126] to avoid adverse interactions among TCSC and other FACTS devices control systems. In [123-124] coordinated control schemes for TCSC and SVC to improve the system transient stability were proposed. In [125-126] coordinated controllers were designed to damp inter-area oscillations with FACTS devices and HVDC links.

**The SSR damping** was studied with TCSC from the frequency response [127] and the active damping controller [128]. The study on TCSC's frequency response was conducted based on the impedance model of TCSC [129-130]. Results indicate that TCSC possesses a different characteristic from FSC and this characteristic improves the SSR damping.

The SSR damping controller is a supplementary scheme for TCSC to mitigate SSR. In [131] the author stated that even though TCSC is found capable of damping SSR, a supplementary SSR damping controller is required to secure SSR mitigation. The design of the SSR damping controller was proposed based on the observed-state feedback method [132-133], the root-locus design method [131] and the electrical damping method [134-136].

## 3.6 SUMMARY

In this chapter, the development of FACTS technology is briefly presented, and some members of FACTS family are introduced. The review highlights the TCSC.

The industrial configuration of TCSC has been described and functions of relevant components are discussed. The basic control of TCSC has been demonstrated in details, including the synchronisation of the gate signals with the capacitor voltage, and

different operational modes of TCSC. The selection of TCSC parameters is also discussed. The determination of the base capacitance is based on the system requirements in future power transfer capability and compensation level, while the inductance of the TCR can affect the impedance characteristic of TCSC. The study with a factor $\omega$, which defines the relationship between the base capacitor impedance and the TCR impedance, shows that the factor $\omega$ with different values can vary the operational range of TCSC. A reasonable range of $\omega$ is between 2.3 and 2.8. Otherwise the operational range of firing angle is narrowed and multi resonant areas may occur.

Existing TCSC projects around the world are discussed along with their key ratings. The application of TCSC is majorly for power transfer boosts but TCSC is also regarded as a solution to system stability problems. Some research on the system transient stability, the power oscillation damping, the coordinated control and the SSR damping are summarised.

# Chapter 4

# Inherent characteristic of TCSC in SSR mitigation

## 4.1 INTRODUCTION

TCSC has been suggested to have better performance than FSC in terms of SSR issues [137-139]. Lots of research have been conducted on SSR mitigation with TCSC controllability [132, 133, 140] and TCSC frequency response [141-142]. These results indicate that TCSC can improve the modal damping within sub-synchronous frequency ranges with the regulation of thyristors. Researches in [135, 142] on TCSC's impedance imply that TCSC could behave inductively within sub-synchronous frequency ranges which can break the conditions of SSR. Some studies also indicate that TCSC behaves negative resistive at synchronous frequency [143, 144], but there is no further investigation into this phenomenon.

In this chapter, the contribution of TCSC in improving SSR damping is explained with the power conversion ability of TCSC. The negative-resistive performance of TCSC is studied and explained with the power conversion ability of TCSC. Various case studies are conducted to investigate the effectiveness of the power conversion ability in improving SSR damping and how TCSC parameters are affecting this ability.

## 4.2 SSR DAMPING VIA POWER CONVERSION OF TCSC

TCSC's controllability is due to the regulation of the anti-paralleled thyristor banks, which is controlled based on the synchronisation with the TCSC capacitor voltage or line current. However, when sub-synchronous components occur in the system and flow through TCSC, thyristors force-regulate these sub-synchronous components and

affect their waveforms, thus changing the energy carried by these sub-synchronous components. In this section, this phenomenon is investigated.

### 4.2.1 Dynamics of TCSC with sub-synchronous injection

The control system of TCSC is based on the synchronisation with the fundamental component of the TCSC capacitor voltage or the line current. The synchronisation is achieved using Phase Lock Loop (PLL) to track the phasor information and eliminate sub-synchronous or super-synchronous harmonics. There have been a lot of research on how to improve the performance of PLL [64, 65, 145].

In a steady state, the capacitor voltage of TCSC is symmetrical to its zero-crossing points if there is no harmonic distorting the system. However, with sub-synchronous components in the capacitor voltage, the zero-crossing instants of the capacitor voltage are varied. Fig. 4.1 shows the waveforms of the capacitor voltage with and without distortions from sub-synchronous components. In this case, if the control system of TCSC is still based on a constant firing angle control, the induced TCR current becomes unsymmetrical and imbalanced.

Fig. 4.1 (a) shows the ideal capacitor voltage and TCR current waveforms without distortions. The zero-crossing points of the capacitor voltage occur every 0.05s based on a 50 Hz system. Fig. 4.1 (b) shows the impact of distortions from a sub-synchronous component. Compared with Fig. 4.1 (a), the first zero-crossing point of the capacitor voltage in Fig. 4.1 (b) is delayed. Since the firing instants of thyristors are kept the same, the larger instantaneous capacitor voltage results in a larger TCR current, which in turn accelerates the discharging and charging procedures of the capacitor voltage. In this way, thyristors try to regulate the sub-synchronous component and bring the zero-crossing point of the capacitor voltage back to the correct instant.

Similarly, the second zero-crossing point of the capacitor voltage in Fig. 4.1 (b) occurs slightly earlier than expected. In this case, the induced TCR current is also reduced and thus the discharging rate of the capacitor voltage is slowed, which indicates that TCSC is trying to delay the zero-crossing of the capacitor voltage back to its synchronised position.
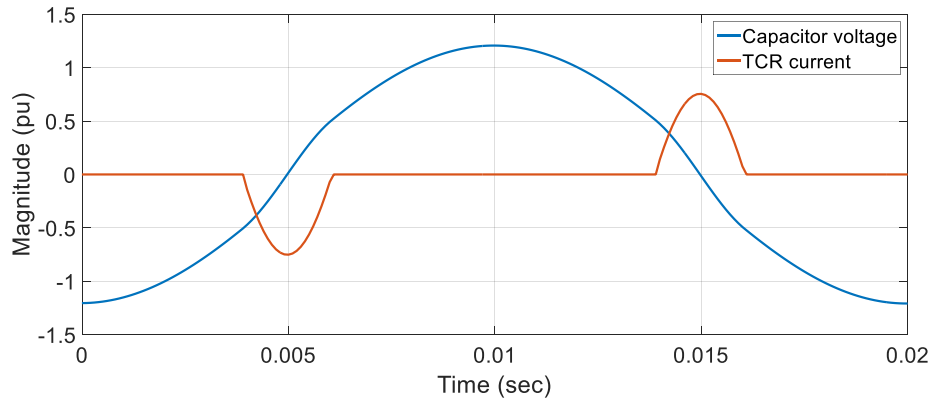


(a) Capacitor voltage and TCR current waveforms without sub-synchronous distortions
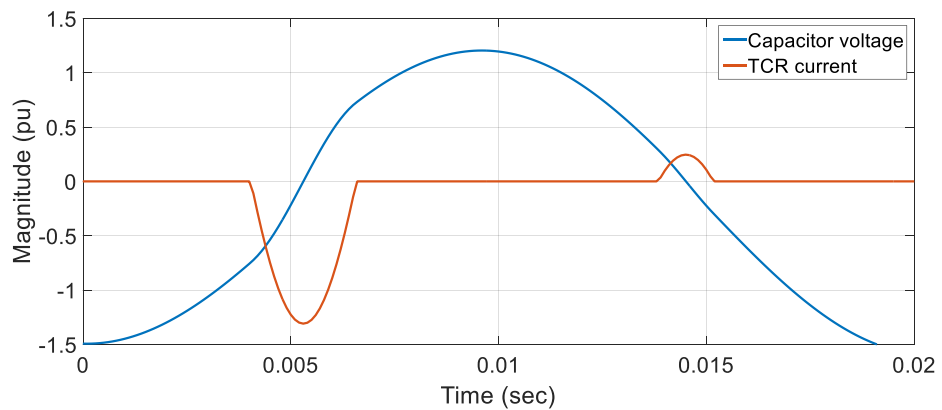


(b) Capacitor voltage and TCR current waveforms with sub-synchronous distortions

Fig. 4.1 Changes in capacitor zero-crossing points affected by sub-synchronous components

As shown in Fig. 4.1 (b), the first zero-crossing point of the distorted waveform is slightly delayed from expected point. If left unattended, the next zero-crossing point

shall be further delayed. However, due to control of thyristors, the second zero-crossing point arrives slightly earlier. This example indicates that TCSC has the ability to bring the capacitor voltage's zero-crossing points back to the synchronous frequency, though sub-synchronous components are not fully eliminated, as can be seen in Fig. 4.1 (b) that the capacitor voltage waveform is still distorted. It should be noted that this ability is not obtained from a closed-loop control scheme but is inherited from the basic operation of TCSC.

### 4.2.2 The resistive behaviour of TCSC

TCSC's characteristic within sub-synchronous frequency ranges has drawn lots of attentions from researchers. The inductive or capacitive sub-synchronous behaviour is modelled and investigated [132-133], and results indicate that TCSC working under high compensation levels can behave inductive within sub-synchronous frequency ranges. Then the circuit becomes inductive and the condition that SSR occurs is broken. Moreover, TCSC is also found to perform negative resistive at the synchronous frequency [140-142]. In this section, the resistive behaviour of TCSC is investigated.

A method to study the resistive behaviour has been proposed in [140], as shown in Fig. 4.2. TCSC is powered by an ideal voltage source at the synchronous frequency and the control of thyristors is based on the synchronous capacitor voltage only. The impact of sub-synchronous components on the operation of TCSC is tested by injecting the sub-synchronous current at a small magnitude, i.e. 0.1 pu.
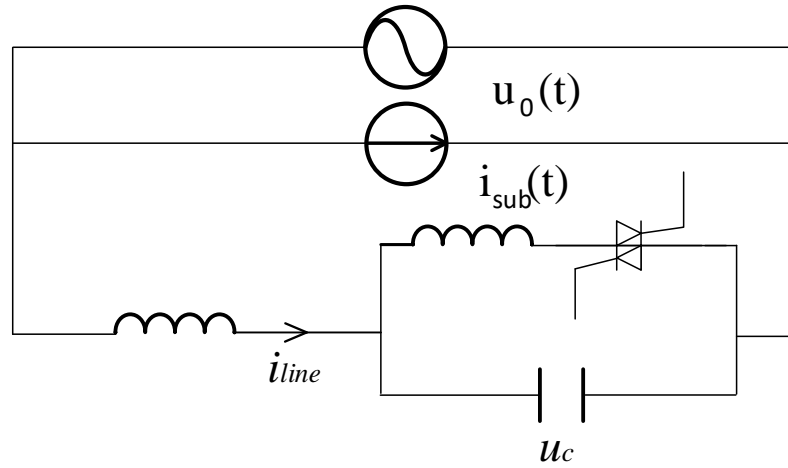
Fig. 4.2 The study of TCSC resistive behaviour with the current injection method

The reaction of TCSC to the injected sub-synchronous current is directly reflected in the capacitor voltage and the line current. Fig. 4.3 shows the procedure of deriving TCSC resistance and reactance at both the synchronous frequency and the sub-synchronous frequency. Fast Fourier Transform (FFT) is used on the capacitor voltage $u_c$ and the line current $i_{line}$, to extract the magnitude and the phase angle of fundamental components and sub-synchronous components. The resistance and the reactance at the synchronous frequency or the sub-synchronous frequency are calculated with corresponding signals in the format as follow:

$$X = \frac{V_m}{I_m} \sin\left(V_p - I_p\right) \tag{4.1}$$

$$R = \frac{V_m}{I_m} \cos\left(V_p - I_p\right) \tag{4.2}$$

where the subscripts 'm' and 'p' refer to the magnitude and the phase angle respectively, and the subscripts 'fun' and 'sub' indicate the fundamental frequency and the sub-synchronous frequency.
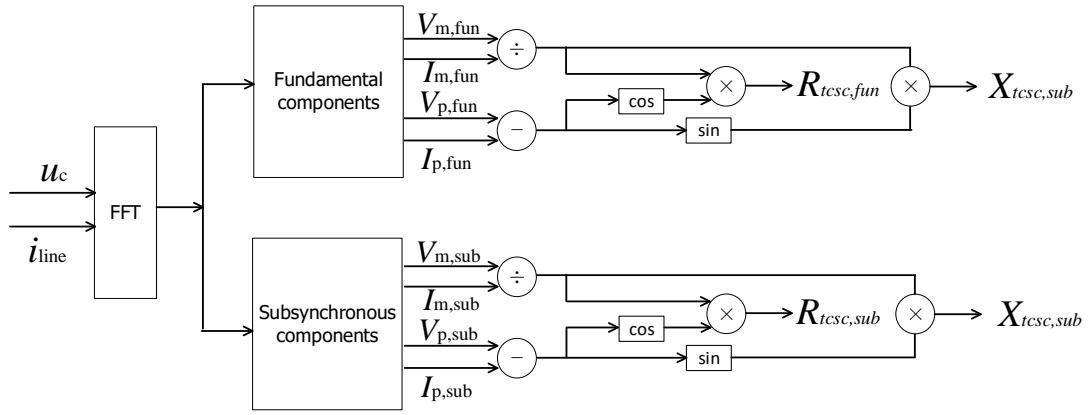
Fig. 4.3 Block diagram used to deduce TCSC impedance at the synchronous frequency and the sub-synchronous frequency

Table 4.1 Parameters of TCSC under test

| TCSC | | Compensation level after boosting (%) |
|---|---|---|
| Capacitance (uF) | Inductance (mH) | |
| 35uF | 40 mH | 46% |

Considering the test system configuration as shown in Fig. 4.2, and making TCSC parameters as shown in Table 4.1, a study on the resistance of TCSC is conducted to investigate the impacts of different firing angles, which is varied from 150° to 175°. The injected sub-synchronous current is maintained the same in both magnitudes and phases, but its frequency is varied at 17 Hz, 27 Hz and 37 Hz, to represent typical sub-synchronous harmonics. The calculated TCSC resistance within sub-synchronous frequencies are shown in below Fig. 4.4.
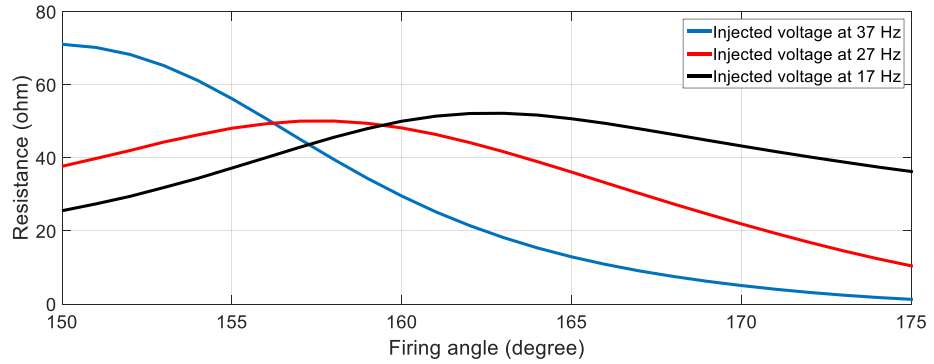
Fig. 4.4 TCSC resistance at 37 Hz, 27 Hz and 17 Hz with varying firing angles

Fig. 4.4 indicates the impacts of firing angle on TCSC resistive behaviours at sub-synchronous frequencies. It shows that the resistance of TCSC within sub-synchronous frequencies increase first with firing angle but then start to decrease after reaching a peak value. The occurrence of this peak value varies within the sub-synchronous frequency ranges. The trend shows that TCSC with a lower firing angle appears more resistive at higher sub-synchronous frequencies, while larger firing angle makes TCSC resistance decrease at the same frequency after reaching the peak point. When the firing angle is approaching to 180°, which means thyristors are fully blocked and TCSC is acting as FSC, the resistances at all sub-synchronous frequencies decreases to zero.
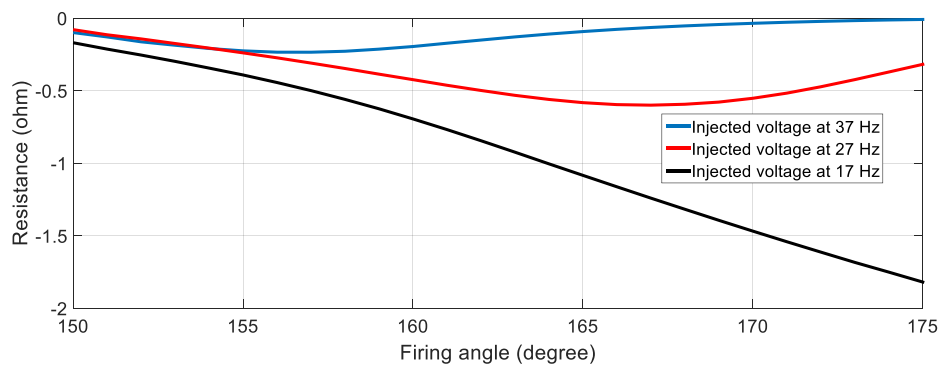


Fig. 4.5 TCSC resistance at the synchronous frequency with varying firing angles

Fig. 4.5 shows that the TCSC synchronous resistance varies with firing angles when injected sub-synchronous current is at 17 Hz, 27 Hz, or 37 Hz. It can be observed that the negative resistance at synchronous frequency is maintained throughout all firing angle ranges. However, when the firing angle is lower, TCSC's synchronous resistance has less response to changes in frequencies of injected voltages. If the firing angle increases, the synchronous resistance is greatly affected by the frequencies of injected current.

## 4.2.3 Relationship between the energy conversion and resistive behaviour of TCSC

In Section 4.2.2, results indicate that TCSC behaves resistively at sub-synchronous frequencies, and it also behaves as a negative resistance at the synchronous frequency. In an AC system, a resistor causes power losses determined as square of current multiplied by resistance. Similarly, a negative resistance at the synchronous frequency represents that energy is transformed and extracted to the synchronous frequency. Therefore, some numerical calculations are conducted upon power changes at both the sub-synchronous frequency and the synchronous frequency, to investigate the relationship between the resistive behaviours and power changes.

Considering the case study in Section 4.2.2, the injected sub-synchronous current is at 37 Hz. The line current is measured and analysed with FFT to obtain information of sub-synchronous components and synchronous components. Fig. 4.6 gives the frequency spectrum of the line current.
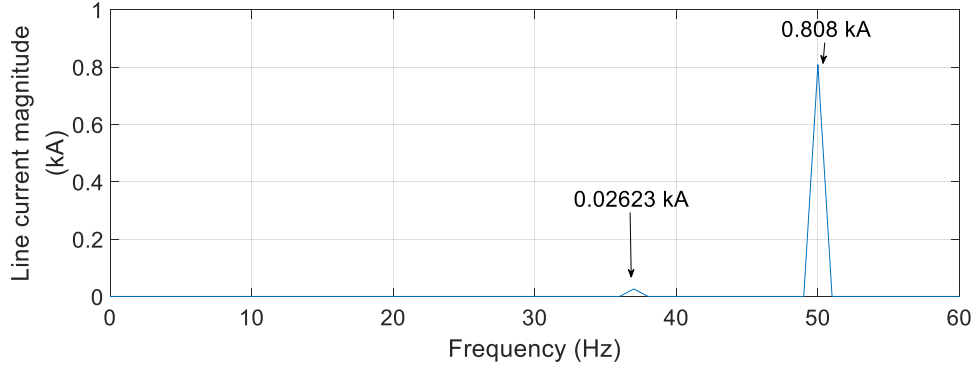
Fig. 4.6 Frequency spectrum of the line current when the injected component is at 37 Hz

With the extracted voltage and current magnitudes using FFT, and the calculated resistances at 37 Hz and 50 Hz, the power losses can be deduced respectively.

At 37 Hz, the current magnitude is 0.02623 kA, and the resistance is 133.4 Ω. Therefore, the power loss at 37 Hz is

$$P_{sub} = I_{sub}^2 \cdot R_{sub} = 0.02623^2 * 133.4 = 0.092 \text{ MW} \tag{4.3}$$

At 50 Hz, the current magnitude is 0.808 kA, while the resistance is -0.14 Ω. Then the power loss caused by the negative resistance is

$$P_{fund} = I_{fund}^2 \cdot R_{fund} = 0.808^2 * (-0.14) = -0.0914 \text{ MW} \tag{4.4}$$

Comparing $P_{sub}$ and $P_{fund}$, the difference between them is around 0.6%, which can be neglected. The positive power loss at 37 Hz is apparently transformed into a synchronous component and the negative power loss can be regarded as a result of injected power tranformed into synchronous power.

Similarly, another study based on case 1 is conducted with the injected sub-synchronous voltage being tuned to 17 Hz instead, while other parameters are kept the same. Fig. 4.7 is the frequency spectrum of the line current in this case.
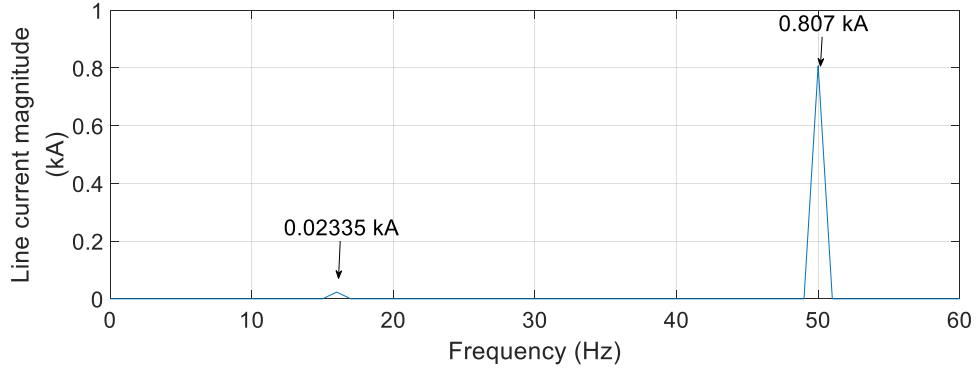
Fig. 4.7 The frequency spectrum of the line current when the injected component is at 17 Hz

At 17 Hz, the current magnitude is 0.02335 kA, and the resistance is 142.99 Ω. Therefore, the power loss at 17 Hz is

$$P_{sub} = I_{sub}^2 \cdot R_{sub} = 0.02335^2 * 142.99 = 0.078 \text{ MW} \tag{4.5}$$

While at 50 Hz, the current magnitude is 0.807 kA, and the resistance is -0.098 Ω. Then the power loss caused by the negative resistance is

$$P_{fund} = I_{fund}^2 \cdot R_{fund} = 0.807^2 * (-0.098) = -0.079 \text{ MW} \tag{4.6}$$

Therefore, it can be observed that the power loss at 17 Hz matches the negative power loss at 50 Hz with ignorable errors, which is around 1.3%.

The above two case studies indicate that TCSC's resistive behaviours at sub-synchronous frequencies are related to its negative resistive behaviour at the synchronous frequency. The positive and negative resistive behaviours are due to power conversions from sub-synchronous components to synchronous components. In this way, since sub-synchronous components are partially transformed into synchronous components, the interaction with these sub-synchronous components is expected to be weakened. Thus the severity of SSR can be reduced.

## 4.3 THE STUDY SYSTEM FOR TCSC'S CONTRIBUTION IN SSR MITIGATION

To investigate the SSR phenomena, an example system model is proposed by the Institute of Electrical and Electronics Engineers (IEEE) Working Group [64]. The FBM system is preferred than the GB three-machine system. The reason is that in both systems only one turbine generator is studied in detail. In the GB three-machine system, the other two grids are modelled as ideal voltage sources. Therefore, there is no actual difference between the FBM system and the GB three-machine system in SSR study. A detailed parameter list is given in Appendix I. Fig. 4.8 shows the system configuration with turbine-shaft which is represented by a multi-mass model. L and R are the transmission line inductance and resistance respectively. The variable capacitor, denoted as C, represents the inserted compensation, which can be either FSC or TCSC.
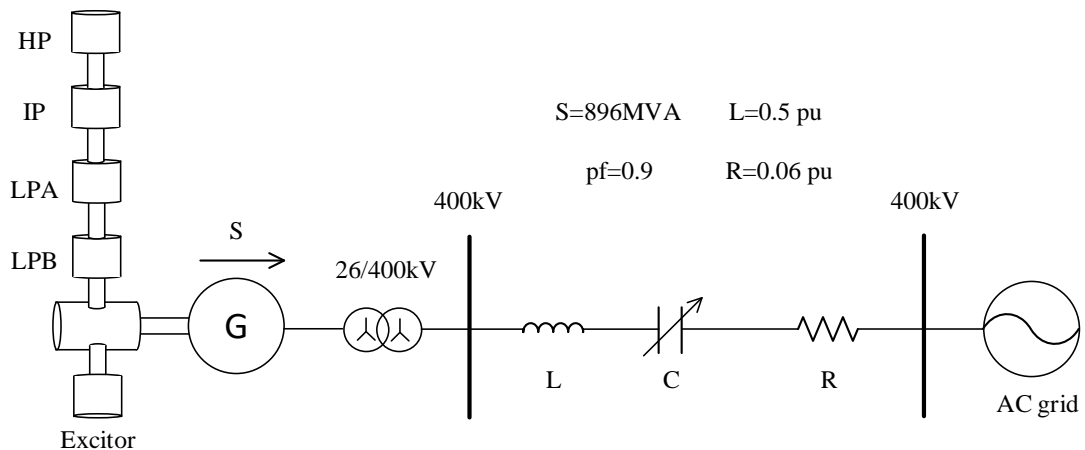


Fig. 4.8 The IEEE FBM system configuration with turbine shaft model and series compensation [64]

The FBM system is used to study a typical series-compensated transmission system. According to [64], there are four torsional modes within sub-synchronous frequency ranges that can be studied. Four masses (HP, IP, LPA and LPB) and an exciter mass

are connected to the generator mass. The series compensation levels that can excite a SSR mode are listed in Table 4.2.

From Table 4.2, it can be concluded that the FBM system can suffer SSR at different compensation levels, and each listed level corresponds to one torsional mode respectively.

Table 4.2 SSR mode and corresponding series compensation level

| Mode of oscillation | Frequency | Series compensation level (in 50 Hz system) |
|:---:|:---:|:---:|
| TM1 | 15.83 Hz | 46% |
| TM2 | 20.22 Hz | 36% |
| TM3 | 25.42 Hz | 24% |
| TM4 | 32.26 Hz | 13% |

## 4.4 TCSC CHARACTERISTIC AND ITS IMPACTS ON MITIGATING SSR PROBLEMS

### 4.4.1 TCSC and FSC comparisons under different compensation levels

Three case studies in Table 4.3 with either FSC or TCSC to provide the compensation individually are tested. In each case, the firing angle of TCSC is kept constant at 160°. As summarised in section 4.2.4, TCSC at this firing angle has a stronger ability to transform sub-synchronous components at higher frequencies than that at lower frequencies. The case studies are used to compare the impacts of TCSC

in improving the electrical damping within sub-synchronous frequency ranges, with that provided by FSC. The electrical damping is obtained with the complex torque coefficient method in each case study.

Table 4.3 Parameters and corresponding compensation levels of TCSC and FSC for defined cases

| | FSC | TCSC | | Compensation level after boosting (%) |
| | | Capacitance (uF) | Inductance (mH) | |
| --- | --- | --- | --- | --- |
| Case 1 | 30uF | 35uF | 40 mH | 46% |
| Case 2 | 60uF | 65uF | 27 mH | 23% |
| Case 3 | 100uF | 110uF | 17 mH | 13% |

The frequency of the injected sub-synchronous current is controlled with the multi-run block in PSCAD, with an increment of 1 Hz in each run. The frequency of the disturbance $\Delta T_m$ ranges from 5 Hz to 45 Hz, to cover the sub-synchronous frequency ranges. The electrical torque and the rotor speed are measured at the synchronous generator side. By using FFT analysis on their derivatives, the phasor information can be obtained. The details of the complex torque coefficient method are introduced in Section 2.5.3 in the previous chapter.
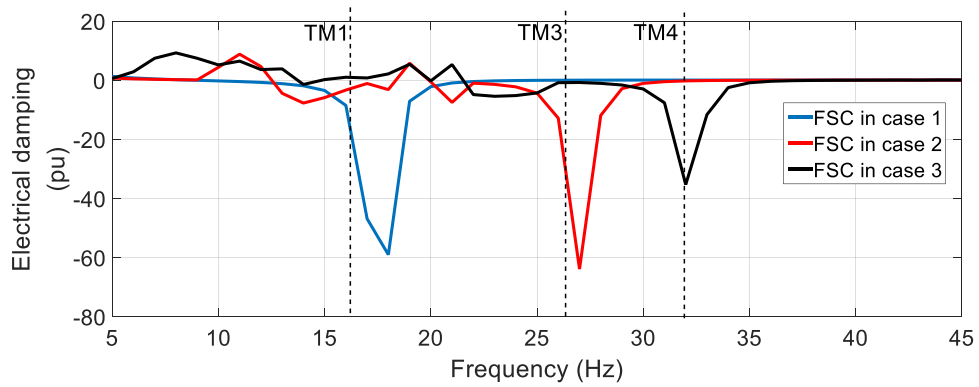
Fig. 4.9 Electrical damping calculated with FSC in different cases

Fig. 4.9 shows the electrical damping measured when only FSC is in the network regarding to the three cases. In case 1, there is a dip in the electrical damping at around 16 Hz, which is the frequency of TM1. Similarly, case 2 and case 3 have dips in damping at around 26 Hz and 32 Hz. These results indicate that the three cases are unstable and suffer SSR modes of TM1, TM3 and TM4 respectively.
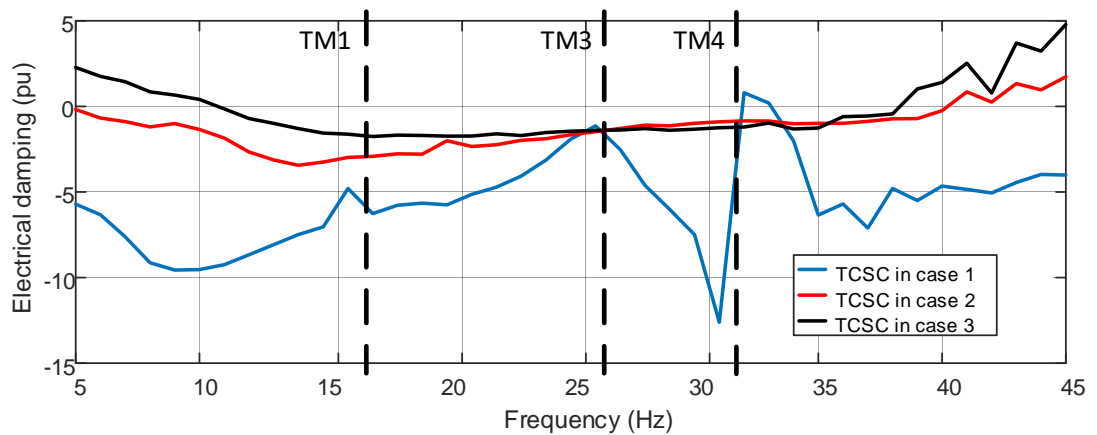


Fig. 4.10 Electrical damping calculated with TCSC in three cases

When TCSC is used to replace FSC, and is operated at a constant firing angle, the electrical damping is shown in Fig. 4.10. Compared with FSC, TCSC with the same compensation level possesses a better overall electrical damping characteristic, which is closer to zero or even positive at some frequencies. If the damping is positive, the

oscillation is expected to be damped. Damping dips caused by FSC are improved at concerned SSR frequencies, from lowest -60 pu to lowest -12 pu. Besides, when TCSC base impedance is lower, the overall damping characteristic is better, as indicated that the overall damping in case 3 is better than that in case 1. Moreover, despite of the dip at around 30 Hz in case 1, the overall trend shows that the electrical damping is better at higher frequencies. This matches with the ability of the power conversion of TCSC when the firing angle is selected to be 160°.

A simulation is conducted using the FBM system as shown in Fig. 4.10, and results are shown in Fig. 4.11.



(a) Active power with FSC at 57% compensation level

(c) Active power with TCSC at 57% compensation level

(b) LPA-LPB torque with FSC at 57% compensation level

(d) LPA-LPB torque with TCSC at 57% compensation level
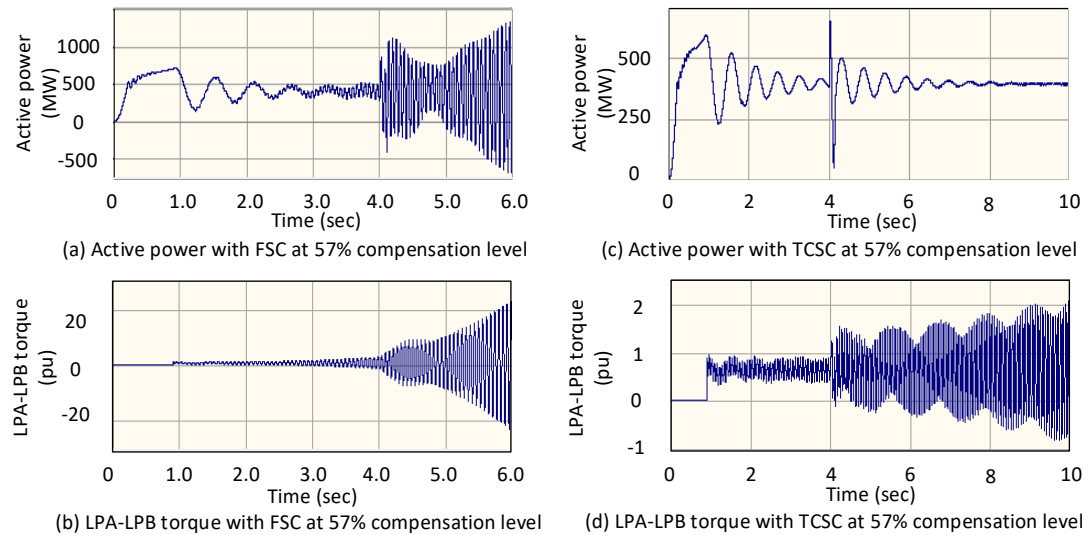
Fig. 4.11 Simulation results of the active power and the LPA-LPB torque considering FSC or TCSC in case 1

In Fig. 4.11, the two plots on the left are the active power and LPA-LPB torque when FSC is in the system. It can be observed that with FSC the system suffers SSR problems when a fault is applied at 4s. The two plots on the right are the corresponding performance with TCSC replacing FSC. A fault is also applied at 4s but the oscillation is limited and grow in a slower rate than that with FSC. In 6s after the fault, the LPA-

LPB torque oscillation reaches around 2 pu, compared with that magnitude reaches around 20 pu in 2s after the fault with FSC. The oscillation frequency is at around 16 Hz, and the result indicates that TCSC is contributing to better damping but it is not enough to mitigate SSR in this case.



(a) Active power with FSC at 27% compensation level

(c) Active power with TCSC at 27% compensation level

(b) LPA-LPB torque with FSC at 27% compensation level

(d) LPA-LPB torque with TCSC at 27% compensation level
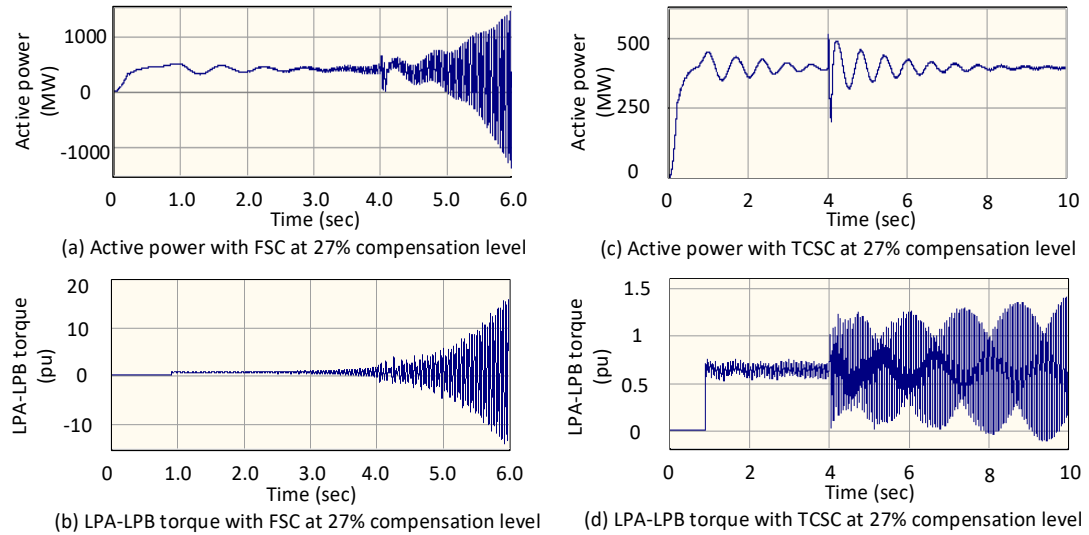
Fig. 4.12 Simulation results of the active power and the LPA-LPB torque considering FSC or TCSC in case 2

In case 2, the system compensation level is reduced to 23% and the SSR frequency is at 26 Hz. With FSC, as shown in Fig. 4.12 (a) and (b), the system performance is very poor. The oscillation in LPA-LPB torque grows to around 15 pu in 2s after the fault. However, as shown in Fig. 4.12 (c) and (d), TCSC provides a better damping performance at 26 Hz and the oscillation in LPA-LPB torque is growing very slowly. This result indicates that TCSC is more capable of damping SSR at higher frequencies than at lower frequencies.

In case 3, the compensation level is further reduced to 13%, and the corresponding SSR frequency is at 32 Hz. Fig. 4.13 (a) and (b) show the system performance with FSC only, where the SSR problem becomes severe and the oscillation magnitude

grows to around 60 pu. However, with TCSC, the SSR is damped. As shown in Fig. 4.13 (c) and (d) that the active power has little distortions from the SSR event and the oscillation in LPA-LPB torque is decreasing in its magnitude.



(a) Active power with FSC at 17% compensation level

(c) Active power with TCSC at 17% compensation level

(b) LPA-LPB torque with FSC at 17% compensation level

(d) LPA-LPB torque with TCSC at 17% compensation level
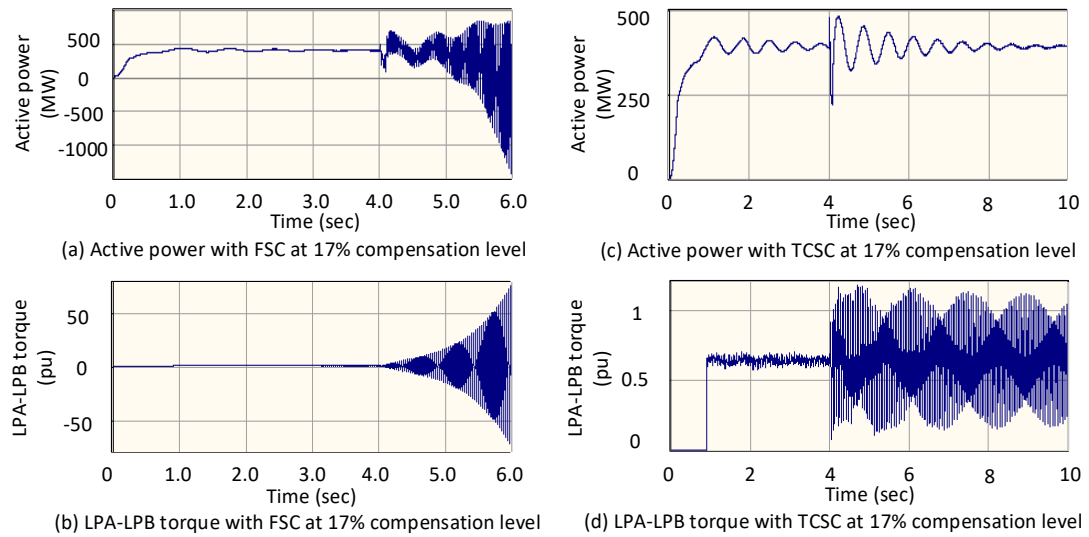
Fig. 4.13 Simulation results of the active power and the LPA-LPB torque considering FSC or TCSC in case 3

In summary, the results of the above case studies are listed in the below table.

Table 4.4 Results summary of the three case studies

| Case number | Stability | | | | |
|---|---|---|---|---|---|
| | FSC | | | | |
| | Stability | LPA-LPB torque at 10s (peak-peak pu) | Stability | LPA-LPB torque at 10s (peak-peak pu) | |
| Case 1 | Not stable | 40 | Not stable | 3 | |
| Case 2 | Not stable | 30 | Not stable | 1.5 | |
| Case 3 | Not stable | 150 | Stable | 0.75 | |

## 4.4.2 Impacts of different TCSC firing angles on the performance of SSR damping

TCSC's firing angle selection also has an impact on SSR damping performance. The study is conducted upon varying firing angles in order to understand how the damping performance can be influenced by varying firing angles. Parameters in case 1 in Table 4.3 are used and only TCSC is inserted in the network to provide the compensation.

Fig. 4.16 shows the simulation results, with firing angles changed at 160°, 165° and 170°. As the compensation level is 46%, the SSR frequency is at 16 Hz. According to the power conversion ability of TCSC and the resistive performance study in section 4.2.2, TCSC with a smaller firing angle has a better damping performance of SSR. The reason for this is that the larger firing angle is, the shorter thyristors are conducted per

cycle. If the firing angle approaches to 180°, thyristors are fully blocked and TCSC acts as FSC. In that case, TCSC has the same damping characteristic with FSC. Simulation results match the study results in section 4.2.2 very well. When the firing angle is 160°, as shown in Fig. 4.14 (a) and (b), the growth of SSR oscillation in LPA-LPB torque is relatively slower. The magnitude in LPA-LPB torque oscillation reaches only 2 pu at 10s. With the firing angle increasing, the damping of SSR provided by TCSC gets poorer. As can be observed in Fig. 4.14 (c) and (d), the oscillation in the LPA-LPB torque grows to 10 pu and the active power flow is obviously distorted with sub-synchronous harmonics. A similar trend can be verified in Fig. 4.14 (e) and (f) that the damping gets even poorer when the firing angle is increased to 170°.



(a) Active power with TCSC firing angle 160

(b) LPA-LPB torque with TCSC firing angle 160

(c) Active power with TCSC firing angle 165

(d) LPA-LPB torque with TCSC firing angle 165

(e) Active power with TCSC firing angle 170

(d) LPA-LPB torque with TCSC firing angle 170
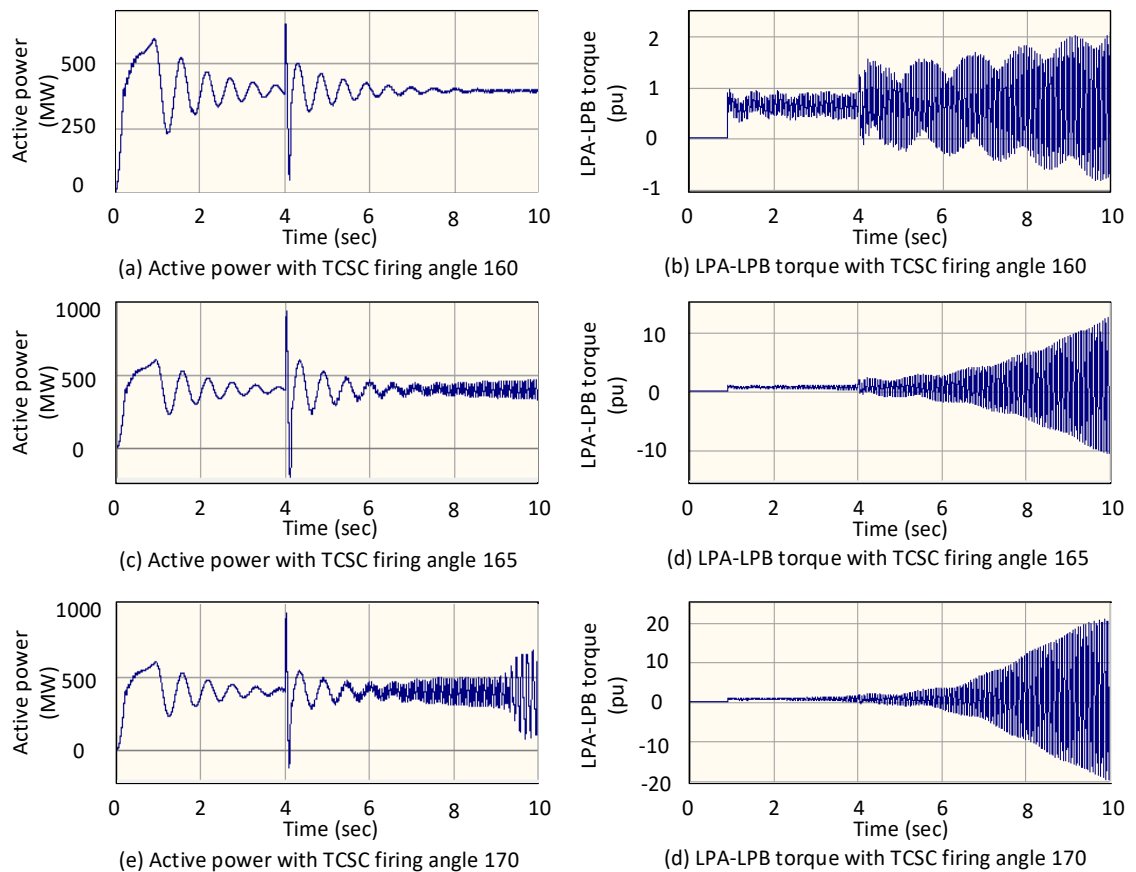
Fig. 4.14 Simulation results of the active power and the LPA-LPB torque with different firing angles

72

### 4.4.3 Impacts of different TCSC/FSC ratios on the performance of SSR damping

Compared with FSC, TCSC is much more expensive. Therefore, a convenient way is to install TCSC in a combination with FSC to reduce the cost. In practical projects [146], TCSC is designed to contribute to 1/3 of the base compensation to maintain a smooth controllability and SSR mitigating capability, but there are few studies on the selection of the compensation level provided by TCSC. Therefore, four cases are defined to investigate the impacts of different TCSC/FSC ratios on the overall damping performance of SSR.

Table 4.5 Definition of studied cases

| Overall compensation 45% | TCSC compensation level (%) | FSC compensation level (%) | Ratio |
|---|---|---|---|
| Case 1 | 22% | 22% | 1:1 |
| Case 2 | 15% | 30% | 1:2 |
| Case 3 | 11% | 33% | 1:3 |
| Case 4 | 9% | 36% | 1:4 |

Table 4.5 gives the percentages of TCSC and FSC in the four cases. The ratio of TCSC/FSC varies from 1:4 to 1:1 to investigate the overall damping performance with different levels of TCSC. TCSC is controlled with a constant firing angle at 160° , the boosting level is around 1.2 pu at this firing angle. The displayed TCSC compensation in Table 4.5 is the boosted compensation level.
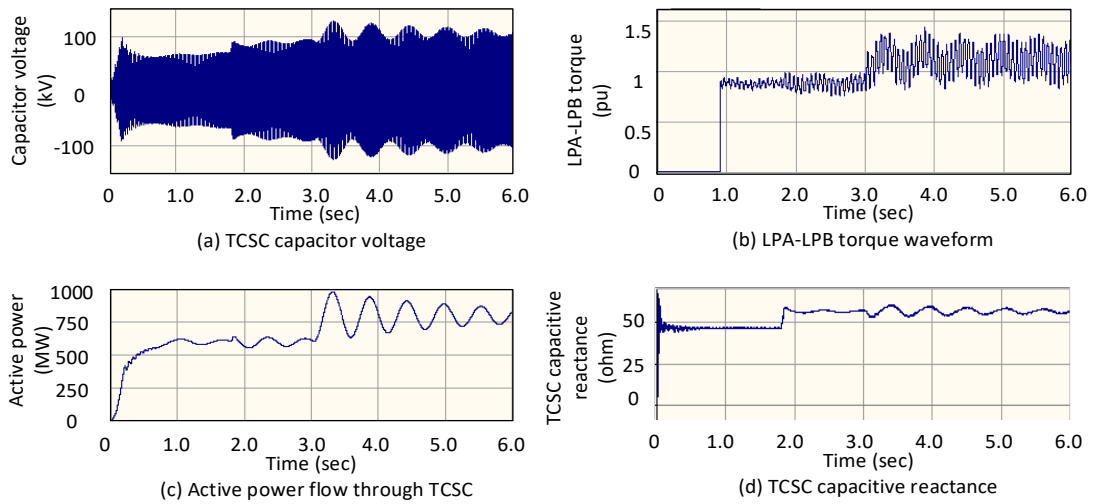
Fig. 4.15 Simulation results of case 1 when the ratio of TCSC/FSC is 1:1

In case 1, half of the compensation levels are provided by TCSC. The system performance is shown in Fig. 4.15. In Fig. 4.15 (b), the LPA-LPB torque is oscillating and the magnitude of the oscillation is growing slowly. This indicates the electrical damping provided by TCSC in this case is good. However, the system is also suffering a low-frequency oscillation, as shown in Fig. 4.15 (c) the active power flow plot. This low-frequency oscillation is slowly damped.
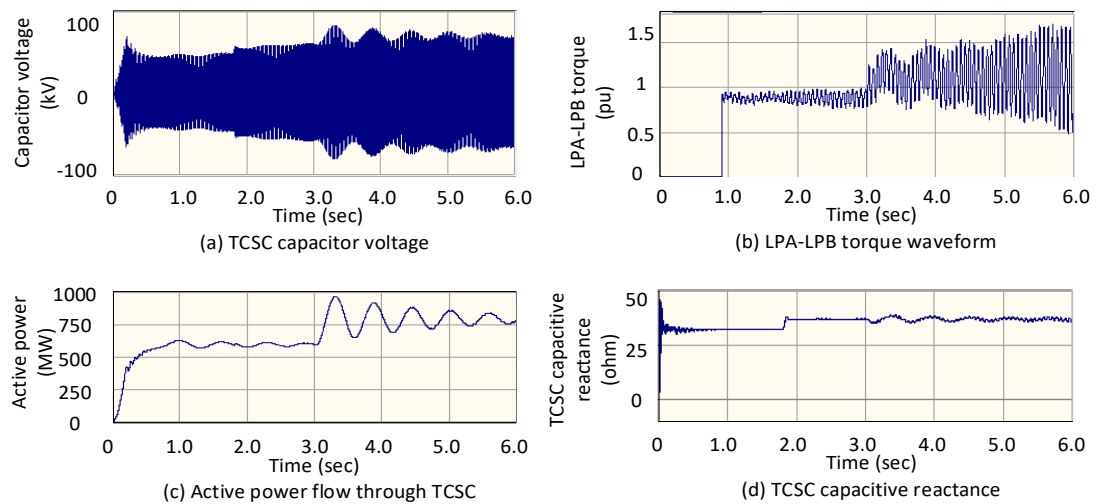


Fig. 4.16 Simulation results of case 2 when the ratio of TCSC/FSC is 1:2

In case 2, the ratio is changed to 1:2 which means the percentage of TCSC is reduced. In Fig. 4.16 (b) the severity of SSR problem gets higher than that in case 1. The oscillation magnitude in Fig. 4.16 (b) reaches 1.5 pu at 6 s. The system still suffers low-frequency oscillation when the fault is applied at 3 s and it is slowly damped.



(a) TCSC capacitor voltage

(b) LPA-LPB torque waveform

(c) Active power flow through TCSC

(d) TCSC capacitive reactance
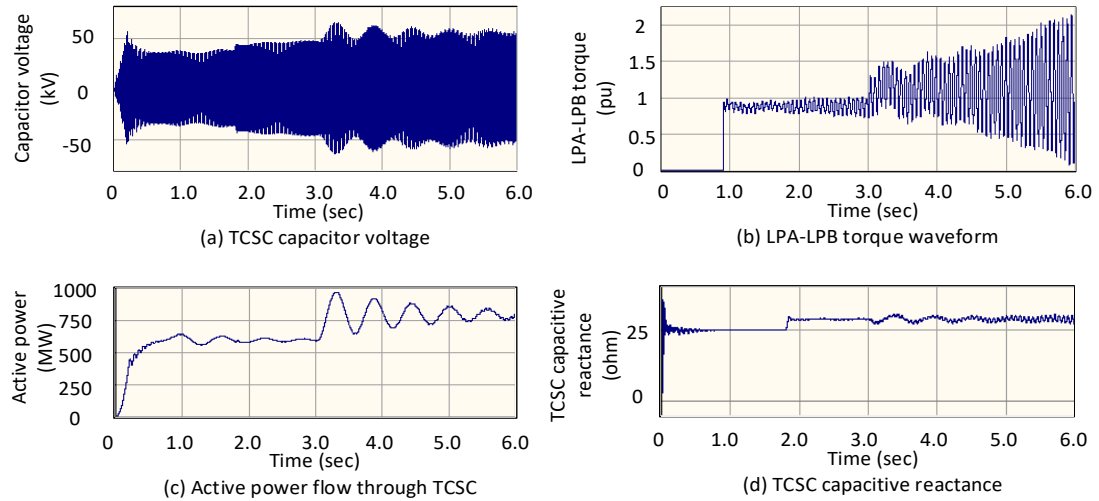
Fig. 4.17 Simulation results of case 3 when the ratio of TCSC/FSC is 1:3

In case 3, Fig. 4.17, with more FSC replacing TCSC to provide compensation, the SSR becomes more severe while the power swing caused by the step change in generator output is not much affected.



(a) TCSC capacitor voltage

(b) LPA-LPB torque waveform

(c) Active power flow through TCSC

(d) TCSC capacitive reactance
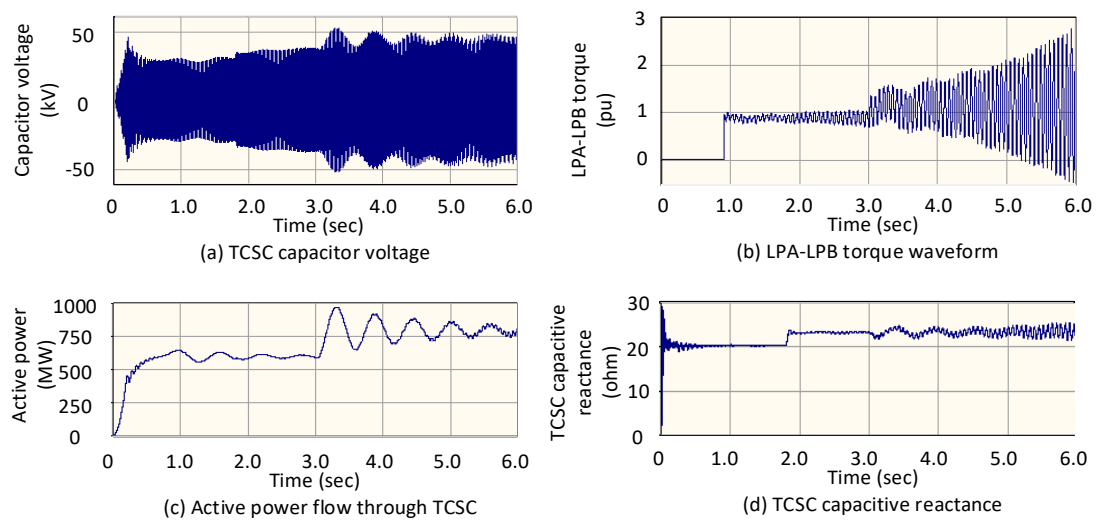
Fig. 4.18 Simulation results of case 4 when the ratio of TCSC/FSC is 1:4

75

With the ratio drops to 1:4, as seen in Fig. 4.18, the SSR problem becomes very severe. Oscillations at the SSR frequency can be clearly observed in the capaccitor voltage, the active power and the measured TCSC impedance. Regarding to the low-frequency oscillation, the change in the ratio between TCSC and FSC fails to improve the low-frequency oscillation damping very much.

From the comparison, it can be seen that the ratio between TCSC base impedance and FSC impedance dramatically influence the SSR damping. With more compensation contributed by TCSC, the SSR damping performance is much better. However, regarding to low-frequency power swings, the ratio between TCSC and FSC does not have obvious impacts on this performance. The low-frequency power swing is more related to the characteristic at synchronous frequency, which are kept the same in above tests. Therefore, the percentage of TCSC plays an important role in affecting the SSR mitigation, but this needs to be balanced between the SSR mitigation capability and the capital cost.

## 4.5 SUMMARY

TCSC inherent characteristic based on the thyristor's regulation provides the ability to transform the sub-synchronous energy into the synchronous energy. This ability can be clearly observed in the dynamic behaviour of TCSC with sub-synchronous distortions, that TCSC tries to bring the zero-crossing points of the capacitor voltage back to the synchronous frequency.

The resistive performance of TCSC is explained by using the power conversion ability. The positive resistance of TCSC at sub-synchronous frequencies consume the energy carried by sub-synchronous components while the negative resistance at

synchronous frequency is the result of the energy being transformed into synchronous components.

The effectiveness of the power conversion ability of TCSC is varied with TCSC firing angles and is also varied with the frequency of the sub-synchronous component. It can be concluded that at a specified sub-synchronous frequency, the best performance of this ability occurs when the firing angle is around 150° to 160°. TCSC at larger firing angle performs poorly in transforming sub-synchronous components and the performance is improved with firing angles decreasing. However, if the firing angle drops to below 150° the performance is still weakened.

Moreover, TCSC with larger firing angles is more capable of transforming sub-synchronous components at lower frequencies than at higher frequencies. This trend is changed when the firing angle decreases. When the firing angle drops to around 155°, TCSC is more capable of transforming sub-synchronous components at higher frequencies.

An investigation is conducted with TCSC or FSC providing different compensation levels, which cause the frequency of SSR to be varied. The results indicate that TCSC with the larger firing angle provides a better damping performance to SSR at higher frequencies. This matches the findings in the power conversion studies.

Another study on the combination of TCSC and FSC with consideration in both the low-frequency oscillation and the SSR damping is conducted. Cases are defined with various ratios between the TCSC base capacitor impedance and the FSC impedance. The results indicate that the ratio has few impacts on system low-frequency oscillations but can affect SSR damping greatly. With more percentages of compensation provided by FSC, the system has a poorer SSR damping. When the ratio is down to 1:4, the SSR

severity is quite strong and the power flow is heavily distorted by sub-synchronous harmonics within 3s.

# Chapter 5

# Experimental platform for sub-synchronous resonance test with Thyristor-Controlled Series Capacitor

## 5.1 INTRODUCTION

An experimental hardware platform has been designed and developed to validate the effectiveness of the proposed controller. This chapter describes the details of the TCSC-SSR experimental platform that has been designed at the laboratory level including a grid emulator connected to a TCSC test rig. The motivation behind this setup is to investigate the functions of the TCSC device in power systems, and sub-synchronous interactions between turbine generator shaft systems and the series compensator. Solutions using TCSC to solve the sub-synchronous problem are proposed and validated on this platform.

In this chapter, the configuration of the platform is presented. The design of the TCSC test rig and the method to select its parameters are demonstrated. Specifications of the platform are introduced, including the TCSC prototype, the grid emulator, the power amplifier and the AC grid. The control system and the software are also demonstrated. To avoid the over-current situation when the main circuit breaker inside the TCSC test rig is closed, a solution is proposed with both simulation and real-time experimental results compared.

## 5.2 OVERVIEW OF THE EXPERIMENTAL PLATFORM FOR TCSC-SSR TEST

### 5.2.1 Configuration of the experimental platform

Fig. 5.1 shows the overview of the experimental platform representing a turbine generator emulator connected to the AC grid through TCSC compensated lines.
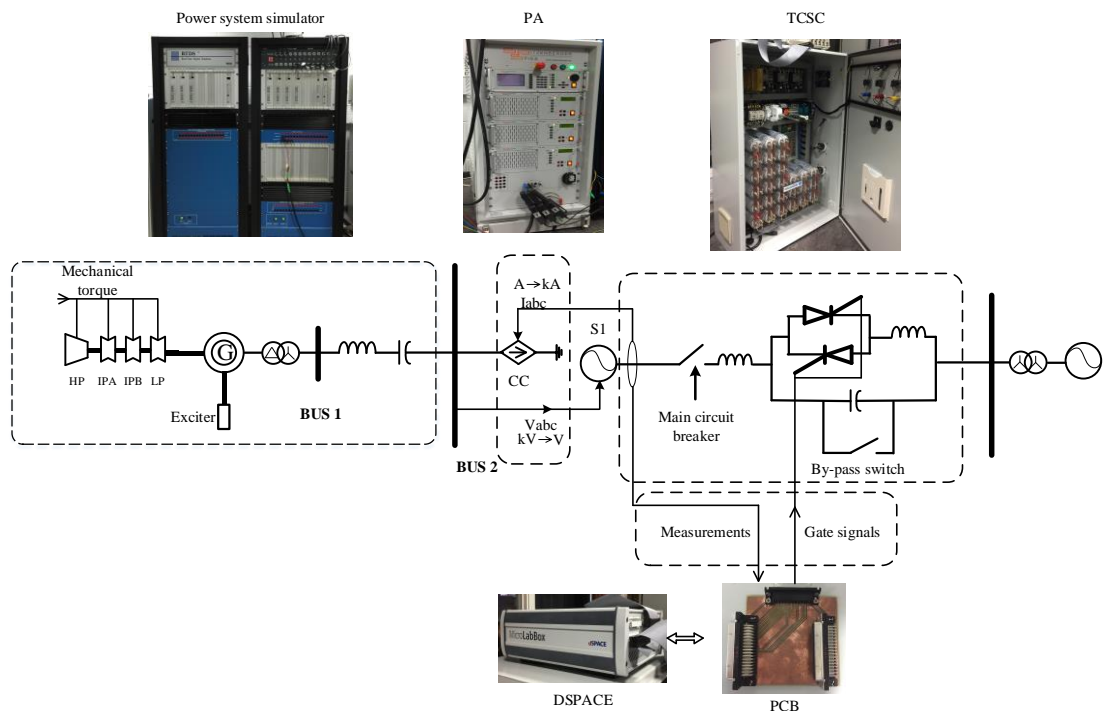


Fig. 5.1 An overview of the TCSC-SSR experimental platform configuration

The platform consists of a power system simulator, a controller platform, a TCSC device connected to the AC grid via transformer, and a PC to monitor/control system dynamics. Fig. 5.1 shows how the system is modelled. The HV generating unit including the mechanical turbine shaft is modelled in RTDS, along with the transformer and part of the transmission cable. The physical TCSC device is embedded in the experimental platform. The connection between TCSC and the power system simulator is achieved with the interface of PA and current feed-back signals. Control

signals of thyristors in the TCSC device are sent via a Printed Circuit Board (PCB) from the dSPACE controller.

All components of TCSC are assembled within a cabinet of size 150cm x 100 cm x 50cm. There are two power sockets and one signal I/O socket on this cabinet. The input power socket is connected to the output of the PA while the output power socket is connected to the AC grid via an auto-transformer. These connections are via power cables of 5-pin and 32A rating. The signal I/O socket is a D-Sub 26-pin connector, and is connected to a PCB via a flat cable. These signals include both analogue measurements of voltage/current within TCSC, and digital control/state signals, i.e. thyristor triggering pulses or the state of a circuit breaker.

The control platform is implemented on the dSPACE MicroLabBox. Due to the design of the dSPACE MicroLabBox, the digital and analogue sockets are separated by the manufacturer. However, all analogue and digital signals of the TCSC are assembled together on one PCB to save room in the cabinet, and are transmitted via one D-Sub socket. To adapt to the digital and analogue socket requirements on the MicroLabBox, a PCB is designed as an interface to re-arrange TCSC I/O signals to individual pins. To achieve this, two 50-pin D-Sub sockets and one 26-pin D-Sub socket are mounted on the PCB. The 26-pin socket is used to send/receive signals to/from the TCSC device, while the two 50-pin sockets are used to separate digital signals from analogue signals. All controls, monitoring, and system modifications are completed on the PC and being downloaded to the dSPACE MicroLabBox.

## 5.3 DESIGN, PARAMETERS AND RATING OF THE TCSC TEST RIG

### 5.3.1 Topology design

To perform effective and flexible validation on the experimental platform, some modifications are added to the general three-phase topology of TCSC. Fig. 5.2 shows the single-line diagram of the designed TCSC device.

The TCSC device has two power connectors. The input socket is connected to the output of the grid simulator amplifier, while the output socket is connected to the AC power grid. The AC grid is also used to power up the internal PCB and measuring units through a AC/DC converter that provides 10V/24V DC.
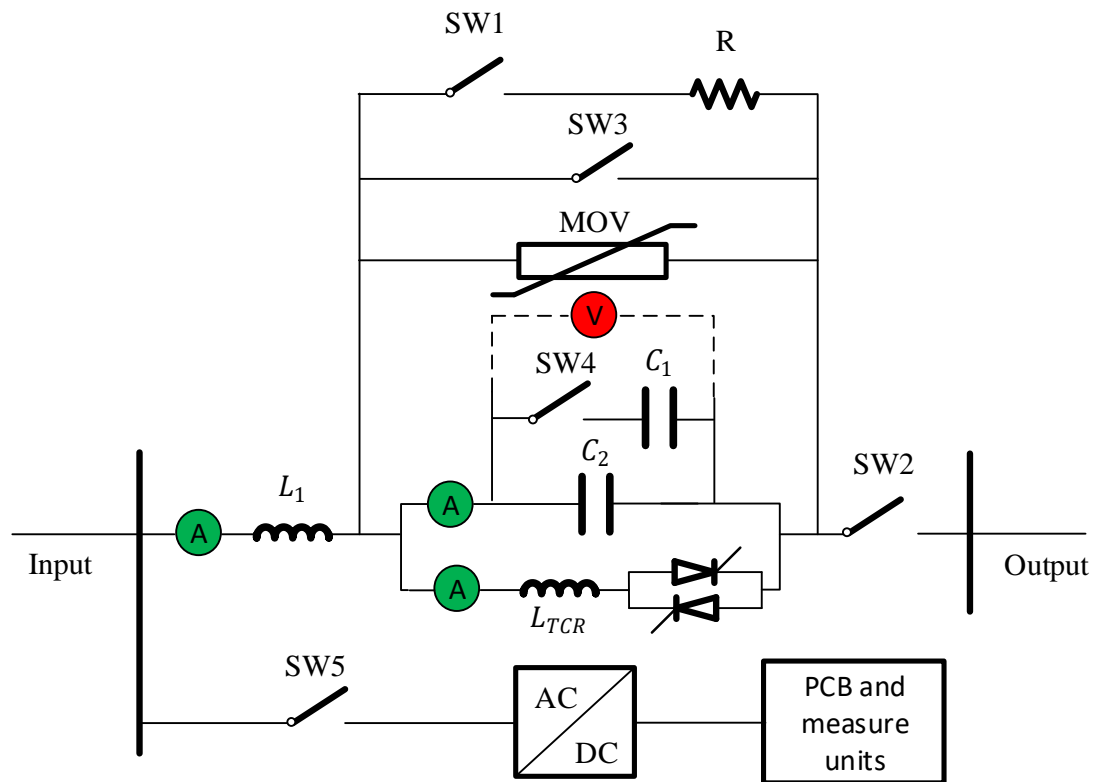


Fig. 5.2 Single line diagram of TCSC cabinet

In Fig. 5.2, the switch SW1 and the resistor R are used to add a fast and safe discharging loop if the capacitors get overcharged. SW1 is the parallel resistor switch and is open in normal conditions, and can be manually controlled.

The inductor $L_{TCR}$ is the TCR, and the inductor $L_1$ represents part of the transmission line inductance.

The circuit breaker located in the main circuit, SW2, is designed as the main circuit breaker, which also acts as a protection scheme that can be opened automatically if the current exceeds a certain level, i.e. 16 A. Manually control over SW2 is also available.

Two capacitors C1 and C2 can be used, and their capacitance are different. A switch SW4 is used to insert/remove C1 into/from the network to enable a different capacitance level. A MOV is used to protect the capacitors from over-voltage risks if the capacitor voltage exceeds 50V.

SW3, the short circuit switch, is used to operate the TCSC in the by-pass mode. This will by-pass capacitors and thyristors, and leave only the inductor L2 in the network. This design is to minimise the influence of the main circuit breaker closure. SW3 can be manually controller.

The power to internal measuring units and PCB is provided by the AC grid via a AC/DC converter. The converter works under 100V/240V AC and outputs 10V/24V DC to supply the operations of PCB and measuring units. A switch, SW5, is used to control the power supply.

Internal measurements are achieved by placements of different sensors, voltage and current measuring units, which are located at different locations to allow a full monitoring during the operation of TCSC. These measurements are 3-phase capacitor

voltage, line current, TCR current and capacitor current. The output terminal voltage are also measured as phase-to-phase voltage.

## 5.3.2  Selection of TCSC parameters

The TCSC device used in the lab is working under 240/415V, and is a scaled down model of the real TCSC project located between the Hark substation and the Hutton substation. The transmission circuit structure [147] is shown in Fig. 5.3.
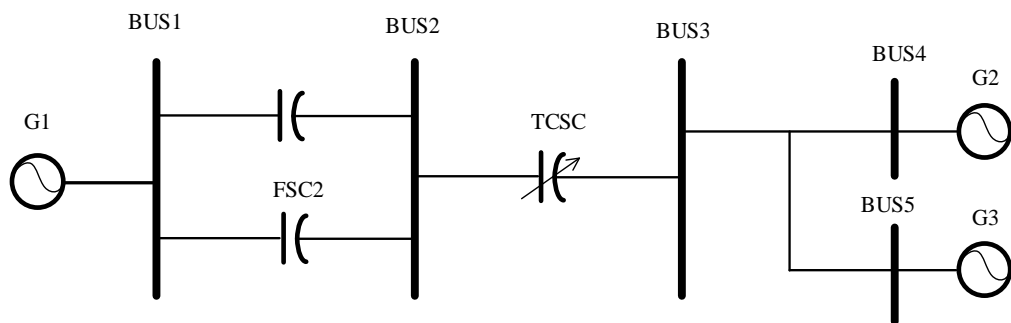


Fig. 5.3 Transmission circuit between Hark and Hutton substation in the UK [147]

The overall transmission system covers an 82 km long transmission line, which is represented by the typical overhead line model, as an R-L circuit with 0.03 ohm and 0.7 mH per kilometre [148]. In Fig. 5.3, G1, G2 and G3 represent the Scottish power system, the Wales power system and the England power system respectively. Bus 2 and Bus 3 are the Hark substation and the Hutton substation which is the main corridor between the Scotland and England transmission systems.

To perform the scaling, the base impedance for the high-voltage and low-voltage systems need to be addressed. For the high-voltage system, the power rating is considered to be [147]:

$$S = 800 + j120 \text{ MVA} \tag{5.1}$$

TCSC is designed to provide variable compensation between 15% and 45%, and in combination with FSC providing an extra 20% compensation. Therefore, the physical capacitor of TCSC should be 15% of the total system impedance:

$$X_{C,TCSC} = X_{SYS} * 15\% = 25 \ ohms * 15\% = 4.15 \ \Omega, \qquad (5.2)$$

$$\text{and } C_{TCSC} = \frac{1}{X_{C,TCSC}*\omega_0} = \frac{1}{4.15*2*\pi*50} = 767 \text{ uF} \qquad (5.3)$$

The selection of the TCR is based on the physical capacitance of the TCSC, and the square root of their impedance ratio should lie between 2.3 and 2.7. Here the ratio is determined as 2.7. Then the TCR inductance is deduced as:

$$X_{TCR} = \frac{X_{C,TCSC}}{2.7^2} = 4.15 \frac{\Omega}{7.29} = 0.569 \Omega \qquad (5.4)$$

$$L_{TCR} = \frac{X_{TCR}}{\omega_0} = \frac{0.569 \ \Omega}{2*\pi*50} = 1.81 \text{mH} \qquad (5.5)$$

Similarly, the capacitance of the FSC can be determined as:

$$X_{FSC} = X_{SYS} * 20\% = 25 \ \Omega * 20\% = 5.53 \ \Omega \qquad (5.6)$$

$$\text{and } C_{FSC} = \frac{1}{X_{FSC}*\omega_0} = \frac{1}{5.53*2*\pi*50} = 575.6 \text{ uF} \qquad (5.7)$$

Table 5.1 Hutton TCSC project parameters: TCSC and FSC

| TCSC | | | FSC |
|---|---|---|---|
| Physical capacitor | TCR | Ratio ($\sqrt{(X\_C/X\_L)}$) | Physical capacitor |
| 4.15 (15% level) $\Omega$ | 0.569 $\Omega$ | 2.7 | 5.53 (20%) $\Omega$ |
| 767 uF | 1.81 mh | | 575.6 uF |

Table 5.1 lists the parameters of the Hutton TCSC. Therefore, the per-unit calculation of the Hutton TCSC project can be expressed with an Real System (RS) and summarized as follow:

$$Vbase_{RS} = 400 \text{ kV}, \ Pbase_{RS} = \ 800 \text{ MVA} \qquad (5.8)$$

$$Ibase_{RS} = \frac{Pbase_{RS}}{Vbase_{RS}} = \frac{800 \text{ MW}}{400 \text{ kV}} = 2 \text{ kA} \qquad (5.9)$$

$$Zbase_{RS} = \frac{Vbase_{RS}}{Ibase_{RS}} = \frac{400 \text{ kV}}{2 \ kA} = 200 \ \Omega \qquad (5.10)$$

Similarly, the base voltage and base power of the TCSC test rig, denoted with subscript 'Rig', are determined as follow:

$$Vbase_{Rig} = 415 \text{ V}, \ Pbase_{Rig} = \ 4.15 \text{ kVA} \qquad (5.11)$$

$$Ibase_{Rig} = \frac{Pbase_{Rig}}{Vbase_{Rig}} = \frac{4.15 \text{ kW}}{415 \text{ V}} = 10 \text{ A} \qquad (5.12)$$

$$Zbase_{Rig} = \frac{Vbase_{Rig}}{Ibase_{Rig}} = \frac{415 \text{ V}}{10 \text{ A}} = 41.5 \ \Omega \qquad (5.13)$$

Then the scaling factor can be obtained by dividing the RS base impedance by the test rig base impedance:

$$Scale\ factor\ (pu) = \frac{Zbase_{Rig}}{Zbase_{RS}} = \frac{41.5}{200} = 0.2075 \qquad (5.14)$$

With the scaling factor, TCSC and FSC parameters given in table 5.1 can be scaled to low-voltage level by multiplying their impedance by the scale factor. This gives designed TCSC parameters and these parameters are given in table 5.2.

Table 5.2 Scaled parameters including the line impedance, the TCSC impedance and the FSC impedance

|  | Line inductor | Line resistor | TCSC capacitor | TCSC inductor |
|---|---|---|---|---|
| Before scaling | 57.4 mH | 2.46 Ω | 767 μF | 1.81 mH |
| After scaling | 11.91 mH | 0.51 Ω | 3696 μF | 0.375 Mh |

These components, TCSC capacitor and TCSC inductor as listed in Table 4.2, their parameters after scaling make the final TCSC device.

### 5.3.3 Protection schemes

As the TCSC test rig is designed for SSR research, some protection schemes are used to prevent the system from getting unstable and damaging the test rig.

Since the device is designed at a current rating of 10 A, an event-triggered scheme under over-current conditions is installed by placing a sensor to monitor the current that flows through the inductor $L_1$, as denoted in Fig. 5.2. When this case occurs, the main circuit breaker, denoted as SW2, will be opened to interrupt the current flow.

The over-voltage risk on capacitor is also considered and can be reduced by the MOV to limit the voltage over capacitors to 50 V maximum. If this is the case, the main circuit breaker will also be triggered to open, and meanwhile the paralleled resistor will be inserted into the network to discharge capacitor voltages. This operation is achieved by closing the circuit breaker next to the resistor, denoted as SW1.

In order to maximise the network impedance during the start-up period, an extra circuit breaker is designed to isolate the series connected capacitors thus leaving the inductor L1 alone in the network to limit the start-up current. This circuit breaker is denoted as SW3 and kept open until needed, i.e. to limit the impact current with closure of the main circuit breaker SW2.

## 5.4 SPECIFICATIONS OF EQUIPMENT IN THE PLATFORM

### 5.4.1 Grid simulator amplifier

The platform uses a Spizenberger & Spies PAS 1000 amplifier. This amplifier composes three four-quadrant amplifiers, resistive dump load, and a control unit. This unit connects directly to the RTDS system and provides a high-fidelity three-phase 400V output to whichever experimental systems may be connected. The combination of the RTDS and the amplifier effectively allows experimental systems to become part of a physical AC network (scaled in power rating). A detailed datasheet can be found in [149].

This grid simulator amplifier allows a rated power of 1000 VA output under continuous operation, and a short-term operation with 20% over-rating for 10 min. Circuit breakers are installed inside to cut emergent over-current or fault conditions if the current exceeds 10 A.

The output control over the grid simulator amplifier is via three digital signal channels, fed from the RTDS to form the waveforms of the three-phase analogue signals. Output terminals are directly connected to the TCSC test rig to provide three-phase voltage.

### 5.4.2  Turbine generator emulator

To emulate the turbine generator, there are generally two aspects to be modelled: the mechanical dynamics within the turbine generator shaft and the electro-magnetic dynamics. RSCAD, a software programme designed suitable for RTDS, is used to model both the mechanical system of the generator shaft and the electrical system. The model in RSCAD is shown in Fig. 5.4.
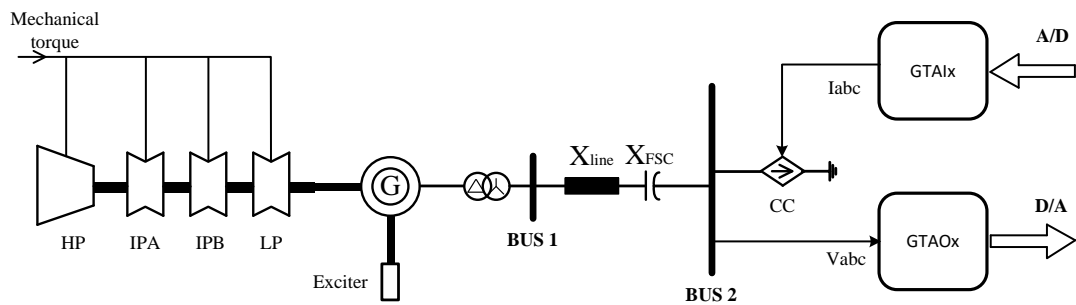


Fig. 5.4 RSCAD model of the turbine generator and transmission system

In Fig. 5.4, the turbine shaft of the synchronous generator is modelled by a four-mass system connected to the generator and the exciter. The parameters of them are obtained from the IEEE FBM system and the operating frequency is modified to 50 Hz [150]. The transmission line is modelled by an inductor denoted as $X_{line}$. A FSC, denoted as $X_{FSC}$, is placed to provide some series compensation of 30%. The analogue signals are exchanged by using an interface which consists of two RTDS I/O cards, GTAIx and GTAOx. In this way, the load is modelled by a controlled current source whose signal is fed by external current measurements via card GTAIx. As for the

external network, the analogue voltage is provided by the grid simulator amplifier, controlled by the digital voltage measurements at BUS 2 and transformed into analogue outputs via card GTAOx with proper scaling.

### 5.4.3 The TCSC device

The TCSC test platform uses a three-phase 7kW TCSC device for power flow and SSR mitigation studies. Upon the design, the TCSC device is supposed to have interoperability with other devices in the lab, i.e. with voltage source converters or the PMSG. In addition to the commonly used modes of a TCSC device, some extra functions are added:

- Capacitor by-passed mode: both thyristors and capacitors in TCSC device are by-passed that TCSC acts as a small inductor in this case

- Two-compensation-level FSC mode: with thyristors un-triggered, the number of capacitors that are connected to the network can be selected between two values

- TCSC mode: with thyristor triggered, the base capacitor value can be selected

The device is assembled in a cabinet as shown in Fig. 5.5. On the front panel, several buttons and switches are placed to enable manually control over the device. For each button, a LED is placed correspondingly to indicate the state of that button. The location of each switch and their functions are related to section 5.3.1.
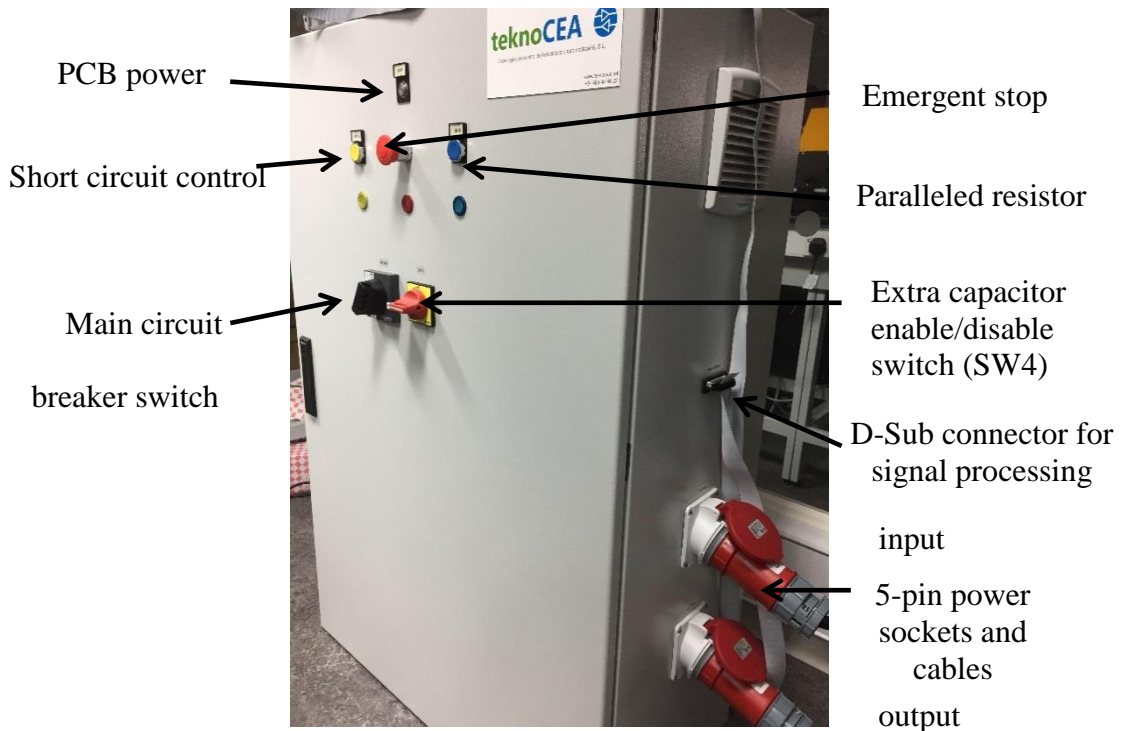
Fig. 5.5 An overview of the TCSC cabinet

The TCSC device is designed with two power connectors and one D-Sub connector for signal exchanging. The input power connector is connected to the output of the grid simulator amplifier, while the output socket is connected to the AC grid. The D-Sub connector allows 26 channels of signals, including both digital and analogue I/O, and is connected to the MicroLabBox for monitoring and control. The analogue signals are measuring signals obtained from measuring units which are placed inside the TCSC device. There are 14 measurements all together, and all the measurements are limited between $\pm9$ V by the PCB adaption board. The measurements ranges go as follows:

- Load output phase-to-phase voltage (pin 3 and pin 6): $\pm981V \rightarrow \pm9V$

- Capacitor voltage (pin 1, pin 2 and pin 4): $\pm324V \rightarrow \pm9V$

- All current measurements (pin 5, pin 7 to pin 13): $\pm55A \rightarrow \pm9V$

The rest signals are digital signals, at either 0V or 5V. Control signals are taken as inputs to control thyristors or switches, while states of some switches are outputted to monitor the operation of the device. Definitions of these pins are given in the Appendix II.

### 5.4.4 onfiguration of the TCSC and the test platform

The layout within the TCSC cabinet is shown in Fig. 5.6. Two capacitor banks lay at the bottom of the cabinet, as C1 and C2. C1 consists of 6 capacitors (600 uF each) per phase and C2 consists of 3 capacitors per phase. The two capacitor banks are connected in parallel, with a selective switch to enable or disable C2 from the network.

In the middle are circuit breakers, AC/DC converters and contactors. The main circuit breaker SW2 is connected to the front panel through the metal rod. On its right is another metal rod which is used to control capacitors connected to the network. Two AC/DC converters are used to supply power to different components at different voltage levels. The black one on the right is providing 24V DC and the light green one on the left is used to generate 15V DC voltage. The two contactors on the left of the Fig. 5.6 represent SW1 (Paralleled resistor control) and SW3 (Short circuit control). Behind them are the three-phase line inductors.

The PCB is used to assemble measurements and control signals for input and output uses. On its left is the voltage measuring units.
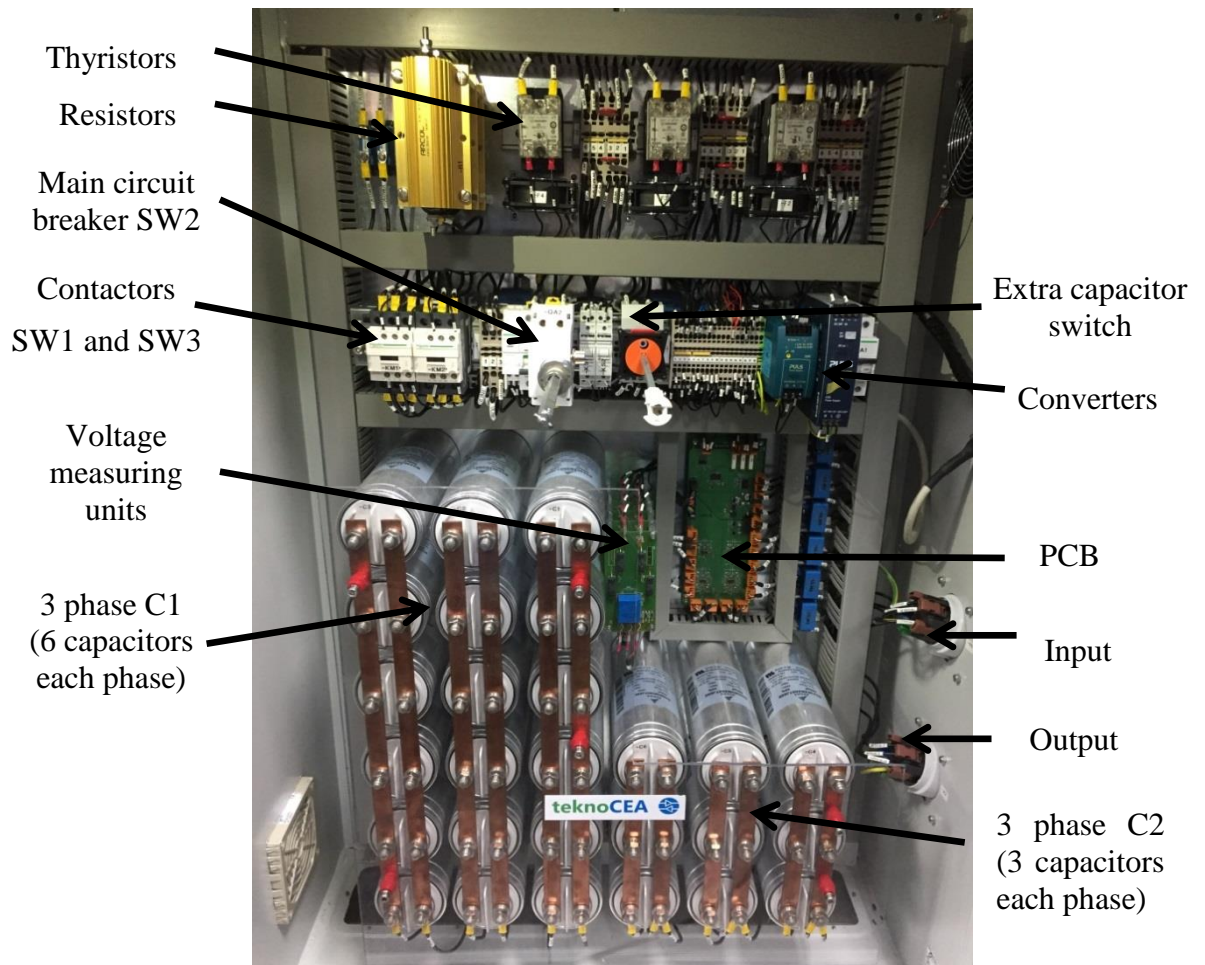
Fig. 5.6 Components inside the TCSC cabinet

The connection between TCSC and the AC grid is via the 3-phase auto-transformer, as shown in Fig. 5.7 (a). The input of the transformer is connected to the AC grid and its output is connected to the output of the TCSC via a 5-pin power cable with banana connectors. In Fig. 5.7 (b) the grid simulator amplifier is connected to the input of the TCSC. Current measurements are taken by three current claps and are fed back to the RTDS.

(a)                                     (b)

Fig. 5.7 (a) The three-phase auto-transformer and (b) the grid simulator amplifier

## 5.4.5 Signal processing and dSPACE MicroLabBox

The measurements and signals control within TCSC device are assembled onto a PCB and transmitted via a 26-pin flat cable. To extend the function of these signals, another PCB is used to divide them to two different connectors, since the MicroLabBox have separate digital and analogue I/Os. Fig. 5.8 shows the schematic diagram and the completed interface PCB.

As shown in Fig. 5.8 (b), the D-Sub connector, denoted as X1, is a 26-pin connector connected to the PCB within the TCSC device. The left and right connectors represent the digital and analogue connectors respectively, as shown on the board, and both of them are of 50 pins to fit the MicroLabBox specifications. The two colours of connections, representing connections on the top and bottom layers of the PCB, are red and blue respectively.

Fig. 5.8 (a) shows the completed PCB using the design of Fig. 5.8 (b). In Fig. 5.8 (a), the bottom layer is upside. Therefore, the copper soldering shown represents the blue connections in Fig. 5.8 (b).
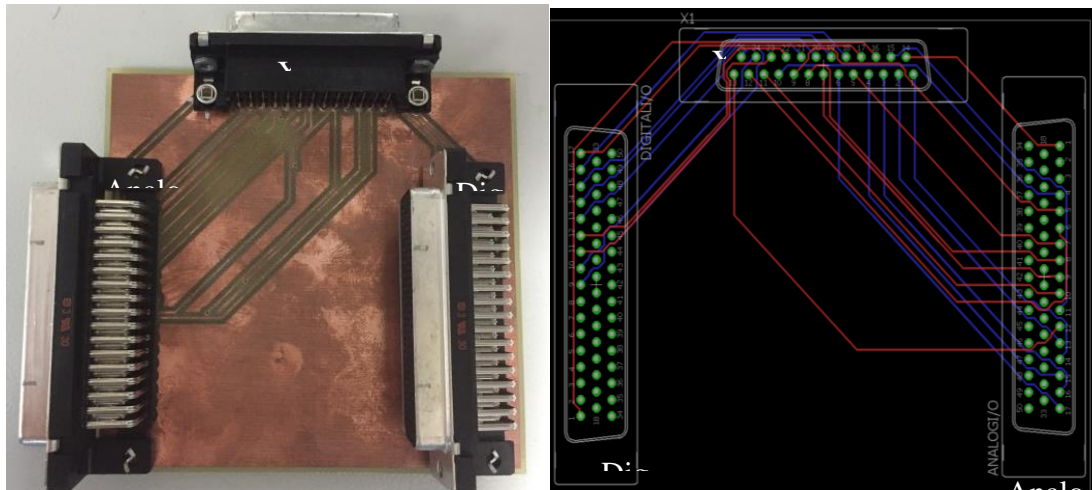


(a)                                              (b)

Fig. 5.8 (a) The completed PCB diversion board and (b) the schematic diagram of the PCB diversion board

Connectors from Fig. 5.8 (a) are connected to digital and analogue sockets on dSPACE MicroLabBox's panel respectively, as shown in Fig. 5.9. For this product, the manufacturer does not allow users to self-define pins but offers a table of pre-defined functions for all pins. The definitions of these pins can be found on the top of the MicroLabBox or in the manual [151].

Fig. 5.9 The front panel of the dSPACE MicroLabBox

As for the digital I/O connectors, the digital reference signal can be connected to several pins pre-defined by the manufacturer, according to [151], these pins are denoted as 'GND'. However, as for analogue I/O connectors, the pin denoted as 'GND' cannot be used as analogue reference as they are shared with digital ground. In that case, analogue measurements would suffer some levels of DC offset. As each pin is allocated to a channel or its reference channel, the correct solution is to connect measurements to different channels, i.e. ch1-ch24 according to [151], while the analogue ground should be connected to corresponding channels with overbar, i.e. $ch1$ and $\overline{ch1}$. Therefore, these reference channels with overbars on the MicroLabBox are parallel-connected to the analogue ground pin of the PCB.

## 5.4.6  dSPACE ControlDesk v5.5

The monitoring and control over TCSC device are achieved by using a dSPACE-developed software suitable for MicroLabBox, the ControlDesk v5.5. This software is linked to Matlab and provides an additional library DS1202 for ADC blocks for MicroLabBox. Connections to DSpace have to be conFig.d and compiled by Matlab Simulink and the supported library before the model runs in the ControlDesk v5.5, as shown in Fig. 5.10.
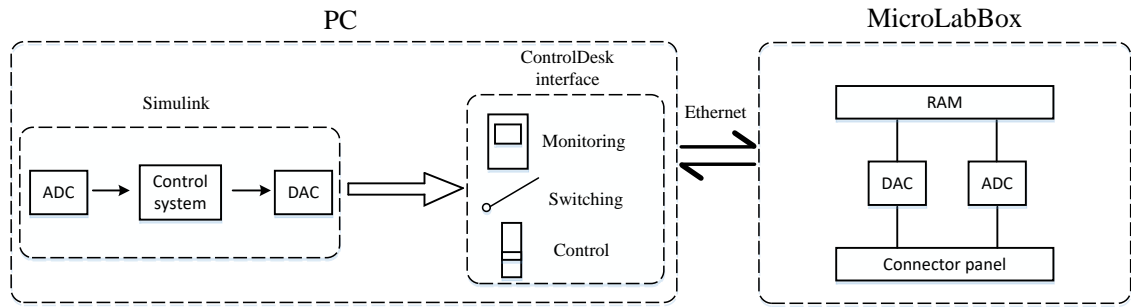
Fig. 5.10 Block diagram of the PC and the dSPACE MicroLabBox connection

In MATLAB Simulink, the ADC/DAC blocks are supported by the Real Time Interface (RTI) block library, DS1202 in this case, which is a pre-defined library by dSPACE [152]. The RTI allows a smart and automatic implementation of Simulink models on the real-time hardware. After compiling, some files are generated by MATLAB Simulink and can be read in ControlDesk v5.5. Particularly, the file xxx.map is of most importance as it contains the information of the MATLAB Simulink model and its variables, which can be monitored or controlled in ControlDesk v5.5.

## 5.5 CONFIGURATION OF THE TCSC TEST RIG FOR SSR STUDY

The studied system is based on the IEEE FBM system and the mechanical parameters of the synchronous generator and multi-mass models are obtained from [150]. However, due to the output limitation is 1kVA from the grid simulator amplifier in the laboratory, the study system is modified and scaled to fit this restriction. This affects both the HV system model in the RTDS and the voltage level of the TCSC test rig at LV.

For the TCSC device in the lab, parameters of its components cannot be changed, i.e. the capacitance or inductance. However, this device is designed with the HV system with a scale factor in base impedances between the LV and HV systems as

discussed in section 5.3.2. The scale factor should be kept the same to maintain a correct information exchange between HV and LV systems, therefore, new ratings are selected for both LV and HV systems. As the power rating of the grid simulator amplifier is 1kVA, therefore, new voltage rating and current rating are needed. Assuming the terminal voltage rating to be 50V rms phase-to-ground, and the current rating is selected to be 6A rms per phase. Thus, the three-phase power can be determined as:

$$S_{3phase} = 3 * V * I = 3 * 50 \text{ V} * 6 \text{ A} = 900 \text{ VA} \qquad (5.15)$$

The single phase power rating is 300VA. Then the per-unit calculation for the LV TCSC test rig can be given as:

$$V'base_{Rig} = 50 \text{ V}, \ P'base_{Rig} = 300 \text{ VA} \qquad (5.16)$$

$$I'base_{Rig} = \frac{P'base_{Rig}}{V'base_{Rig}} = \frac{300 \text{ VA}}{50 \text{ V}} = 6 \text{ A} \qquad (5.17)$$

$$Z'base_{Rig} = \frac{V'base_{Rig}}{I'base_{Rig}} = \frac{50 \text{ V}}{6 \text{ A}} = 8.33 \ \Omega \qquad (5.18)$$

The new base parameters are denoted with a superscript to indicate that they are designed for the modified study system. To keep the scaling factor obtained in section 5.3.2 unchanged, the new base values for the RS should be derived as:

$$Z'base_{RS} = \frac{Z'base_{Rig}}{scale \ factor} = \frac{8.33 \ \Omega}{0.2075 \text{ pu}} = 40.16 \ \Omega \qquad (5.19)$$

$$Make \ V'base_{RS} = 50 \ kV, thus \ I'base_{RS} = \frac{V'base_{RS}}{Z'base_{RS}} = \frac{50 \text{ kV}}{40.16 \ \Omega} = 1.24 \text{ kA} \quad (5.20)$$

$$P'base_{RS} = V'base_{RS} * I'base_{RS} = 50 \text{ kV} * 1.24 \text{ kA} = 62.25 \text{ MVA} \quad (5.21)$$

Therefore, parameters of the modified FBM system can be determined using above calculation results. Their per-unit values are kept the same from [150], but their actual

values are changed with the new base values presented above. These components that modelled in RSCAD/RTDS are given in Table 5.3, and the modified study system is shown in Fig. 5.11.

Table 5.3 Parameters of components in the modified FBM system in RSCAD/RTDS

| | Modified FBM system model parameters | | | | |
|---|---|---|---|---|---|
| | Voltage | Power | Transformer leakage impedance | Line inductor | FSC capacitor (20% compensation) |
| per-unit | 1 pu | 1 pu | 0.14 pu | 0.5 pu | 0.128 pu |
| Actual value | 50 kV | 186.75 MVA | 18 mH (5.62 ohm) | 64 mH (20.08 Ω) | 620 µF (5.14 Ω) |
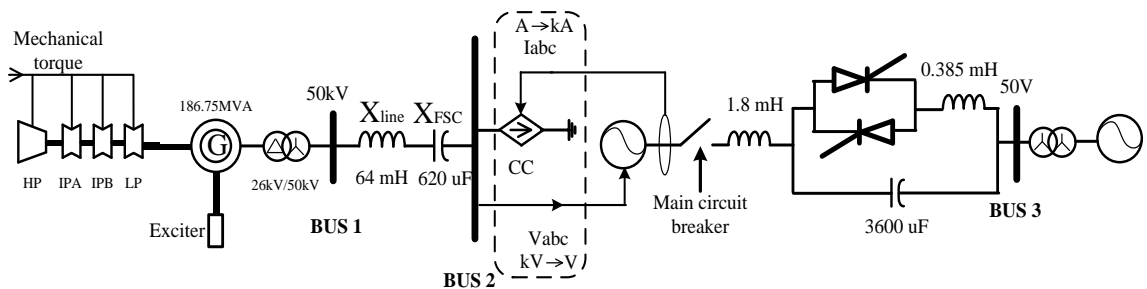


Fig. 5.11 Single line diagram of the modified study system

## 5.6 SYNCHRONISING AND INTERCONNECTING GRIDS

In the AC system, the synchronization between two grids can be a challenge as the transient current can exceed the rating level and cause damages to equipment when two grids are interconnected. As in the TCSC test rig, the closure of the main circuit breaker stands for the connection between the AC grid and the power system simulator. As the phase angle of the AC grid is uncontrollable, a large phase angle difference

between the AC grid and the output of the power amplifier can cause high current flowing through the TCSC test rig. This condition should be avoided and some countermeasures must be taken.

Inserting external resistors will limit the transient current when closing the main circuit breaker, and these resistors are by-passed when the test rig gets stable. However, this requires additional three-phase resistors along with corresponding by-pass switches, which is beyond the scope at the moment of design. Therefore, in this TCSC test rig, the solution is to add a virtual temporary voltage source within the RTDS and control the voltage output to limit the current during the start-up period. In this way, a link between the AC grid and the simulated high-voltage system is established. Then it can be regarded as the AC grid has been synchronized to the power system simulator through a paralleled link.

Fig. 5.12 shows the configuration of for network synchronizing. Before the closure of the main circuit breaker, the test rig stands as an open circuit. The voltage at bus 2 is regulated to be slightly lagging that at bus 3, by adding a time delay of 10 us to the voltage measurements from the VT located at bus 3, and feeding that waveform to S2 with proper scaling up. This small time delay of 10 us is only 0.05% of a full cycle time at 50 Hz, so it can be roughly neglected. The reason of applying this delay is to make sure the simulation in RTDS runs smoothly during start-up period. Since the phase difference between S2 and S3 is very small, i.e. 10us, it can be assumed that S2 represents S3 in the HV system in RTDS. In this way, the power system simulator, whose voltage output is determined by the synchronous generator G, is synchronized to S3 with some power flow through link between generator G and S2. Meanwhile, the mechanical torque input to the generator G is reduced to make the output current as small as possible. The power flow between generator G and load S2 can be

100

monitored and be limited to a secured level. When the main circuit breaker is closed, the link between generator G and S3 is established and part of the power is delivered through this link. This ensures that the power flowing between generator G and the load S3 is limited to safe level and the transient current is controlled by regulating the output of the generator G.
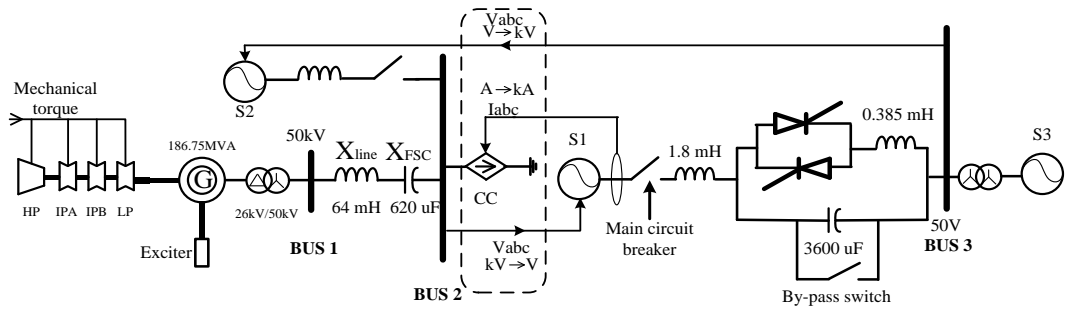


Fig. 5.12 The modified network for grid synchronizing

Once the system is stable, the link between S2 and Bus 2 will be removed by opening the circuit breaker located next to S2. Then the system is restored to the system depicted in Fig. 5.11.

## 5.7 COMPARISON BETWEEN SIMULATION AND REAL TIME EXPERIMENT RESULTS

An initial test is carried out to examine the dynamics of the platform, with the current mitigation technique. A simulation using RSCAD/RTDS is conducted based on the system shown in Fig. 5.12, to check the transient current that would occur with the main circuit breaker closed. All the physical components, the TCSC device and the AC grid are modelled within RSCAD with the scaled parameters indicated in Fig. 5.12. Fig. 5.13 shows the real-time simulation results of phase A current in RTDS. The change in Fig. 5.13 (a) indicates the main circuit breaker is closed, which happens at around 1s in the timeline. At this moment the capacitors and TCR are by-passed. The

transient current grows to -10 A peak value and oscillates at around 0.833 Hz, which is a low-frequency oscillation. The oscillation is slowly damped that even after 4s the oscillation is still observable. The steady-state current is expected to be around 5A peak-to-peak.
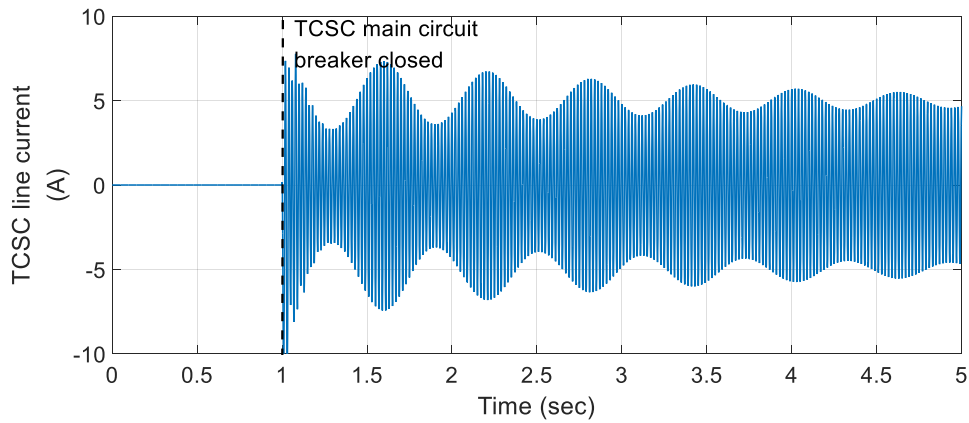


(a)
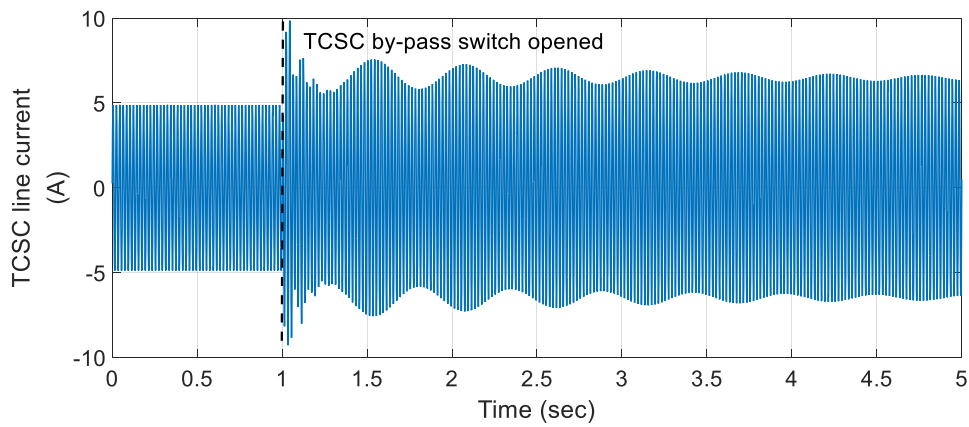


(b)

Fig. 5.13 (a) Simulated phase A current after the closure of the main circuit breaker and (b) after the opening of by-pass switch to put capacitors in the network

In Fig. 5.13 (b), continued from Fig. 5.13 (a), the change is due to the opening of the by-pass switch. This puts capacitors into the network and causes the transient

current to grow to around 10 A peak value. Compared with the current in Fig. 5.13 (a), the oscillation is damped in a faster way, which indicates the series compensation is helpful in damping low frequency oscillation. After 2.5s the oscillation is damped and the current gets steady to around 6A peak-to-peak.
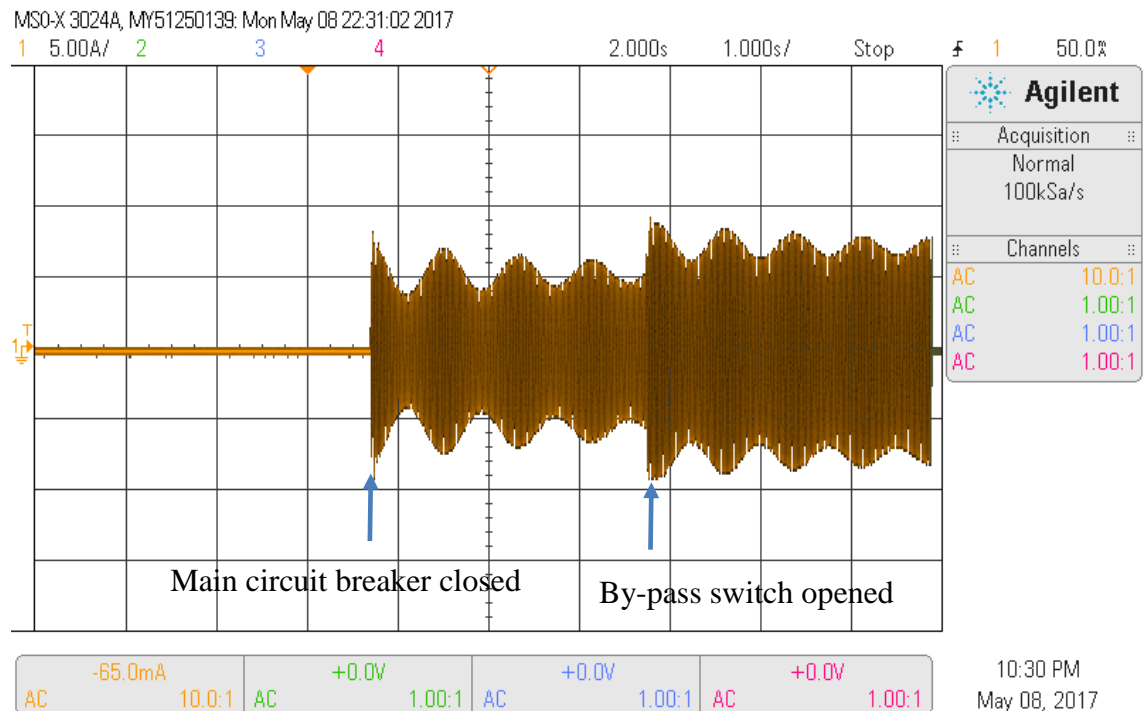


Fig. 5.14 TCSC test rig phase A current measured by a CT during start-up period

Fig. 5.14 shows the real-time experimental phase A current obtained from a CT and monitored on an oscilloscope, with the TCSC test rig connected. The CT is measuring current that flows out of the grid simulator amplifier. The Y axis is the current magnitude of 5A/step, and the X axis is the time of 1s/step. When the main circuit breaker is closed, the current flow increases to around 9A peak value at its first swing, which is slightly smaller than that in the simulation. The low frequency oscillation still exists as that was illustrated in the simulation and it is slowly damped. After 3s, the by-pass switch is opened to put capacitors in the network. This increases the current

peak value to around 9.5A, which is within our limitations (<10A) and a bit smaller than simulation results. These results indicate that the actions of synchronizing are successful and the real-time experimental results match the simulation results with very small difference.

## 5.8 SUMMARY

In this chapter, the TCSC platform for SSR testing is presented. The combination of the grid emulator, RTDS, and the hardware TCSC device, allows a detailed research into but not limited to SSR problems.

The connection of the TCSC platform is validated successfully with some basic tests. An interconnection challenge is found in the commissioning mission and a solution is proposed to solve the challenge by inserting a virtual parallel transmission line. The effectiveness of the solution is tested in the simulation and then validated by real-time experiments. The simulation results agree with the experimental result, which proves the solution is working properly.

Other sub-synchronous interaction phenomena can also be studied on this platform, i.e. SSCI between series compensation (provided by TCSC) and wind turbines (modelled in RTDS). And the implementation of control systems based on the DSpace module allows flexible modification to suit different scenarios.

# Chapter 6

# Mitigation of SSR– a supplementary damping controller for TCSC

## 6.1 INTRODUCTION

There have been a lot of research on TCSC's controllability and its application in SSR mitigation. Among those installed TCSC projects around the world, TCSC is usually operated with a constant firing angle control under normal conditions, while a closed loop controller can be activated for power oscillation damping purposes, i.e. the Kayenta TCSC project and the Slatt TCSC project [153]. In terms of SSR mitigation, researchers have stated that the commonly used closed-loop controllers of TCSC cannot mitigate SSR events but can contribute more damping compared with open-loop control scheme [154-156].

To fully eliminate SSR impacts, some supplementary damping controllers have been proposed [134, 157-161]. However, the robustness and adaptability of these supplementary controllers limit their applications in real power systems. Therefore, this chapter proposes a new supplementary controller for SSR mitigation. This controller can effectively distinguish sub-synchronous components from fundamental components, and act quickly to mitigate SSR. The novelty of this control scheme is provided by the high-performance filter and multi-channel control loops. However, some disadvantages may exist as the design of the control scheme need information about the generator torsional modes, which is difficult to be obtained. Its control structure and advantages compared with conventional controllers are discussed.

Validation of the effectiveness of the proposed controller is provided with simulation results in PSCAD/EMTDC and hardware experimental platform.

## 6.2 REVIEW OF TCSC SUPPLEMENTARY DAMPING CONTROLLER FOR SSR

The intention of actively using TCSC to mitigate SSR problems raises a lot of research ideas. Among these ideas, a critical topic is the development of a supplementary SSR damping control scheme. Unlike other closed-loop control schemes of TCSC, the supplementary damping control scheme is only designed for SSR mitigation. The control scheme should be only activated when SSR phenomenon is detected in the network, which can be observed in the generator mechanical torques and the electrical power output.

There have been several TCSC control schemes proposed in [162-165]. The Synchronous Voltage Reversal (SVR) scheme discussed in [163, 164] presents the maintenance of TCSC fundamental impedance through synchronising the voltage zero-crossing points under impacts of SSR. An iterative calculation based on instantaneous measurements is conducted within each cycle to vary the instants of thyristor triggering. However, the control objective of this scheme is the impedance of TCSC at synchronous frequency, and its effectiveness in SSR mitigation is limited within lower TCSC boosting factors. A Sub-Synchronous Damping Controller (SSDC) is proposed in [134, 157-158] and [160, 161] to measure and control the electrical damping within sub-synchronous frequency ranges with TCSC. The generator rotor speed derivation is used to extract the sub-synchronous information and to derive the firing angle variation. The design of these SSDC is also difficult that the phase lags caused by the conventional bandpass filter are varying at different sub-synchronous

frequencies. This increases the difficulty in designing phase compensators for different SSR modes. In [159], the author proposed a solution with multi-channels to individually design the phase compensator for different SSR mode. But the poor performance of conventional bandpass filters is still causing problems in designing when the sub-synchronous frequency is close to its cut-off frequency.

In the above control schemes, to detect the phasor information of sub-synchronous components, remote signals at the generator side, including the rotor speed and the generator electrical torque. This increases the phase delay between the actual sub-synchronous components and measured sub-synchronous components and requires careful phase compensation before these components can be used in the SSDC.

In order to utilise advantages of the supplementary SSDC, the adaptability and robustness of SSDC needs to be improved. The priority is to extract the sub-synchronous information with local measurements which can provide a faster response, and to solve the variable phase lags caused at different sub-synchronous frequencies caused by conventional bandpass filters.

### 6.3 A NEW CONTROLLER WITH LOCAL MEASUREMENTS ONLY

### 6.3.1 Control principle

To monitor SSR problems in power systems, there are several features that can be used to indicate SSR occurrence. The sub-synchronous component in the line current is one of them. In the GB power system, the compensated line is the main corridor connecting the Scottish power system and the England power system. Therefore, if a SSR event occurs, the sub-synchronous current must flow through TCSC device. Compared with the remote information at generator side, the benefits of using the local current measurements to extract sub-synchronous information are as follow:

- Local current measurements are easier to be obtained with CTs and the communication delay caused by distant data transmitting can be avoided.

- By using D-Q transformation on the current measurement, the Q-axis current contains only DC component and sub-synchronous components, which solves the challenge to distinguish sub-synchronous component from synchronous component.

- To detect SSR events, monitoring units are distributed at different generators under SSR risks. This is simplified by centralising the SSR detection at TCSC site only.

The mechanism of SSR problem is the sub-synchronous current flowing back to turbine generator rotor to cause the interaction. Therefore, a solution to mitigate SSR problems is to eliminate these sub-synchronous currents so that the interaction is weakened or even removed.

The small signal test is a conventional method to investigate the frequency response of TCSC [166-168]. Based on the test system configuration in [166], when the firing angle is replaced by an oscillating component sub-synchronous frequency $\omega_{sub}$, the TCSC will induce a sub-synchronous current accordingly at a frequency of $\omega_0 - \omega_{sub}$. In this way, if a sub-synchronous current $i_{sub}$ is observed in the system, the supplementary controller can inject a harmonic $\Delta\alpha$ into the firing angle of TCSC to induce another sub-synchronous current $i_{sub}{}'$. The target is to make sure the phase different between $i_{sub}$ and $i_{sub}{}'$ is around 180°.

According to the simulation results using the small signal test, the phase angle of the induced sub-synchronous current $\overline{i_{sub}}{}'$ is between 80~100° lagging the phase angle of $\Delta\alpha$. Therefore, when the sub-synchronous current $i_{sub}$ is given, the

supplementary control can measure its phase angle and generate the harmonic firing angle $\Delta\alpha$ compensated by 90° lagging. In this way, the two sub-synchronous currents are almost in opposite directions and will cancel each other. Fig. 6.1 shows the polar diagram of the sub-synchronous current $\overline{i_{sub}}$, and how $\dot{\Delta\alpha}$ can be varied to induce the $\overline{i_{sub}}'$ to cancel $\overline{i_{sub}}$.
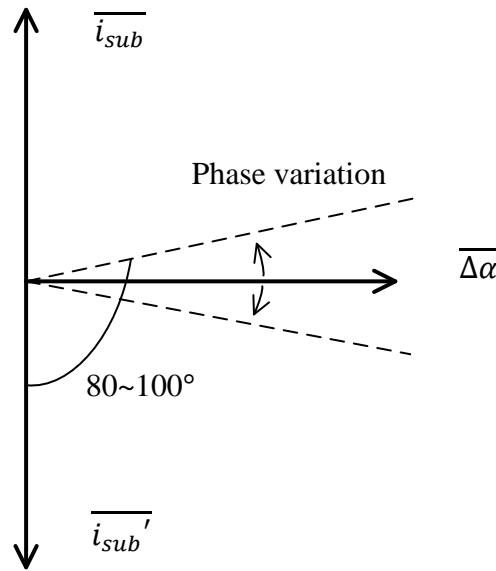


Fig. 6.1 Polar diagram of $\overline{\boldsymbol{i_{sub}}}$, $\overline{\Delta\boldsymbol{a}}$ and induced $\overline{\boldsymbol{i_{sub}}}'$

It should also be noted that the SSR risks are all due to the installation of the series compensation between the Scottish and England power systems. This means sub-synchronous components can only be flowing through this corridor and can be controlled by the series connected TCSC. With this control SSDC scheme, the mitigation of SSR via this link can be achieved.

### 6.3.2 Structure of the SSDC

Compared with normally used closed-loop Constant-Impedance (CI) or Constant-Current (CC) control, the supplementary SSDC is more focused on SSR mitigation rather than normal TCSC operation. Therefore, the supplementary controller is only activated when SSR problem is observed in the system, while the normal open-loop or closed-loop control are operated throughout the time. This allows TCSC to recover to designed compensation level fast after the occurrence of SSR.

The structure of the proposed SSDC cooperating with the basic control loop of TCSC is depicted in Fig. 6.2. The input to the supplementary controller is the local current measurement. For conventional damping schemes with bandpass filters, one of the limitations is that their poor performance at frequencies close to the synchronous frequency. For example, in a 50 Hz system, most bandpass filters can only cover up to 40 Hz. If a SSR event is at higher frequency that is close to 50 Hz, that sub-synchronous component cannot be distinguished from the synchronous component. To solve this challenge, a DQ transformation is conducted to obtain the d-axis component of the line current. In this way, the synchronous component in the line current is transformed into DC component, while the sub-synchronous component is changed to its complementary frequency. Different from conventional bandwidth filters, several independent Resonant Filters (RF) are used to replace the bandwidth filter. Each RF focuses on a potential SSR frequency which can be obtained from manufacturers or pre-studies. The d-axis current, $i_d$, is sent to these RFs. The outputs of the RFs will be sub-synchronous components which will be considered as $\Delta\alpha_i$ after scaling and phase compensation. Here $i$ denotes the ith torsional mode in potential. The sum of all $\Delta\alpha_i$ gives the overall $\Delta\alpha$ forms the final firing signal input with $\alpha_0$.

Fig. 6.2 The structure of TCSC control strategy

The synchronisation signal is obtained based on the TCSC capacitor voltage $V_{TCSC}$ through PLL block. Along with the finalised firing angle which is the sum of $\alpha_0$ and $\Delta\alpha$, the synchronisation signal are sent to the pulse generator to produce the firing pulses. These pulses are delivered to thyristors accordingly. $\alpha_0$ is the reference firing angle used in the open-loop control loop for TCSC.

### 6.3.3 Phase compensation

The phase compensation is to make sure the induced sub-synchronous current would cancel each other to weaken the interaction between them and turbine shafts. In conventional solutions, the phase compensators for different torsional modes have to be approximated as the phase shifts caused by filters are varying at different frequencies. Compared with conventional bandpass filters, whose bode diagram is shown in Fig. 6.3 (a), an ideal RF has the advantage in its very high gain at the

111

characteristic frequency while very little gain at other frequencies. This allows a more accurate information extraction than conventional bandpass filters. Moreover, a RF does not cause phase shift at the characteristic frequency, as depicted in Fig. 6.3 (b). This allows an easier design of phase compensator for each torsional mode and better performance.

Fig. 6.3 (a) shows the typical band-pass filter with bandwidth from 20 Hz to 40 Hz. When the input signal is through this filter, the phase shift caused by the filter varies at different frequencies, up to $\pm 45°$. This is causing a lot of difficulties in designing phase compensators for different SSR modes located within this bandwidth with conventional SSDCs. An average phase compensation is to be made to approximately compensate the phase shifts caused by the band-pass filter, where the performance of the SSDC can be poor. However, in Fig. 6.3 (b), the phase shift challenge is solved since the RF has very narrow frequency response and ideally zero phase shift. For any given SSR modes, different RFs can be designed to extract the sub-synchronous components without causing phase shift. This allows the designer to only consider the phase compensator based on the polar diagram as shown in Fig. 6.1 to induce an opposite sub-synchronous current.

The control diagram is constructed as shown in Fig. 6.3. The phase compensation is provided by a fixed delay block, which compensates one quarter of a cycle time related to the sub-synchronous component. The term $\omega_c$ is referring to the sub-synchronous frequency, while $T_c$ is the corresponding cycle time. Since the delay block does not affect the gain-frequency characteristic of the filter, its accuracy is secured in this way.
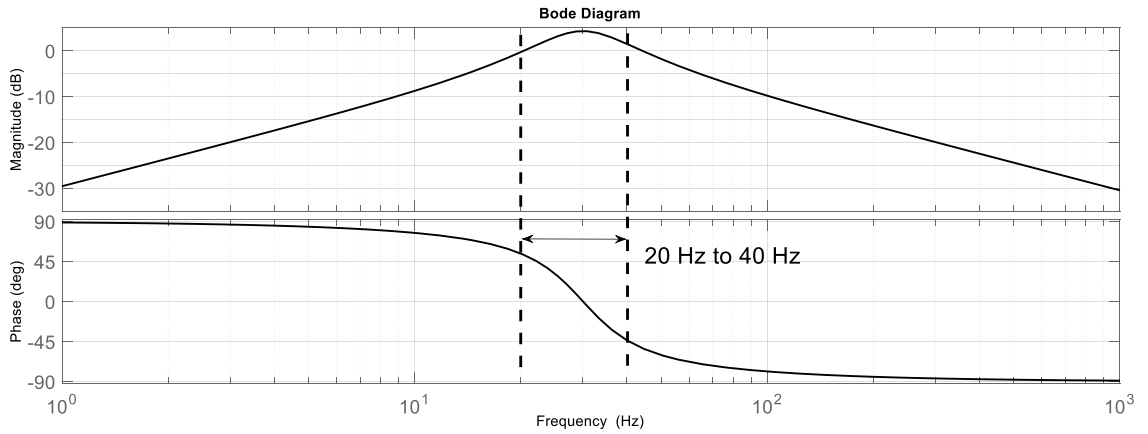
(a) Frequency response for a conventional band-pass filter covering 20-40 Hz
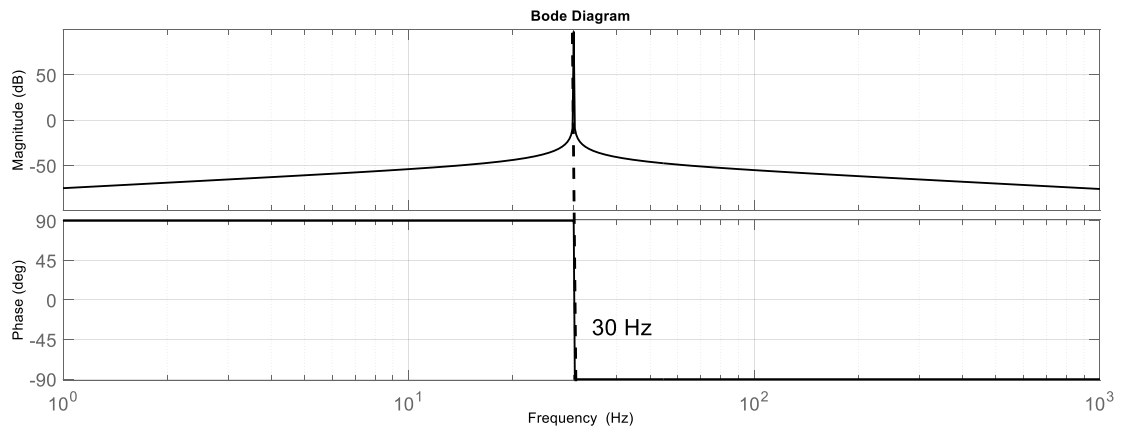


(b) Frequency response for a RF with characteristic frequency at 30 Hz

Fig. 6.3 Comparisons between band-pass filter and RF in gain and phase margins
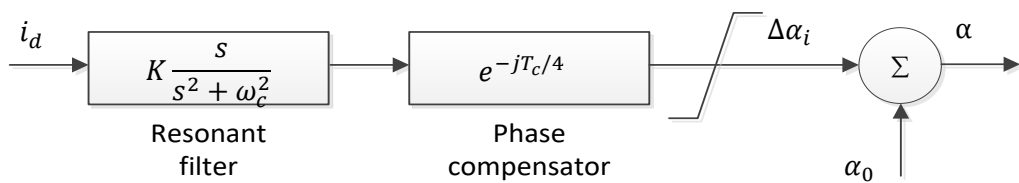


Fig. 6.4 Control block diagram

For each potential torsional mode, a control loop as shown in Fig. 6.4 is designed. The output of each control loop is denoted as $\Delta\alpha_i$ and represents the harmonic at

specific sub-synchronous frequency. The outputs of all control loops considering all torsional modes will be summed together with the initial firing angle $\alpha_0$ to form the final firing angle α sent to trigger TCSC device. However, it should be noted that if a torsional mode is not excited at all, the corresponding output of that control loop will be quite small so that it will not affect the overall control of TCSC.

### 6.4 SOFTWARE SIMULATION AND HARDWARE VALIDATION

### 6.4.1 Test system

The system under test is a single line transmission system as shown in Fig. 6.5. The mechanical dynamics of the turbine generator is modelled as 4 masses, denoted as HP, IPA, IPB and LP. The voltage rating of the high voltage system is at 50 kV and the power rating is 186.75 MVA. The line inductance is 64 mH and a FSC of 620 uF is inserted to provide a basic compensation of 30%. The low voltage circuit is to represent the TCSC test rig in the lab, which is working at 50 V and 6 A rating. The equivalent compensation provided by TCSC under 160° firing angle is around 15%. The parameters of the multi-mass model are kept the same from the IEEE FBM system [64], therefore, at 45% compensation the system is about to suffer SSR at 16 Hz. To solve the problem, the proposed SSDC with local current measurements is implemented.
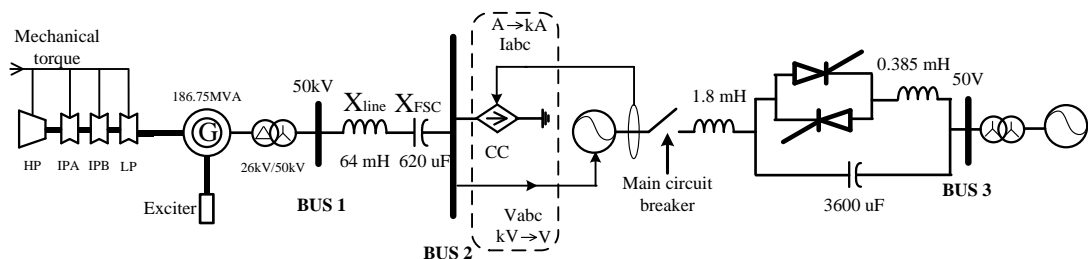


Fig. 6.5 Single line diagram of the test system in PSCAD/EMTDC

### 6.4.2  Simulation results and hardware validation

In this test, the effectiveness of the proposed SSDC is validated. The synchronous generator with multi-mass model to model the turbine mechanical dynamics is delivering power along the transmission line to the AC load. Notice that the voltage level is scaled down from 50 kV to 50 V in the TCSC test rig. in PSCAD simulation, this is realised through controlled three-phase voltage source and current source, with proper scaling up or scaling down respectively, as indicated in Fig. 6.5.

TCSC is activated throughout the test and the system is having a compensation of 45%. A disturbance is applied at 4s to excite SSR event. The SSDC is not activated until 6s after SSR event. This is to allow SSR event to grow so that it can be clearly observed. In real projects, a threshold of the magnitude of SSR in line current can be used to trigger the SSDC.

Results from both digital simulation and experimental tests indicate the effectiveness of the proposed SSDC (see Fig. 6.6 and Fig 6.7 respectively). Before the SSDC is activated at around 10 s, the firing angle of TCSC is kept at 160 degree as an open-loop control. During this period, the SSR event triggered at 4 s by the disturbance is growing. This can be reflected from figure (b) rotor speed and figure (d) exciter-generator torque waveforms. The zoomed-in plot of the exciter-generator torque illustrates that the SSR event is at around 16 Hz. After 10s, when the SSDC is activated, the firing angle is injected with an oscillating component which is derived based on the sub-synchronous component in the line current. With this control, the growing oscillations in the rotor speed and exciter-generator torque are being damped.
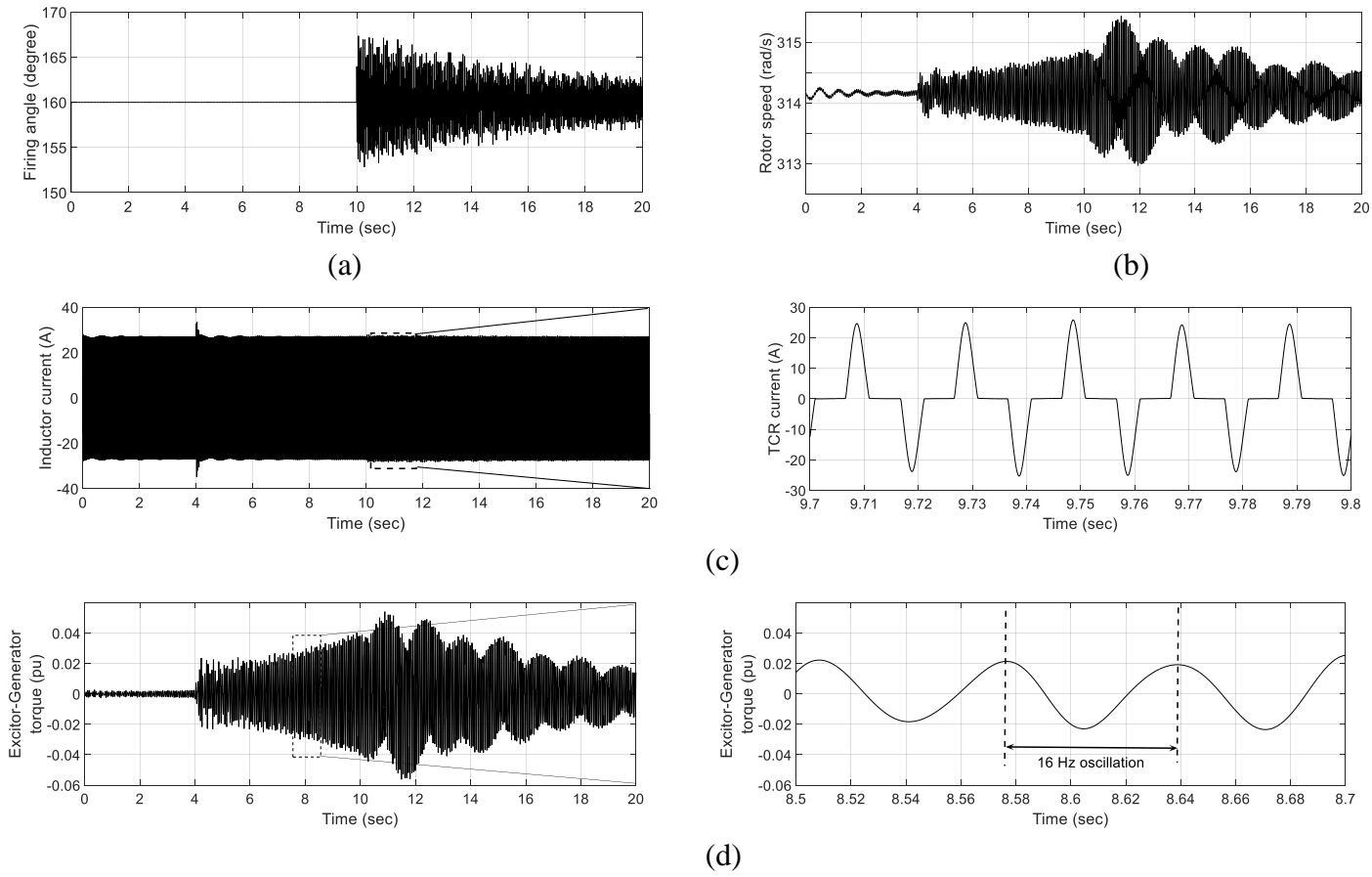
Fig. 6.6 Waveforms of (a) TCSC firing angle (b) Generator rotor speed (c) TCR current and its Zoom-in (d) Excitor-Generator torque and its zoom-in obtained from PSCAD
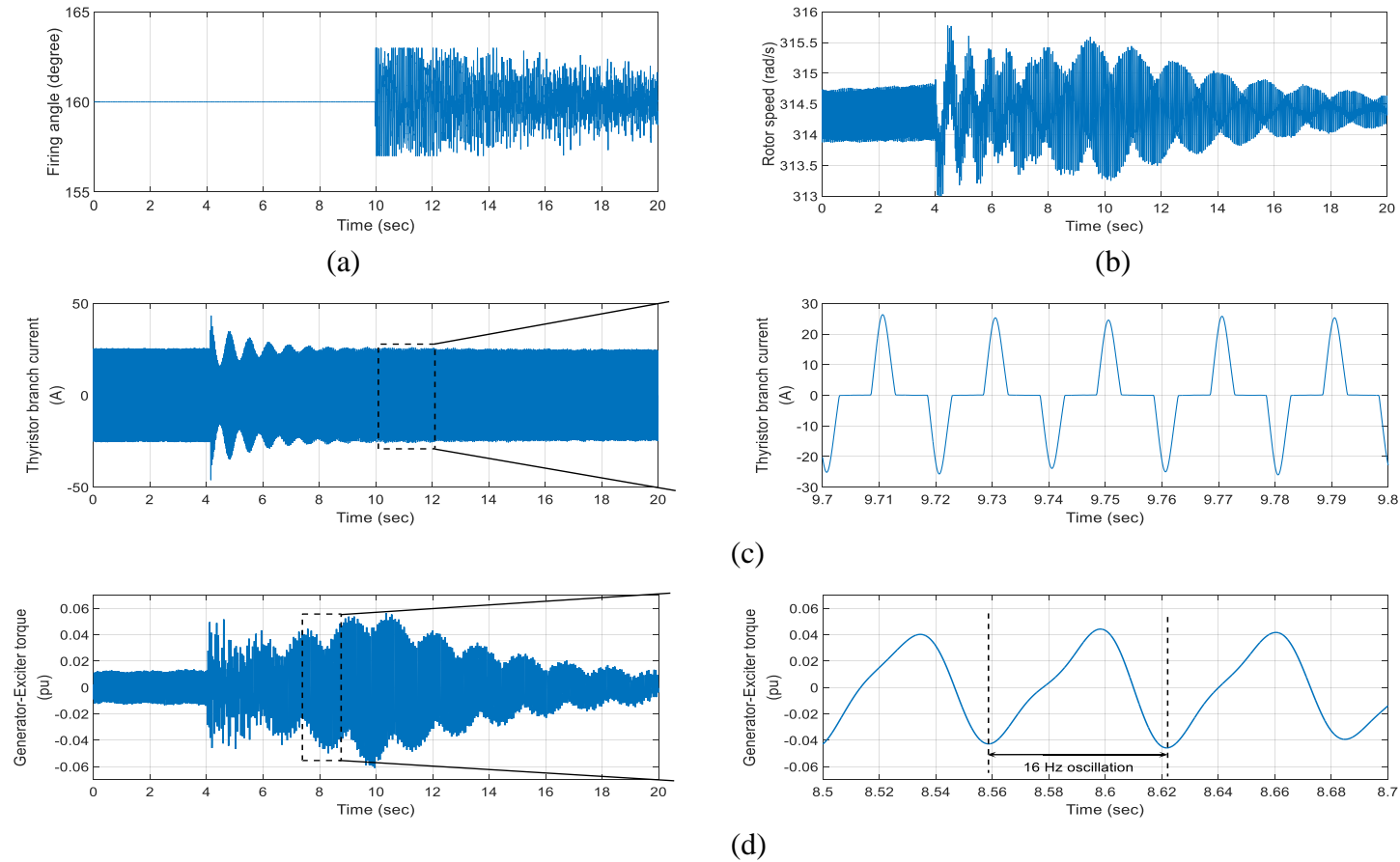
Fig. 6.7 Waveforms of (a) TCSC firing angle (b) Generator rotor speed (c) TCR current and its Zoom-in (d) Excitor-Generator torque and its zoom-in obtained on the experimental platform

By comparing the Fig. 6.6 and Fig. 6.7, the simulation results and experimental results match each in the trend very well. There are a few differences in the start-up period before 4s. This is due to the start-up period in PSCAD is very short while the experimental platform has to be operated for a few minutes to get into the steady-state. Therefore, the initial rotor speed and exciter-generator torque are much higher on the platform than that in the PSCAD simulation. Additionally, the disturbance applied at 4s is causing more oscillations on the experimental platform than in the PSCAD simulation. But the overall trend in SSR damping and control dynamics indicate the experimental platform is following the simulation model.

## 6.5 SUMMARY

This chapter presents the limitation of conventional SSDCs and the challenge in practical projects. The low adaptability of conventional SSDCs with band-pass filters requires lots of work to redesign the control system for new SSR problems. Besides, the unavoidable delay caused by remote information transmitting from the generator side to the SSDC reduces the accuracy and reliability of conventional SSDC scheme.

To solve the above limitations and challenges, modifications are conducted to propose a new supplementary damping control scheme. This new scheme uses only line current as input to extract sub-synchronous information. The conventional band-pass filter is replaced by the resonant filter with better performance in the phase and gain margins. This increases the accuracy of sub-synchronous extraction and the performance in discriminating sub-synchronous components from fundamental components. Moreover, multiple control loops are designed to individually focus on each known SSR frequency. As each control loop is operated and phase shifted

separately, it is easier to insert new control loops for new SSR modes without distorting other loops.

The effectiveness of the proposed SSDC scheme is validated in PSCAD simulation and the results are promising. A physical TCSC device is used to perform real-time experiments. The matching of simulation results and experimental results indicate the proposed SSDC is effective and the method is practical to be implemented on real TCSC sites.

# Chapter 7

# Conclusions and future work

## 7.1 CONCLUSIONS

### 7.1.1 Inherent capability of TCSC in SSR mitigation

TCSC has been installed in the GB power system. To investigate the damping contribution of TCSC in mitigating SSR, the inherent characteristic of TCSC is studied in this work.

Due to thyristor regulation, a TCSC can behave as a resistor within sub-synchronous frequency ranges even the thyristors are fired at a constant firing angle. This resistive behaviour is caused by the power conversion ability of TCSC. Power carried by sub-synchronous currents is transformed into components at the synchronous frequency. In this procedure, sub-synchronous power seems to be consumed by TCSC thus TCSC behaves like a resistor at these frequencies. At synchronous frequency, additional power transformed from sub-synchronous frequencies is induced by TCSC thus TCSC behaves as a negative resistor at synchronous frequency.

With the power conversion ability, TCSC weakens the interaction between the turbine shaft system and the electrical resonant component. The investigation into the electrical damping provided by TCSC with the complex torque coefficient method indicates that the trend of the improved electrical damping is similar with the resistance-frequency curve of TCSC within sub-synchronous frequency ranges. It

proves the improved electrical damping is highly related to the power conversion ability of TCSC at different frequencies.

### 7.1.2  Physical TCSC platform

A physical TCSC device is designed and configured to form the experimental platform. The control system of the TCSC device is implemented on a master computer via dSPACE MicroLabBox and the dSPACE ControlDesk software. The platform is interconnected with the grid emulator, which consists of a RTDS and a power amplifier, to establish the interaction with a HVAC system. Currents flowing through the TCSC platform are fed back to the grid emulator to reflect dynamics in the platform.

The commissioning of the device is completed with some early tests on the basic operations of TCSC and switching of circuit breakers. The results indicate that the TCSC platform is working correctly. SSR is implemented on the platform for testing, and can be clearly observed in the power and current flow through the platform. Experimental tests find that TCSC with a constant firing angle control scheme is not able to damp SSR. The proposed SSR damping controller is implemented on the platform and the effectiveness is validated on the platform.

### 7.1.3  Control scheme of TCSC for SSR mitigation

The mechanical dynamics of the turbine generator shaft is modelled in the grid emulator and the SSR problem is realised on the TCSC platform. The voltage output of the grid emulator is observed with distortions of sub-synchronous components.

Supplementary damping controllers for TCSC to solve SSR have been proposed by many researchers. But the limitations of conventional SSDC make it impractical in industrial projects, due to the low adaptability of traditional band-pass filters and the

remote information required at the generator side. A modified damping control scheme is proposed in this thesis to eliminate above limitations. The proposed damping control scheme uses only local current measurements as input and adopts resonant filters to replace conventional band-pass filters. Besides, the application of multi-channel control loops allows the SSDC to be modified for new SSR modes since each control loop is individually designed for one SSR mode only.

Validations of the effectiveness of the proposed SSDC scheme are conducted both on the PSCAD/EMTC simulation software and on the experimental platform of TCSC. The comparisons between the simulation results and the experimental results show good agreements with each other. Both results indicate that the proposed SSDC scheme provides a fast damping performance to SSR problems.

## 7.2 FUTURE WORK

The work presented in the thesis can be extended in the future as follow:

### 7.2.1 Integration of TCSC platform with Multi-Terminal DC (MTDC) network

With the integration of the HVDC links into the GB power system, the interaction between MTDC network and the AC system is drawing lots attention. Topics in this area can be the impacts of faults in AC/DC systems on DC/AC networks, interactions between DC converter control systems and power electronics devices in AC systems, and protection schemes. At Cardiff University, a 4-terminal MTDC network has been constructed and can be interconnected with the TCSC platform to form an AC-DC interconnection.

### 7.2.2 Self-adaptive SSR damping controller for TCSC

Adaptability is an important feature of a damping controller. A controller with good self-adaptability allows the controller to self-detect SSR frequency and activate corresponding damping mode.

Under a SSR event, a reliable SSR damping controller is expected to fast discriminate the SSR frequency from other components. By selecting reasonable thresholds for the SSR detection and discrimination, the controller can switch to different SSR damping modes when the detected SSR frequency moves from one mode to another. However, this requires detailed case studies and an algorithm to detect and analyse SSR frequencies. In conventional studies, SSR detection is usually achieved by FFT analysis. This method is not practical in real projects as it requires longer response time which is not acceptable under SSR impacts. A solution can be based on Phasor Measurement Units (PMUs) which allows real time analysis and fast response. The phase delay caused by remote communication can be compensated with a fixed phase shift. Therefore, the future work should consider modifications in the SSR detection method with PMUs.

### 7.2.3 Eigenvalue analysis of the proposed scheme

Eigenvalue analysis is a strong tool for system stability study. However, due to the complexity of the power system and the high non-linearity of the proposed control scheme, eigenvalue analysis is not realised in the thesis. It is recommended to model the control scheme along with the studied system with space equations and work out the eigenvalues to predict the stability of the system under certain operation points.

# Reference

[1]. 2020 renewable heat and transport targets, [Online]. Available: https://publications.parliament.uk/pa/cm201617/cmselect/cmenergy/173/17305.htm#footnote-198

[2]. UK Energy Statistics, Q2 2017, [Online]. Available: https://www.gov.uk/government/uploads/system/uploads/attachment_data/file/647750/Press_Notice_September_2017.pdf

[3]. Road map, [Online]. Available: https://www.gov.uk/government/uploads/system/uploads/attachment_data/file/48128/2167-uk-renewable-energy-roadmap.pdf

[4]. ENSG 'Our Electricity Transmission Network: A Vision for 2020', Full report, July 2009.

[5]. System Operability Framework 2015, [Online]. Available: https://www.nationalgrid.com/sites/default/files/documents/44046-SOF%202015%20Full%20Document.pdf

[6]. Our Electricity Transmission Network: a vision for 2020, [Online]. Available: https://www.gov.uk/government/uploads/system/uploads/attachment_data/file/48274/4263-ensgFull.pdf

[7]. C. Hor, J. Finn, G. Thumm and S. Mortimer, "Introducing series compensation in the UK transmission network," 9th IET International Conference on AC and DC Power Transmission (ACDC 2010), London, 2010, pp. 1-5.

[8]. Working on high voltage series compensation equipment, [Online]. Available: https://www.spenergynetworks.co.uk/userfiles/file/31B_OPSAF-11_078%20Issue_1_MSP2.13_Working_on_HV_Series_Compensation_Equipment.pdf

[9]. GE-Exclusive Technology Helps Scottish Utility Integrate Renewable Energy and Meet Complex Grid Challenges, [Online]. Available: http://www.gegridsolutions.com/press/GEExclusiveTechnology/

[10]. Mechanically Switched Capacitor with Damping Network (MSCDN) [Online]. Available: https://www.spenergynetworks.co.uk/pages/mscdn_series_compensation.aspx

[11]. China National Bureau of Energy, "Technical specifications of series capacitor installation for 1000 kV system", 2013

[12]. System Operability Framework 2014, [Online]. available: https://www.nationalgrid.com/sites/default/files/documents/35435-SOF%202014%20Final.pdf

[13]. Lesson Learned, "Sub-Synchronous Interaction between Series-Compensated Transmission Lines and Generation", published by NERC, July 26, 2011

[14]. M. Henderson, D. Bertagnolli, D. Ramey, "Planning HVDC and FACTS in New England," *IEEE/PES Power Systems Conference and Exposition*, 2009, PSCE '09. pp. 1-3, 15-18 Mar. 2009.

[15]. M. Bongiorno, A. Petersson and E. Agneholm, "The impact of Wind Farms on Subsynchronous Resonance in Power Systems", April 2011

[16]. J. Adams, V. A. Pappu and A. Dixit, "Ercot experience screening for Sub-Synchronous Control Interaction in the vicinity of series capacitor banks," 2012 IEEE Power and Energy Society General Meeting, San Diego, CA, 2012, pp. 1-5.

[17]. A. S. Subburaj, et al. "Determination of Sub Synchronous Control Interaction between Wind Turbines and Series Compensated Transmission Lines." *International Journal of Renewable Energy Research (IJRER)* 6.3 (2016): 987-994.

[18]. Subsynchronous Torsional Interaction, [Online]. available: http://www.tdworld.com/grill-grid-masters/subsynchronous-torsional-interaction

[19]. Y. Jiang-Hafner, et al. "Improvement of subsynchronous torsional damping using VSC HVDC." Power System Technology, 2002. Proceedings. PowerCon 2002. International Conference on. Vol. 2. IEEE, 2002.

[20]. Electric Power Research Institute, "HVDC Systems Control for Damping of Subsynchronous Oscillations", EPRI EL-2708, Final Report, October 1982.

[21]. H. Björklund, K.-E. Johansson and G. Liss, "Damping of Subsynchronous Oscillations in Systems Containing Turbine Generators and HVDC Link", International Conference on Large High Voltage Electric Systems, Paris, 1980 Session, August 27 – September 4.

[22]. Y. Wang, J. Meng, X. Zhang, L. Xu, "Control of PMSG-based wind turbines for system inertial response and power oscillation damping", *IEEE Transactions Sustain. Energy*, vol. 6, no. 2, pp. 565-574, Apr. 2015.

[23] E. Giraldo, A. Garces, "An adaptive control strategy for a wind energy conversion system based on PWM-CSC and PMSG", *IEEE Transactions on Power Systems*, vol. 29, no. 3, pp. 1446-1453, May 2014.

[24]. H. Liu *et al*., "Subsynchronous Interaction Between Direct-Drive PMSG Based Wind Farms and Weak AC Networks," in *IEEE Transactions on Power Systems*, vol. 32, no. 6, pp. 4708-4720, Nov. 2017.

[25]. C. Xia, J. Wang, and K. McMenemy, "Short, medium and long term load forecasting model and virtual load forecaster based on radial basis function neural networks", *International Journal of Electrical Power & Energe Systems*, Vol. 32, No. 7, pp. 743-750

[26]. K. Clark, "Overview of subsynchronous resonance related phenomena," *PES T&D 2012*, Orlando, FL, 2012, pp. 1-3.

[27] IEEE Committee Report, "First benchmark model for computer simulation of subsynchronous resonance," *IEEE Transactions on Power Apparatus and Systems*, vol. 96, no. 5, pp. 1565-1572, Sept. 1977.

[28]. IEEE SSR Working Group, "Proposed Terms and Definitions for Subsynchronous Oscillations," *IEEE Transactions on Power Apparatus and Systems*, vol. PAS-99, no. 2, pp. 506-511, March 1980.

[29]. IEEE SSR Working Group, "Terms, Definitions and Symbols for Subsynchronous Oscillations," *IEEE Transactions on Power Apparatus and Systems*, vol. PAS-104, no. 6, pp. 1326-1334, June 1985.

[30]. P. Kundur, *Power system stability and control*. Vol. 7. New York: McGraw-hill, 1994. Chapter 15, pp. 1026-1060

[31]. P. M. Anderson, B. L. Agrawal, and J. E. Van Ness. *Subsynchronous resonance in power systems*. Vol. 9. John Wiley & Sons, 1999, Chapter 1, pp 3-4

[32]. M. C. Jackson, et al. "Turbine-Generator Shaft Torques and Fatigue: Part I-Simulation Methods and Fatigue Analysis." *IEEE Transactions on Power Apparatus and Systems* 6 (1979): 2299-2307.

[33]. D. N. Walker, S. L. Adams, and R. J. Placek. "Torsional vibration and fatigue of turbine-generator shafts." *IEEE Transactions on Power Apparatus and Systems* 11 (1981): 4373-4380.

[34]. R. Qual and A. C. Schwalb, discussion of reference 4, *IEEE Transactions on Power Apparatus and systems*, Vol. PAS-94, No. 5, pp. 1887-1888, Sep/Oct 1975

[35]. D. N. Walker, et al. "Results of subsynchronous resonance test at Mohave." *IEEE Transactions on Power Apparatus and Systems.Vol.* 94. No. 5 pp. 1878-1889, 1975.

[36]. D. G. Ramey, A. C. Sismour, and G. C. Kung. "Important parameters in considering transient torques on turbine-generator shaft systems." *IEEE Transactions on Power Apparatus and Systems* Vol. 1, pp. 311-317, 1980.

[37]. W. Watson, and M. E. Coultes. "Static exciter stabilizing signals on large generators-mechanical problems." *IEEE Transactions on Power Apparatus and Systems* Vol. 1 , pp. 204-211, 1973.

[38]. IEEE Committee Report, "Countermeasures to Subsynchronous Resonance," ibid, v. PAS-99, n. 5, Sept/Oct 1980, p. 1810-1817.

[39]. G. D. Jennings, R. G. Harley and D. C. Levy, "Subsynchronous resonance of a power station with two identical generating units," *IEEE Proceedings -Generation, Transmission and Distribution*, vol. 133, no. 1, pp. 33-43, January 1986.

[40]. B. L. Agrawal and R. G. Farmer, "Use of Frequency Scanning Techniques for Subsynchronous Resonance Analysis," *IEEE Transactions on Power Apparatus and Systems*, vol. PAS-98, no. 2, pp. 341-349, March 1979.

[41]. J. M. Undrill and T. E. Kostyniak, "Subsynchronous oscillations part 1 - comprehensive system stability analysis," *IEEE Transactions on Power Apparatus and Systems*, vol. 95, no. 4, pp. 1446-1455, July 1976

[42]. EPRI/DCG Report EL-7321, "Electromagnetic transients program – version 2: revised application guide," Nov 1991

[43]. B. Porkar, etc., "Multi-port frequency-dependent network equivalent for electromagnetic transient studies," *Proceedings of the 37th Annual North American Power Symposium,* 2005, pp. 287-295.

r[44]. D. N. Walker, C. E. J. Bowler, R. L. Jackson, and D. A. Hodges, "Results of subsynchronous resonance test at Mohave", *IEEE Transactions on Power Apparatus and Systems*, vol. PAS-94, no. 5, Sep./Oct. 1975

[45]. B. L. Agrawal, R. G. Farmer, "Use of Frequency Scanning Techniques for Subsynchronous Resonance Analysis", *IEEE Transactions. on Power Apparatus and Systems*,Vol.PAS-98, No.2, pp.341-349, Mar./Apr. 1979.

[46]. Y. Cheng, M. Sahni, D. Muthumuni, and B. Badrzadeh, "Reactance Scan Crossover-Based Approach for Investigating SSCI Concerns for DFIG-Based Wind Turbines", *IEEE Transactions On Power Delivery*, VOL. 28, NO. 2, pp. 742-751, Apr. 2011.

[47]. P. Belkin, "Event of 10-22-09," presented at the CREZ Tech. Conference, [Online]. Available: www.ercot.com/content/meetings/rpg crez/keydocs/2010/0126/8Belkin_Event%20of%2010.ppt

[48]. J. Milanovic and A. Adrees, "Identifying Generators at Risk of SSR in Meshed Compensated AC/DC Power Networks", *IEEE Transactions On Power Systems*, VOL. 28, NO. 4, pp. 4438-4437, Nov. 2013.

[49]. Y. Cheng, S. H. Huang, J. Rose, V. A. Pappu and J. Conto, "ERCOT subsynchronous resonance topology and frequency scan tool development," *2016 IEEE Power and Energy Society General Meeting (PESGM)*, Boston, MA, 2016, pp. 1-5.

[50]. P. M. Anderson, B. L. Agrawal and J. E. Van Ness, "SSR Eigenvalue Analysis- Subsynchronous Resonance in Power Systems", 1, *Wiley-IEEE Press*, 1990, pp.288-298

[51]. M. Ilic, J. Zaborsky, "Dynamics and control of large electric power systems", New York, US, John Wiley & Sons, Inc., 2000

[52]. J. G. Sllotweg, J. Persson, and A. V. Voorden, "A study of the eigenvalue analysis capabilities of power system dynamics simulation software", 14 th PSCC, Sevilla, June 2002.

[53]. S. K. Gupta, A. K. Gupta and N. Kumar, "Damping subsynchronous resonance in power systems," *IEEE Proceedings - Generation, Transmission and Distribution*, vol. 149, no. 6, pp. 679-688, Nov 2002.

[54]. D. Y. Wong, G. J. Rogers, and B. Porretta, "Eigenvalue analysis of very large power systems," *IEEE Transactions,* Vol. PWRS-3, No. 2, May 1988

[55]. N. G. Hingorani, "A new scheme for sub-synchronous resonance damping of torsional oscillations and transient torque – part 1," *IEEE Transactions*, Vol. PAS-100, pp. 1852-1855, April 1981

[56]. Z. Zhang, X. Xiao, "Analysis and Mitigation of SSR Based on SVC in Series Compensated System", International Conference on Energy and Environment Technology, ICEET '09. Beijing, China, 16-18 Oct. 2009.

[57] D. Nazarpour, H. Ghahramani, "Novel Methods with Fuzzy Logic and ANFIS Controller Based SVC for Damping Sub-Synchronous Resonance and Low-Frequency Power Oscillation",20th Iranian Conference on Electrical Engineering (ICEE), 15-17 May 2012.

[58] R. K. Varma and S. Auddy, "Mitigation of subsynchronous oscillations in a series compensated wind farm using static var compensator," IEEE Proceeding Power Energy Soceity General Meeting Conference, 2006, pp. 1–7.

[59]. B. Li, H. Xie, M. M. de Oliveira, Carl Heyman, Mauro Monge, "Mitigation of Subsynchronous Resonance in a DFIG Based Wind Power Plant Connected to Series-Compensated Lines Using STATCOM", in Proceeding 12th International Workshop on Large-Scale Integration of Wind Power into Power Systems as well as on Transmission Networks for Offshore Wind Power Plants, London, UK, 22-24 Oct. 2013

[60]. M. S. El-Moursi, B. Bak-Jensen, M. H. Abdel-Rahman, "Novel STATCOM Controller for Mitigating SSR and Damping Power System Oscillations in a Series Compensated Wind Park," *IEEE Transactions Power Delivery*., vol. 25, no. 2, pp. 429–441, Feb 2010.

[61]. S. Golshannavaz, M.Mokhtari, and D.Nazarpour, "SSR Suppression via STATCOM in Series Compensated Wind Farm Integrations", Electrical Engineering (ICEE), 2011 19th Iranian Conference

[62]. H. Khalilinia and J. Ghaisari, "Improve Sub-Synchronous Resonance (SSR) damping using a STATCOM in the transformer bus," *IEEE EUROCON 2009*, St.-Petersburg, 2009, pp. 445-450.

[63]. R. K. Varma, "Mitigation of subsynchronous oscillations in a series compensated wind farm with Thyristor Controlled Series Capacitor (TCSC)", Power Systems Conference: Advanced Metering, Protection, Control, Communication, and Distributed Resources, 2007.

[64]. A. Timbus, R. Teodorescu, F. Blaabjerg, and M. Liserre, "Synchronization methods for three phase distributed power generation systems. an overview and evaluation", Power Electronics Specialists Conference, 2005, pp. 2474-2481.

[65]. L. G. B. Rolim, D. R. da Costa, and M. Aredes, "Analysis and software implementation of a robust synchronizing PLL circuit based on the pq theory", *IEEE Transactions on Industrial Electronics*, vol. 53, no. 6, pp. 1919-1926, December 2006.

[66]. D. J. N. LIMEBEER, R. G. HARLEY, and S. M. SCHUCK, "Subsynchronous resonance of the Koeberg turbo-generator and of a laboratory systems", *IEEE Transactions on Power Apparatus and Systems ,* 1979, Vol. 70, pp. 278-297

[67]. D. J. N. Limebeer, R. G. Harley and M. A. Lahoud, "Suppressing subsynchronous resonance with static filters," in *IEEE Proceedings - Generation, Transmission and Distribution*, vol. 128, no. 1, pp. 33-44, January 1981.

[68]. X. Xie, P. Liu, K. Bai and Y. Han, "Applying Improved Blocking Filters to the SSR Problem of the Tuoketuo Power System," in *IEEE Transactions on Power Systems*, vol. 28, no. 1, pp. 227-235, Feb. 2013.

[69] Huakun Liu, Xiaorong Xie, Jingbo He, Hui Liu and Yunhong Li, "Damping DFIG-associated SSR by adding subsynchronous suppression filters to DFIG converter controllers," *2016 IEEE Power and Energy Society General Meeting (PESGM)*, Boston, MA, 2016, pp. 1-5.

[70]. H. Liu, X. Xie, Y. Li, H. Liu and Y. Hu, "Mitigation of SSR by embedding subsynchronous notch filters into DFIG converter controllers," in *IET Generation, Transmission & Distribution*, vol. 11, no. 11, pp. 2888-2896, 8 3 2017.

[71]. B. S. Nagabhushana, Chandrasekharaiah, 'SSR analysis using artificial neural networks', Proceedings ofthe International Conference on Intelligent Systems Applications to Power Systems, IEEE, Feb 1996.

[72]. B. S. Nagabhushana, Chandrasekharaiah, L. L. Lai and D. Vujatovic, "Neural network approach to identification and control of sub-synchronous resonance in series compensated systems," *Power Electronics and Drive Systems,* 1999, pp. 683-687 vol.2.

[73]. C. E. J. Bowler, J. A. Demcko, L. Mankoff, W. C. Kotheimer and D. Cordray, "The Navajo SMF Type Subsynchronous Resonance Relay," in *IEEE Transactions on Power Apparatus and Systems*, vol. PAS-97, no. 5, pp. 1489-1495, Sept. 1978.

[74]. S. Rezaei, "Behavior of protective relays during Sub Synchronous Resonance," 2017 IEEE International Conference on Environment and Electrical Engineering and 2017 IEEE Industrial and Commercial Power Systems Europe (EEEIC / I&CPS Europe)*, Milan, 2017, pp. 1-5.

[75]. G. Taylor, "Power quality hardware solutions for distribution systems: Custom power", *IEEE Symposium on the Reliability, Security and Power Quality of Distribution systems*, April 1995, Durham, UK, pp. 11/1-11/9.

[76]. M. Iravani and etc, "Application of static phase shifter in power systems", *IEEE Transaction on Power Delivery,* Vol. 9, No. 3, July 1993, pp. 1600-1608.

[77]. IEEE/CIGRE: "FACTS overview", *IEEE Special Issue*, Piscataway, NJ, USA, 1995.

[78]. N. Christl, P. Luzelberger, and K. Sadek, "System studies and basic design for and advanced series compensation scheme (ASC)", Proceedings of IEEE International Conferences on Advances in Power System Control, Operation and Management, Nov. 1991, HongKong, pp. 123-128.

[79]. E. Larsen, C. Borwler, B. Damsky, and S. Nilsson, "Benefits of thyristor controlled series compensation", CIGRE Session 1992, 14/37/38-04, Paris.

[80]. A. Edris, "FACTS technology development: an update", *IEEE Power Engineering Review,* March 2000, Vol. 20, No. 3, pp.4-9.

[81]. E. Larsen, K. Clark, S. Miske, and J. Urbanek, "Characteristic and rating consideration of thyristor controlled series compensation", *IEEE Transactions on Power Delivery,* Vol. 9, No. 2, April 1994, pp. 992-1000.

[82]. B. K. Perkins and M. R. Iravani, "Dynamic Modeling of a TCSC with Application to SSR Analysis Modular modeling," *IEEE Transactions on Power systems,* vol. 12, no. 4, pp. 1619–1625, 1997.

[83]. C. R. Fuerte-Esquivel, E. Acha, and H. Ambriz-PBrez, "A Thyristor Controlled Series Compensator Model for the Power Flow Solution of Practical Power

Networks", *IEEE Transactions on Power Systems.* vol. 15, no. 1, pp. 58- 64, February 2000.

[84]. J. Geng, L. Tong, Z. Wang, and J. Ge, "Mathematical Model for describing characteristics of TCSC", [Power System Technology, 2002. Proceedings. PowerCon 2002. International Conference on](#).

[85]. S. Meikandasivam, R. K. Nema and S. K. Jain, "Selection of TCSC parameters: Capacitor and inductor," India International Conference on Power Electronics 2010 (IICPE2010)*,* New Delhi, 2011, pp. 1-5.

[86]. M. H. Abardeh and J. Sadeh, "Effects of TCSC parameters and control structure on damping of sub-synchronous resonance," 2010 4th International Power Engineering and Optimization Conference (PEOCO), Shah Alam, 2010, pp. 26-32.

[87]. N. G. Hingorani and L. Gyugyi, *Understanding FACTS Concepts and Technology of Flexible AC Transmission Systems*, Wisley online library, 2000

[88]. S. J. GMey, W. A. Mittelstadt and R. W. Suhrbier Bonneviue, "Power Administration, Test Results and Initial Operating Experience for the BPA 500 kV Thyristor Controlled Series Capacitor Design, Operation, and Fault Test Results," Northcon 95. IEEE Technical Applications Conference and workshops Northcon95, 1995, pp 268 – 273.

[89]. K. Ahlgren, D. Holmberg, P. Halvarsson, and L. Ängquist, 'Thyristor Controlled Series Capacitor Used as a Means to Reduce Torsional Interaction Subsynchronous Resonance', Sweden.

[90]. TCSC in Brazil: power system interconnection, [Online]. Available: http://www.modernpowersystems.com/features/featuretcsc-in-brazil-power-system-interconnection/

[91]. C. Gama l. Ängquist, G. Ingeström, and M. Noroozian, "Commissioning and operative experience of TCSC for damping power oscillation in the Brazilian North-South interconnection," CIGRE, Session 2000.

[92]. C. Gama , "Brazilian North-South interconnection - Control application and operating experience with a TCSC," IEEE Power Engineering Society Summer Meeting, 1999. , pp 1103 – 1108.

[93]. M. Arunachalam, G. L. Rajiv, C. G. BHEL, "Performance verification of TCSC control and protection equipment using RTDS", 15th PSCC, Liege, pp 22-26.

[94] S. Subhash, A. K. Tripathy, and K. R. Padiyar, "SSR study for the Thyristor Controlled Series Compensation application on the Kanpur-Ballabgarh 400kV line in India," International Conference on Power Systems Transients, , No. 05 – 043.

[95]. ABB, TCSC for stable transmission of surplus power from eastern to western India, ABB power technologies, [Online]. Available: www.abb.com/powersystems.

[96]. K. Braun, etc, It's a FACTS – India gets closer to completing its national grid, Siemens PTD, Erlangen, Germany (2008), Transmission & Distribution.

[97]. Z. Yin, etc. "A study on the characteristics of TCSC based on digital simulations and physical experiments," Power System Technology, Proceedings. POWERCON '98. 1998 International Conference on, Beijing, 1998, pp. 328-332 vol.1.

[98]. J. Liang, J. Guo and X. Zhou, "Theory analysis and engineering study of Yimin-Fengtun 500 kV TCSC transmission system," Power System Technology, 1998. Proceedings. POWERCON '98. 1998 International Conference on, Beijing, 1998, pp. 377-381 vol.1.

[99]. X. Zhou, J. Guo, Q. Guo, EPSR (2000), "Studies on Application of TCSC in power systems of China", Power System Technology, 2000. Proceedings. PowerCon 2000. International Conference on, pp 387 – 390.

[100]. TCSC projects in China – TIANGUANG project, Simens, [online], available:https://www.energyportal.siemens.com/static/de/de/products.../12805_1070 17_tian%20guan g%20tcsc%20in%20china.html.

[101]. Case studies Hutton 400kV Thyristor Controlled Series Compensation, [Online]. Available: http://www.poweng.net/case-studies/index.php?id=13

[102]. J. C. Nambo-Martinez, K. Nieradzinska, and O. Anaya-Lara, "Dynamic series compensation for the reinforcement of network connections with high wind penetration", EERA Deep Wind 2014, Norway

[103]. Y. Pipelzadeh, et al. "Role of smart grid technology and corrective control in enhancing network capacity utilisation in great britain with HVDC links." CIGRE Symposium HVDC System and Markets Integration. Lund, Sweden. 2015.

[104]. G. N. Taranto, J. H. Chow, "A robust frequency domain optimisation technique for tuning series compensation damping controllers", *IEEE Transactions on Power Systems,* 1995, Vol. 10**, No.** *3,* pp. 1219-1225

[105]. G. N. Taranto, J. K. Shiau, and H. A. Othman, "A robust decentralized control design for damping controllers in FACTS applications". Proceedings of the 4th IEEE conference on Control applications, 1995, pp. 233-238

[106]. H. Othman, R. Vedam, and J. Finney, "Robust supplementary control controllers". *International symposium on Electric power engineering,* Stockholm, Sweden, 18-22 June 1995, pp. 244-249

[107]. M. Noroozian, G. Anderson, "Damping of inter-area and local modes by use of controllable components", *IEEE Transactions on Power Delivery,* 1995, (4), pp. 2007-2012

[108]. X. R. Chen, etc, "Controlled series compensation for improving the stability of multi-machine power systems", *IEEE Proceedings - General Transmission Distribution,* 1995, 142, (4)

[109]. F. J. Swift and H. F. Wang, "Application of the controllable series compensator in damping power system oscillations," in *IEEE Proceedings - Generation, Transmission and Distribution*, vol. 143, no. 4, pp. 359-364, Jul 1996.

[110]. Q. Liu, V. Vittal and N. Elia, "LMI pole placement based robust supplementary damping controller (SDC) for a thyristor controlled series capacitor (TCSC) device," *IEEE Power Engineering Society General Meeting,* 2005, pp. 1381-1386 Vol. 2.

[111]. H. Chen, G. Anderson, "A versatile approach for the control of FACTS equipment in multi-machine power systems", *Electrical Power Energy System,* 1995, **17,** *(3),*pp. 215-221

[112]. H. Chen, "Enhancement of power system stability by controllable series compensation", *Automation Electric Power Systems,* 1996, 20, (1 0), pp. 1617

[113]. K. C. S. Thampatty, E. P. Cheriyan and M. P. Nandakumar, "Design of a discrete Linear Quadratic Gaussian (DLQG) compensator for SSR damping using a sample invariant discrete model of TCSC," TENCON 2009 - 2009 IEEE Region 10 Conference*,* Singapore, 2009, pp. 1-6.

[114]. W. Chetan, K. Jadhao, and K. Vadirajacharya, "Optimal placing of FACTS devices to improve power system security," *International Journal of Engineering Research & Technology (IJERT),* Vol. 4 Issue 05, May, 2015

[115]. Y. Manganuri, etc, "Optimal location of TCSC using sensitivity and stability indices for reduction in losses and improving the voltage profile," 2016 IEEE 1st International Conference on Power Electronics, Intelligent Control and Energy Systems (ICPEICES)*,* Delhi, 2016, pp. 1-4.

[116]. X. Zhou and J. Liang, "Overview of control schemes for TCSC to enhance the stability of power systems," *IEEE Proceedings - Generation, Transmission and Distribution*, vol. 146, no. 2, pp. 125-130, Mar 1999.

[117]. M. Abapour, M. R. Haghifam, "On-line assessment of the transient instability risk", *IET Generation, Transmission, and Distribution,* 2013, **7**, pp. 602–612

[118]. V. Vittal, etc. "Transient instability risk assessment". Power Engineering Society Summer Meeting, 1999, pp. 206–211

[119]. M. K. Dosoglu, A. B. Arsoy, "Transient stability investigation of a power system with multiple SVC and TCSC", *Energy Education Science and Technology Part A: Energy Science and Research.* 2012, 29, pp. 1445–1456

[120]. M. Abapour, P. Aliasghari and M. R. Haghifam, "Risk-based placement of TCSC for transient stability enhancement," *IET Generation, Transmission & Distribution*, vol. 10, no. 13, pp. 3296-3303, 10 6 2016.

[121]. B. Wang, D. Zou. "Design of Adaptive Terminal Sliding Mode Controller of TCSC for Power System Stability Enhancement." Proceeding of the CSU-EPSA, Vol. 4, No.5, 344-350, 2011.

[122]. L. Zhang, A. Zhang and J. Junfeng, "I&I stabilization based novel nonlinear adaptive TCSC control algorithm for improving transient stability," The 26th Chinese Control and Decision Conference (2014 CCDC), Changsha, 2014, pp. 1610-1615.

[123]. M. Hanyi and D. Chen, "Multi-objective Coordinated Design of TCSC and SVC for Improving Transient Stability," 2015 Fifth International Conference on Instrumentation and Measurement, Computer, Communication and Control (IMCCC), Qinhuangdao, 2015, pp. 246-250.

[124]. X. M. Mao, Y. Zhang, L. Guan, and X. C.Wu, "Coordinated control of inter-area oscillation in the China Southern power grid," *IEEE Transactions on Power Systems*, vol. 21, no. 2, pp. 845–852, May 2006.

[125]. Y. Zhang and A. Bose, "Design of wide-area damping controllers for inter-area oscillations," *IEEE Transactions on Power Systems*, vol. 23, no. 3, pp. 1136–1143, Aug. 2008.

[126]. Y. Li, etc, "Wide-Area Robust Coordination Approach of HVDC and FACTS Controllers for Damping Multiple Interarea Oscillations," in *IEEE Transactions on Power Delivery*, vol. 27, no. 3, pp. 1096-1105, July 2012.

[127]. R. Zheng, G. Li and J. Liang, "Capability of TCSC on SSR Mitigation." *Journal of Power and Energy Engineering* 3.04 (2015): 232-239.

[128]. R. Zheng, T. Joseph, S. Wang and J. Liang, "A control strategy for TCSC to mitigate SSR with local measurements," 13th IET International Conference on AC and DC Power Transmission (ACDC 2017), Manchester, 2017, pp. 1-6.

[129]. L. Piyasinghe, Z. Miao, J. Khazaei and L. Fan, "Impedance model-based SSR analysis for TCSC compensated type-3 wind energy delivery systems," 2015 IEEE Power & Energy Society General Meeting, Denver, CO, 2015, pp. 1-1.

[130]. T. K. Oh, Z. Z. Mao, "Analysis on thyristor controlled series capacitor for subsynchronous resonance mitigation," *ISIE 2001. 2001 IEEE International Symposium on Industrial Electronics Proceedings (Cat. No.01TH8570)*, Pusan, 2001, pp. 1319-1323 vol.2.

[131]. H. A. Mohammadpour, A. Ghaderi, and E. Santi, "Analysis of subsynchronous resonance in doubly-fed induction generator-based wind farms interfaced with gate controlled series capacitor ," *IET Generation, Transmission & Distribution*, June 2014.

[132]. H. A. Mohammadpour, J. Siegers and E. Santi, "Controller design for TCSC using observed-state feedback method to damp SSR in DFIG-based wind farms," *2015 IEEE Applied Power Electronics Conference and Exposition (APEC)*, Charlotte, NC, 2015, pp. 2993-2998.

[133]. S. R. Joshi, E. P. Cheriyan and A. M. Kulkarni, "Output feedback SSR damping controller design based on modular discrete-time dynamic model of TCSC," in *IET Generation, Transmission & Distribution*, vol. 3, no. 6, pp. 561-573, June 2009.

[134]. X. Zheng, Z. Xu and J. Zhang, "A supplementary damping controller of TCSC for mitigating SSR," *2009 IEEE Power & Energy Society General Meeting*, Calgary, AB, 2009, pp. 1-5.

[135]. F. Zhang; Z. Xu, "SSR damping study on a generator connected to TCSC," Power Systems Conference and Exposition. IEEE PES, pp. 673-678 vol.2, 10-13 Oct. 2004

[136]. R. J. iwko, C.A. egner, S.J. inney, J.D. Eden, "Subsynchronous resonance performance tests of the Slatt thyristor-controlled series capacitor," *Power Delivery, IEEE Transactions on*, vol.11, no.2, pp.1112-1119, Apr 1996

[137]. P. Vuorenpaa, T. Rauhala, and P. Jarventausta, "Applying TCSC frequency response data derived using electromagnetic transient analysis in SSR frequency scanning studies", PowerTech, 2009 IEEE Bucharest., 2009: 1-6.

[138]. M. O. Hassan, Z. A. Zakaria, and S. J. Cheng, "Impact of TCSC on enhancing power system stability", Power and Energy Engineering Conference, 2009. APPEEC 2009. Asia-Pacific. IEEE, 2009: 1-6.

[139]. S. K. Kerahroudi, etc. "Investigating the impact of stability constraints on the future GB transmission system", Universities Power Engineering Conference (UPEC), 2012 47th International. IEEE, 2012: 1-6.

[140]. J. Ling, Z. Guo and W. Feng, "Design of adaptive TCSC damping controller based on oscillation energy analysis", Transmission and Distribution Conference and Exhibition: Asia and Pacific, 2005 IEEE/PES. IEEE, 2005: 1-5.

[141]. X. Tan, etc, "Characteristics and firing control of thyristor controlled series compensation installations", Power System Technology, 1998. Proceedings. POWERCON'98. 1998 International Conference on. IEEE, 1998, 1: 672-676.

[142]. A. Kazemi, S. Jamali and H. Shater, "Measured impedance by distance relay with positive sequence voltage memory in presence of TCSC." Power Systems Conference and Exposition, 2009. PSCE'09. IEEE/PES, 2009.

[143]. K. Khosro, S. Henschel, and H. W. Dommel, "Resistive behavior of thyristor-controlled series capacitors at subsynchronous frequencies." *IEEE transactions on Power Delivery* 19.1 (2004): 374-379.

[144]. Y. Tang and Y. Qian, "Mechanism analysis of using thyristor controlled serious compensation to mitigate Subsynchronous Resonance." IPEC, 2010 Conference Proceedings. IEEE, 2010.

[145]. Z. Hao, C. Dai and S. Wu, "Research on single-phase PLL for the synchronization of thyristor controlled series capacitor." Power and Energy Engineering Conference (APPEEC), 2012 Asia-Pacific. IEEE, 2012.

[146]. S. Meikandasivam, K. N. Rajesh, and K. J. Shailendra, "Performance of installed TCSC projects." Power Electronics (IICPE), 2010 India International Conference on. IEEE, 2011.

[147]: "Dynamic series compensation for the reinforcement of network connection with high wind penetration". [Online]. Available: www.sciencedirect.com/science/article/pii/S1876610214010947.

[148]: "Overhead transmission lines and underground cables". [Online]. Available:

www.tkne.net/downloads/power/transmissionlines1/transmission%20lines/overhe ad.pdf. [Accessed: 2014]

[149]. "PAS series of 4-Quadrant Amplifiers". [Online]. available: http://www.spitzenberger.de/download.ashx?Weblink=1002/.

[150]: C. E. Loo Ugalde, J. Ekanayake and N. Jenkins, "Subsynchronous resonance in a series-compensated Great Britain transmission network", *IEEE Generation, Transmission and Distribution 7(3)*, pp. 209-217, 2013.

[151]: "MicroLabBox product information". [Online]. Available:

http://www.dspace.com/shared/data/pdf/2017/dspace_microlabbox_product_infor mation_2017-02_english_170413e.pdf.

[152]: "Real-time interface (RTI)". [Online]. Available:

http://www.dspace.com/shared/data/pdf/2017/dspace_rti_catalog2017_e.pdf. [Accessed: 2017]

[153]. Working Group, "Performance evaluation and applications review of existing thyristor control series capacitor devices – TCSC", CIGRE Report B4.49, session 2013

[154]. A. S. Luiz Pilotto, et al. "Impact of TCSC control methodologies on subsynchronous oscillations." *IEEE Transactions on Power Delivery* 18.1 (2003): 243-252.

[155]. A. Lennart. "Synchronous voltage reversal control of thyristor controlled series capacitor." PhD diss., Elektrotekniska system, 2002.

[156]. T. Yi, R. Yu, and M. Yan, "Research on the synchronous voltage reversal control model of TCSC." Power System Technology (POWERCON), 2010 International Conference on. IEEE, 2010.

[157]. P. Vuorenpaa, T. Rauhala, and P. Jarventausta, "Applying EMT analysis based target function approach for designing SSDC implementation for TCSC." *Modern Electric Power Systems (MEPS), 2010 Proceedings of the International Symposium*. IEEE, 2010.

[158]. X. Xie, H. Liu, and Y. Han, "Coordinated Design of Supplementary Excitation Damping Controller and Voltage-sourced Converter Based Generator Terminal Subsynchronous Damping Controller for Subsynchronous Resonance Suppression: A Case Study." *Electric Power Components and Systems* 44.5 (2016): 565-577.

[159]. X. Wu, et al. "An SSR multichannel damping control scheme for TCSC considering multiple operating conditions." *International Transactions on Electrical Energy Systems* 26.12 (2016): 2759-2773.

[160]. X. Wu, et al. "Mitigation of Sub-synchronous Oscillation Caused by Thyristor Controlled Series Capacitor Using Supplementary Excitation Damping Controller." *Journal of international Conference on Electrical Machines and Systems*. Vol. 1. No. 2. Journal of International Conference on Electrical Machines and Systems, 2012.

[161]. K. S. Mecha, K. N. Shubhanga. "Design of a subsynchronous damping controller using a dynamic phasor-based model of TCSC." Power and Energy Systems:

Towards Sustainable Energy (PESTSE), 2016 Biennial International Conference on. IEEE, 2016.

[162]. C. Balarko, B. C. Pal, "Robust damping of multiple swing modes employing global stabilizing signals with a TCSC." *IEEE Transactions on Power Systems* 19.1 (2004): 499-506.

[163]. K. R. Varma, A. Soubhik, and S. Ysni, "Mitigation of subsynchronous resonance in a series-compensated wind farm using FACTS controllers." *IEEE Transactions on Power Delivery* 23.3 (2008): 1645-1654.

[164]. Q. Liu, et al. "Using TCSC scheme for SSR mitigation in a radial transfer corridor." Power System Technology, 2006. PowerCon 2006. International Conference on. IEEE, 2006.

[165]. H. Xie and A. Lennart, "Synchronous Voltage Reversal control of TCSC–impact on SSR conditions." *Proceedings of the Nordic Workshop on Power and Industrial Electronics (NORPIE)*. 2004.

[166]. K. Khosro, S. Henschel, and H. W. Dommel, "Resistive behaviour of thyristor-controlled series capacitors at subsynchronous frequencies," *IEEE transactions on Power Delivery,* no. 19, vol. 1, pp. 374-379, (2004)

[167]. K. Kabiri, et al. "A discrete state-space model for SSR stabilizing controller design for TCSC compensated systems." *IEEE Transactions on power delivery* 20.1 (2005): 466-474.

[168]. Q. Liu, et al. "A novel active damping control of TCSC for SSR suppression in a radial corridor." Electric Utility Deregulation and Restructuring and Power Technologies, 2008. DRPT 2008. Third International Conference on. IEEE, 2008.

[169]. M. Bongiorno, S. Jan and A. Lennart, "On control of static synchronous series compensator for SSR mitigation." *IEEE Transactions on Power Electronics* 23.2 (2008): 735-743.

[170]. P. Anderson, B. Agrawal, J. V. Ness, *Subsynchronous Resonance in Power Systems*, New York:IEEE Press, 1989.

# Appendix I

IEEE First Benchmark system model

System ratings:

$S_b = 892.4$ MVA, $V_b = 500$ kV, $f_b = 50$ Hz, $\omega_b = 2\pi f_0$.

The following parameters are defined in per unit unless stated otherwise.

Parameters of the synchronous generator :

$R_a = 0.0015, X_l = 0.13, X_q = 1.71, X_q' = 0.228, X_q'' = 0.2, X_d = 1.79,$

$X_d' = 0.169, X_d'' = 0.135, X_{mq} = 1.58, X_{md} = 1.66, R_{kq1} = 0.0053,$

$X_{kq1} = 1.695, R_{kq2} = 0.0182, X_{kq2} = 1.825, R_{fd} = 0.001, X_{fd} = 1.7,$

$R_{kd} = 0.0037, X_{kd} = 1.666, \tau_{d0}' = 4.3$ s, $\tau_{q0}' = 0.85$ s, $\tau_{d0}'' = 0.032$ s, $\tau_{q0}'' = 0.05$ s

Parameters of multi-mass shaft:

Inertias (in MWs/MVA):

$H_H = 0.092897, H_I = 0.155589, H_{LA} = 0.858670, H_{LB} = 0.884215,$

$H_G = 0.868495, H_X = 0.0342165.$

Self and mutual damping coeffiecients (in per unit T/ per unit speed dev.):

$D_H = D_I = D_{LA} = D_{LB} = 0.1, D_G = D_X = 0, D_{HI} = D_{IA} = D_{AB} = D_{BG} = 0.2$

$D_{GX} = 0.005$

Torsional stiffness (in per unit T/rad):

$K_{HI} = 19.303, K_{IA} = 34.929, K_{AB} = 52.038, K_{BG} = 70.858, K_{GX} = 2.822$

Transformer and transmission line:

$$R_T = 0, X_T = 0.14, R_L = 0.02, X_L = 0.5, X_{SYS} = 0.06$$

# Appendix II

| pins | Signal Description | pins | Signal Description |
|---|---|---|---|
| 1 | Phase B Capacitor voltage | 14 | Analogic ground |
| 2 | Phase C capacitor voltage | 15 | Phase B thyristor current |
| 3 | Phase A to phase B voltage | 16 | Digital ground |
| 4 | Phase A capacitor voltage | 17 | Phase A thyristor triggering signal (0V – 5V) |
| 5 | Phase C input line current | 18 | Phase B thyristor triggering signal (0V – 5V) |
| 6 | Phase B to phase C voltage | 19 | Phase C thyristor triggering signal (0V – 5V) |
| 7 | Phase A input line current | 20 | Fans activation signal (0V: off – 5V: on) |
| 8 | Phase B input line current | 21 | Resistor switch control pulse (0V: open – 5V: closed) |
| 9 | Phase B capacitor current | 22 | Short-circuit reset pulse ((0V:nothing – 5V:open) |
| 10 | Phase C capacitor current | 23 | State of main circuit breaker (0V: closed – 5V: open) |
| 11 | Phase C thyristor current | 24 | State of the resistor switch (0V: closed – 5V: open) |
| 12 | Phase A capacitor current | 25 | State of short-circuit breaker (0V:closed – 5V:open) |
| 13 | Phase A thyristor current | 26 | |

# Publications

Journal paper related to the thesis:

[1]. Zheng, Rui, Gen Li, and Jun Liang. "Capability of TCSC on SSR Mitigation." *Journal of Power and Energy Engineering*3.04 (2015): 232-239.

Conference paper related to the thesis:

[2]. R. Zheng, T. Joseph, S. Wang and J. Liang, "A control strategy for TCSC to mitigate SSR with local measurements," *13th IET International Conference on AC and DC Power Transmission (ACDC 2017)*, Manchester, 2017, pp. 1-6.

Jounal paper not related to the thesis:

[3]. S. Wang, J. Guo, C. Li, S. Balasubramaniam, R. Zheng and J. Liang, "Coordination of DC power flow controllers and AC/DC converters on optimising the delivery of wind power," in *IET Renewable Power Generation*, vol. 10, no. 6, pp. 815-823, 7 2016.